PERFORMANCE COMPARISON BETWEEN COMMERCIAL DYE AND NATURAL DYE BASED FROM DYE-SENSITIZED SOLAR CELL USING TITANIUM GRAPHENE FILM

SITI ZUBAIDAH BINTI MOHAMED SIDDICK

INSTITUTE GRADUATE STUDIES
UNIVERSITY OF MALAYA
KUALA LUMPUR

2018

PERFORMANCE COMPARISON BETWEEN COMMERCIAL DYE AND NATURAL DYE BASED FROM DYE-SENSITIZED SOLAR CELL USING TITANIUM GRAPHENE FILM

SITI ZUBAIDAH BINTI MOHAMED SIDDICK

THESIS SUBMITTED IN FULFILMENT OF THE REQUIREMENTS FOR THE DEGREE OF MASTER OF PHILOSOPHY

INSTITUTE GRADUATE STUDIES,
UNIVERSITY OF MALAYA
KUALA LUMPUR

2018

UNIVERSITY OF MALAYA
ORIGINAL LITERARY WORK DECLARATION

Name of Candidate: SITI ZUBAIDAH BINTI MOHAMED SIDDICK

Matric No: HGA140015

Name of Degree: MASTER OF PHILOSOPHY IN SCIENCE

Title of Thesis: **Performance Comparison Between Commercial Dye And Natural Dye Based From Dye-Sensitized Solar Cell Using Titanium Graphene Film**

Field of Study: MATERIAL ENGINEERING (NANOTECHNOLOGY)

I do solemnly and sincerely declare that:

(1) I am the sole author/writer of this Work;
(2) This Work is original;
(3) Any use of any work in which copyright exists was done by way of fair dealing and for permitted purposes and any excerpt or extract from, or reference to or reproduction of any copyright work has been disclosed expressly and sufficiently and the title of the Work and its authorship have been acknowledged in this Work;
(4) I do not have any actual knowledge nor do I ought reasonably to know that the making of this work constitutes an infringement of any copyright work;
(5) I hereby assign all and every rights in the copyright to this Work to the University of Malaya ("UM"), who henceforth shall be owner of the copyright in this Work and that any reproduction or use in any form or by any means whatsoever is prohibited without the written consent of UM having been first had and obtained;
(6) I am fully aware that if in the course of making this Work I have infringed any copyright whether intentionally or otherwise, I may be subject to legal action or any other action as may be determined by UM.

Candidate's Signature Date:

Subscribed and solemnly declared before,

Witness's Signature Date:

Name:

Designation:

UNIVERSITI MALAYA
PERAKUAN KEASLIAN PENULISAN

Nama: SITI ZUBAIDAH BINTI MOHAMED SIDDICK

No. Matrik: HGA 140015

Nama Ijazah: MASTER OF PHILOSOPHY IN SCIENCE

Tajuk Tesis ("Hasil Kerja ini"): **Performance Comparison Between Commercial Dye And Natural Dye Based From Dye-Sensitized Solar Cell Using Titanium Graphene Film**

Bidang Penyelidikan: MATERIAL ENGINEERING (NANOTECHNOLOGY

Saya dengan sesungguhnya dan sebenarnya mengaku bahawa:

(1) Saya adalah satu-satunya pengarang/penulis Hasil Kerja ini;
(2) Hasil Kerja ini adalah asli;
(3) Apa-apa penggunaan mana-mana hasil kerja yang mengandungi hakcipta telah dilakukan secara urusan yang wajar dan bagi maksud yang dibenarkan dan apa-apa petikan, ekstrak, rujukan atau pengeluaran semula daripada atau kepada mana-mana hasil kerja yang mengandungi hakcipta telah dinyatakan dengan sejelasnya dan secukupnya dan satu pengiktirafan tajuk hasil kerja tersebut dan pengarang/penulisnya telah dilakukan di dalam Hasil Kerja ini;
(4) Saya tidak mempunyai apa-apa pengetahuan sebenar atau patut semunasabahnya tahu bahawa penghasilan Hasil Kerja ini melanggar suatu hakcipta hasil kerja yang lain;
(5) Saya dengan ini menyerahkan kesemua dan tiap-tiap hak yang terkandung di dalam hakcipta Hasil Kerja ini kepada Universiti Malaya ("UM") yang seterusnya mula dari sekarang adalah tuan punya kepada hakcipta di dalam Hasil Kerja ini dan apa-apa pengeluaran semula atau penggunaan dalam apa jua bentuk atau dengan apa juga cara sekalipun adalah dilarang tanpa terlebih dahulu mendapat kebenaran bertulis dari UM;
(6) Saya sedar sepenuhnya sekiranya dalam masa penghasilan Hasil Kerja ini saya telah melanggar suatu hakcipta hasil kerja yang lain sama ada dengan niat atau sebaliknya, saya boleh dikenakan tindakan undang-undang atau apa-apa tindakan lain sebagaimana yang diputuskan oleh UM.

Tandatangan Calon　　　　　　　　　　　　Tarikh:

Diperbuat dan sesungguhnya diakui di hadapan,

Tandatangan Saksi　　　　　　　　　　　　Tarikh:

Nama:

Jawatan:

PERFORMANCE COMPARISON BETWEEN COMMERCIAL DYE AND NATURAL DYE BASED FROM DYE-SENSITIZED SOLAR CELL USING TITANIUM GRAPHENE FILM

ABSTRACT

Dye-sensitized solar cell (DSSC) has attracted interest in the renewable energy community due to the ability of the photoelectrochemical device for converting sunlight directly to electricity with easy fabrication process and known as a low-cost solar cell. In this present study, the performance of DSSC based on graphene-titania (TrGO) photoanode using conventional N719 (synthetic dye), natural red anthocyanin dye (organic dye) and natural green chlorophyll dye (organic dye) were extensively studied, analyzed and discussed. One of the main components in DSSC is the dye sensitizer where it is the main contributor to the photovoltaic characteristic efficiency. Dye-sensitized must possess wider absorption spectra to maximize the absorption of light. Nowadays, extensive study of natural dyes DSSC conducted due to its promising alternative to conventional synthetic sensitizer because they are inexpensive, flexible, abundant, suitable, and reduce the usage of noble metals. However, to increase the performance of natural dye-based DSSC, an efficient isolation and fast extraction methods for purification were explored with the ability of the natural dye attached to the semiconductor oxide photoanode. Dye acts as an electron contributor to the semiconductor oxide surface. A highly conductive surface of photoanode is needed to ensure the photogenerated electron travels efficiently. By introducing rGO to the TiO_2 semiconductor oxide, rGO network will lower down the electron migration length of the nanocrystalline TiO_2 semiconductor oxide. TrGO was successfully synthesized via one-step sol precipitation peptization technique using titanium (IV) isopropoxide (TTIP) and reduced graphene oxide (RGO) was used as starting materials. In this thesis, the first parameter covers on to achieve the best nanocomposite morphology an film is the different weight ratio of rGO in the photoanode. A continuous effort was made to further improve on the synthesis pH of the nanocomposite and lastly, the calcination temperature (400 ^{o}C and 450 ^{o}C) was explored to attain the best anatase crystalline phase for the nanocomposite film. From the modification, the best performance DSSC was TrGO-3 with pH3 photoanode. It was found TrGO works with all type of dye (commercial N719 dye, red anthocyanine dye, and green chlorophyll dye). Green chlorophyll dye exhibit 4.77mAcm^{-2} current density with the efficiency of 1.41% and red anthocyanin dye producing 4.08 mAcm^{-2} current density with the efficiency of 1.36% compared to commercial N719 dye with 12.98 mAcm^{-2} current density with the efficiency of 4.79 %. Although natural dye (green chlorophyll dye and red anthocyanin dye) shows lower efficiency compared to commercial N719 dye, natural dye exhibits good properties such as environmentally friendly, cheap, abundant and good in energy production if numerous study is conducted to improving the energy production. Energy band gap of the device also shows improvements than pure TiO$_2$ where it lowers down from 3.2eV to 2.82eV for TrGO-3 and 2.72eV for TrGO-3 450. In terms of photovoltaic efficiency, TrGO-3 shows the best characteristics with the highest efficiency 4.76 %, with 695.81mV for V$_{oc}$ and current density, J_{sc} of 12.98mAcm^{-2}. The enhancement of DSSC mainly contributes from the integration of conductive rGO to TiO$_2$ where it contributed to the enhancement in porosity on the surface of the semiconductor oxide. Porosity helps in increasing the dye loading and thus enhancing the photovoltaic characteristics. The electron lifetime also obtained to prove the improvement in DSSC performance when rGO incorporated in TiO$_2$ photoanode in terms of reducing electron loss between the surface interface and lower down electron migration length.

Keyword: Dye-sensitized Solar cell; Graphene; Titanium Graphene Nanocomposite; Electron Transfer; Natural Dye.

PERBANDINGAN PRESTASI ANTARA PEWARNA KOMERSIAL DAN PEWARNA SEMULAJADI UNTUK SEL SOLAR SENSETIF PEWARNA MENGGUNAKAN TITANIUM GRAFIN FILM

ABSTRAK

Sel solar sensetif pewarna telah menarik perhatian dalam industri tenaga yang boleh diperbaharui kerana peranti sel ini mudah difabrikasi dan menjimatkan kos pengeluaran serta berupaya menukarkan cahaya matahari kepada elektrik secara langsung. Dalam skop penyelidikan ini, prestasi sel solar sensetif pewarna di fabrikasi dengan menggunakan grafin dan titanium dioksida dan menambah pewarna sentetik (N719), pewarna asli merah antosianin dan pewarna asli hijau klorofil untuk dianalisis dan dibincangkan. Salah satu komponen yang penting dalam DSSC adalah pewarna sensetif cahaya berupaya menyerap spectrum warna dari cahaya matahari dengan lebih luas. Trend uji kajian kini lebih tertumpu pada bahan - bahan semula jadi yang mempunyai potensi seperti pewarna asli yang digunakan dalam eksperimen ini sebagai alternatif kepada pewarna sintetik yang digunakan kini oleh kerana pewarna semula jadi lebih murah, mudah didapati, fleksibel, sesuai digunakan dalam peranti dan boleh mengurangkan penggunaan bahan logam adi. Walaubagaimanapun, untuk meningkatkan prestasi pewarna semula jadi di dalam peranti sel solar, memelukan usaha untuk meringkaskan teknik pengasingan dan menyaringan bahan pewarana semula jadi disamping kemampuan pewarna untuk menyalut permukaan semikonduktor. Permukaan yang konduktif diperlukan pada lapisan photoanode untuk memastikan electron yang terbias oleh cahaya untuk bergerak secara efisyen di antara perukaan komposit. Dengan mengsintesis rGO dan TiO_2 semikonductor oksida, diramalkan rGO akan membantu memendekkan laluan untuk eketron dari TiO_2 semikonduktor oksida. Titanium (IV) isopropoksida dan grafin oksida yang di ringkaskan digunakan sebagai bahan utama untuk mengsintesis titanium nano-sintesis rGO (TrGO) dengan menggunkan teknik selangakah sol titisan peptidisasi berjaya dihasilkan. Parameter pertama dikaji untuk mencari komposisi peratusan berat yang sesuai bagi rGO untuk disintesis menjadi photoanod. Tambahan, sinthesis pH dan suhu pembakaran (400 ^{o}C and 450 ^{o}C) semikonduktor juga diuji untuk memperoleh hablur berstruktur anatase yang berkualiti tinggi. Perolehan dari kajian ini menunjukkan walapun menggunakan pewarna yang berlainan jenis (semulajadi dan sintetik), TrGO-3 dengan sintesis pH3 menghasilkan aliran elektrik yang tinggi untuk semua sel solar. Pewarna hijau klorofil menghasilkan arus eletrik 4.77mAcm^{-2} dengan kecekapan 1.41% dan pewarna merah antosainin menghasilkan 4.08 mAcm^{-2} dengan kecekapan 1.36% berbanding pewarna sinetik N719 dengan 12.98 mAcm^{-2} arus eletrik dengan kecekapan 4.79% . Walaupun pewarna semula jadi menunjukkan kecekapan yang rendah berbanding pewarna sintetik, pewarna semual jadi terkenal dengan ciri mesra alam sekitar, lebih murah, senang untuk diperolehi berbanding pewarna sintetik dan banyak usaha dijalankan bagi mengkomersilkan sel solar yang menggunakan pewarna semulajadi bagi kegunaan diluar bandar serta menjamin masa depan pengurusan kuasa. Salah satu perolehan positif di dalam eksperimen ini adalah dari pada plot tauc berjaya mengkecilkan jurang jalur elektron dari TiO_2 3.2 –eV kepada 2.82 –eV TrGO-3 dan 2.72-eV untuk TrGO-3 450. Grafin memanjangkan kadar resapan cahaya photoanod ke cahaya visibal. rGO juga memberi impak kepada semiconductor dengan menabah liang-liang antara partikel yang membolehkan pewarna untuk menyerap masuk ke dalam liang tersebut. Peningkatan serapan pewarna senistif cahaya dapat menambahkan prestasi solar cell kerana lebih banyak cahaya boleh diserap ke dalam sel dan menambah bilangan elektron permukaan semikonduktor untuk meningkatkan pengambungan pemukaan antara TiO_2 dengan rGO dan menghasilkan rintangan cas elektron.

Kata Kunci: Sel Solar Sensetif Pewarna; Grafin; Nanocampuran Titanium Grafin; Pemindahan Elektron; Pewarna Semulajadi.

ACKNOWLEDGEMENTS

My sincere appreciation to everyone that contribute in my master degree research entitled: Degradation Analysis of Natural Dye in Dye-Sensitized Solar Cell using Titanium Dioxide-Graphene Film. I would like to express the biggest appreciation to all my supervisors, especially Dr Lai Chin Wei, Assoc. Prof. Dr. Juan Joon Ching, and late Prof. Dr. Sharifah Bee Hamid for the guidance throughout my research, publication, provides research facilities and studies. Secondly, thank you to all dear nanocat labmates especially to Low Foo Wah and Nur Azimah Abd Samad for the assistance throughout my experimentation and studies. I am gratitude to Mr. Hafiz Ahmad for the guidance in organic chemistry and natural dye studies. A big appreciation to Rekabina Utama; Mr. Ruhi Anuar Ruslan, Mr. Ruslan M.Shah and Mrs. Halimahton Abd Jalil for sponsoring natural dyes resources from their plantation throughout my master studies. My biggest acknowledgements to Nanotechnology and Catalysis Research Centre for the lab facilities throughout the research and Institute Graduate Studies for the study facilities. Last but not least, thank you to my family members and close friends for unconditional support throughout my master studies and research. My biggest grateful to God for His blessings throughout every great journey of life and throughout this master degree research was conducted.

TABLE OF CONTENTS

LIST OF FIGURES

LIST OF TABLES

LIST OF SYMBOLS AND ABBREVIATIONS

For examples:

TiO_2 : Titanium Dioxide

rGO : Reduced Graphene Oxide

TrGO : rGO nanocomposite Titanium Dioxide

PV : Photovoltaic

V_{oc} : Voltage/ Voltage open circuit

J_{sc} : Current Density

DSSC : Dye Sensitized Solar Cell

FF : Fill Factor

ŋ% : Efficiency

P_{max} : Maximum Power

P_{in} : Initial Power

XRD : X-ray diffraction

HRTEM : High-resolution Transmission Electron Microscope

FESEM : Field Scanning Electron Microscope

PL : Photoluminesence Spectra

FTIR : Fourier Transform Infrared Spectroscopy

Uv-Vis : Uv-Visible Spetrcoscopy

EIS : Electron Impedance Spectroscopy

R_s : Series resistance

R_{CT} : Charge Transfer resistance of photoanode/dye/electrolyte

R_{CE} : Charge Transfer resistance of counter electrode/electrolyte

f_{max} : Reduced Graphene Oxide

τ_n : rGO nanocomposite Titanium Dioxide

D : Debye Scherrer Equation

K : Sharp factor with a value close to unity

λ : X-ray wavelength

β : Line broadening at half maximum intensity (FWHM)

θ : Bragg angle

LIST OF APPENDICES

CHAPTER 1: INTRODUCTION

1.1 Introduction

At present, our research is motivated by interesting challenges arising from the future growth in energy demand and depletion of fossil fuels for our future energy management. In addition of that, many scientists aware that the extraction and combustion of our current fossil fuels will generate the significant amount of greenhouse gases to our atmosphere and this is a major threat to the environment because it causes pollution to from combustion of fossil fuels (Hemmatzadeh & Mohammadi, 2013). One of the steps taken by many countries to find an alternative clean energy source to ensure the availability of the source to producing the electricity (Grätzel, 2005). In this manner, an alternative clean energy source such as sunlight shows the characteristics of inexhaustible, most easily exploitable, and adjustable to many application such as solar cell, solar water heater and solar absorber (Gong, Sumathy, Qiao, & Zhou, 2017; Su'ait, Rahman, & Ahmad, 2015). The finding of alternative clean energy source is crucial in leading a high quality of life, which is in harmony with nature (Wan, 2004).

To date, Solar/ Sun energy has been established as a potential primary energy that is abundantly available and possibly the best substitute for fossil fuel to secure the future supply of a clean and sustainable energy. It's a well-known fact that Sunlight is a low-carbon technology to harness renewable energy from the Sun, which can be used in the photovoltaic technology industry. In order to bring photovoltaic technology to the point of commercial readiness, substantial research on the development of highly efficient photovoltaic cell to produce electrical energy has been developed over the past two decades (Nazeeruddin, Baranoff, & Grätzel, 2011). photovoltaic cell to produce electrical energy has been developed over the past two decades.

Among viable renewable PV solar energy approaches, the use of third generation solar cell is dye-sensitized solar cell (DSSCs) has become one of the most promising systems and has high potential in generating electricity to secure our future supply of clean and continuous energy is the 3rd generation solar cell at where it focused on environmental electricity generation from DSSC system. Dye-sensitized solar cell first developed by Michael Gratzel and Brian O'Regan (de Souza, de Andrade, & Polo, 2013; Narayan, 2012) by the combination of nanostructures electrode and efficient charge inject dyes (Narayan, 2012). Taking into account of the processes involved in the DSSC system on particulate photoanodes under solar irradiation, the materials used as photoanode as well as the dye sensitizer played a crucial role in the determination of their photoconversion efficiency. In this manner, the dye sensitizer absorbs light to excite electrons and then photo-induced electrons would then migrate to an electrode which produces a current (Basheer, Mathew, George, & Reghunadhan Nair, 2014); the photoanode is the path for the electron transport.

This research focuses more on the dye sensitizer and photoanode which they are two major essential parts in DSSCs, where the sensitizer absorbs light to excite electrons; the electrons would then migrate to an electrode which produces a current (Basheer et al., 2014); the photoanode is the path for the electron transport. The techniques of fabricating photoanode are relatively important aspect in the production of higher DSSCs efficiency (Seigo Ito et al., 2008). In recent years, natural resources have been extensively studied as the possible inexpensive and eco-friendly alternatives to the conventional material. Reduced graphene oxide (rGO) which is inexpensive and abundance has attracted tremendous research interest in the field of DSSC and will be applied as a photoanode enhancer in this study. In order to elevate the third-generation solar cell mainly DSSC, substantial research efforts towards the development of hybrid semiconductor/photoelectrode for the highly-efficient solar cell, particularly DSSCs, have been widely developed in recent years. Basically, in this study**,** the N719 commercialize dye, red anthocyanin dye and green chlorophyll dye used as photosensitizer (Figs.1.1) for photoanode to enhance the absorption of light in DSSC. On top of that, dyes derived from natural sources as the photo-sensitizer for DSSCs have been extensively studied associated with their large absorption coefficient, good light-harvesting efficiency, low cost and environmental friendliness (Seigo Ito et al., 2008; S. Ito, Saitou, Imahori, Uehara, & Hasegawa, 2010; Maurya, Srivastava, & Bahadur, 2016).

Figure 1.1: (a) N719 commercialize dye, (b) natural green chlorophyll dye, and (c) red anthocyanin dye.

In the present research work, an easy fabrication method to encapsulate TiO_2 into rGO photoanode film to enhance the photocurrent of DSSCs system using a natural dye sensitizer and commercial N719 (Fig.1.1) dye as comparison purpose will be developed and studied. In this case, several crucial issues, such as designing of the highly active surface area of photoanode morphology, dye loading amount on TiO_2 and rGO photoanode, lower down electron transfer resistance in the DSSCs device as well as the intensify the photo-induced electron transport rate will be focused and investigated in detail. In fact, the optimization of TiO_2 dopants into rGO film via sol precipitation technique is critical in order to improve their active surface area of the photoanode for efficient electron transfer pathway. To the best of our knowledge, literature reported about TiO_2 nanocomposite on rGO through via sol precipitation method to improve the DSSCs performance is still lacking. Making intuitive guesses on their properties are more or less impossible, and a focused research on this area is a very challenging task, including optimization of processing parameters in our sol precipitation synthesis formation of TrGO thin film for improving the DSSCs system performance using green chlorophyll dye, red anthocyanin dye, and conventional N719 dye sensitizers.

1.2 Problem Statements

The 3rd generation of the solar cell is focused more on the clean, abundant, low cost and easy fabricated solar cell. The problem is to design a simple and high efficiency and have a longer lifetime of the solar cell. DSSCs must have long-term stability and the function must retain after millions of times, in turn, over for the catalytic cycle which is excitation, charge injection and regeneration. The choice of material and structure of each layer are the critical issues as they can have a strong impact on the reliability and the efficiency of the solar cells. Graphene (Gr) is a new novel material that has unique properties where it is in form two-dimensional crystal thin. Gr is considered to be an ideal two-dimensional catalytic which consider having excellent electrical and thermal conductivities, mechanical strength, large surface area, and incredible high mobility of charge carriers(Gong et al., 2017). However, in practical, Gr films produced via solution processing will contain lattice defects and grain boundaries that act as recombination centers and decrease the electrical conductivity of the material significantly. Besides, Gr only can absorb 2.3% of visible light from the solar illumination. Thus, continuous efforts have been exerted to further improve the Gr textural and electronic properties by loading an optimum content of TiO_2 nanoparticles for a high photoactive electrode for further improvement photoconversion efficiency and their immigration of photo-induced charge carriers. In fact, the dye-sensitized solar cell has a major problem need to overcome to make a presentable and as a main product of the organic solar cell. Therefore, the study was critique based on natural dye DSSCs performance for both chlorophyll and anthocyanin dyes. To the best of our knowledge, the formation of Gr-composited with TiO_2 nanocrystals to improve the natural dye-based DSSC photovoltaic performance is still lacking and still a matter of debate. Thus, the development of efficient electrode for natural dye-based DSSC generation remains to be determined.

1.3 Objective

The objectives of this study are listed as follow:

i. To synthesis and characterize the synthesized TiO_2 loaded reduced graphene oxide using sol precipitation method. (eg: rGO weight, pH, and calcination temperature)

ii. To study the dye-sensitized solar cell performance based on natural dyes sensitizer (green chlorophyll dye and red anthocyanin dye) in terms of photocurrent efficiency, impedance spectroscopy and corporation with a different kind of dye.

1.4 Research Scope

In the present research study, synthesis of nanocomposite TiO_2 into the rGO photo-anode film using sol precipitation technique was developed with the ultimate study aim is to enhance the DSSCs performance. A comprehensive study was conducted to tailor the photoanode morphology at the same time optimizing natural dye loading on the TiO_2 and rGO photoanode and minimizing the electron transfer resistance in the device to intensifying the electron transport rate. Furthermore, the performance of the photoanode sensitized with natural dyes as well as the commercial dye has also been studied to evaluate the photocurrent performances and absorption compatibility between the dye and TrGO photoanode. In order to provide more conductive pathways for electron transfer within the DSSCs system, TiO_2/rGO thin film TiO_2 nanotubes with controlled dimensional features by controlling the ratio of the TiO_2 and rGO in the composites via sol precitation technique has been investigated in detail. The growth mechanism of TrGO nanocomposite with desired crystalline phase was investigated too. In addition, detailed studies regarding the relationship of the rGO content incorporated into TiO_2 for DSSCs performance have been established in this work. To the best of our knowledge, one-step synthesis of TrGO nano-composite through sol precipitation technique to improve DSSCs performance is still lacking. Thus, a comprehensive study was conducted to optimize weight content parameters (e.g., 0.01g - 0.05g), synthesis pH (pH1 – pH5) of TrGO nanocomposite and calcination temperature (400^{o}C and 450^{o}C) to obtain the desired TrGO nanocomposite thin film, resulting in best DSSC performance. To the best of our knowledge, there have been very limited reports of using sol precipitation of TrGO nano-composite through that resulted in enhanced are relatively limited for enhanced photovoltaic characteristics. In this respect, a comprehensive study on optimization of TiO2/ rGO ratio in the green chlorophyll-dye, red anthocyanin dye and N719-sensitized DSSC was also reported in this report.

1.5 Outline of the dissertation

This dissertation is organized into five chapters consecutively.

Chapter 1

In chapter 1, the introduction of this research work, research objectives, problem statement, the scope of research as well as dissertation overview is presented.

Chapter 2

Literature review where presents in this chapter where it tells on the past research that was done in the dye-sensitized solar cell. Further elaboration about the mechanism, fundamental of DSSCs and literature of each layer in DSSCs (semiconductor oxide, dye-sensitized, electrolyte, a cathode electrode and the modification of study) for reference purpose will be present. This chapter also reviews about other researcher studies with the different material used for this study. The importance of this research will be the highlight for further understanding of this research.

Chapter 3

The specifications of the raw materials, research methodology, and the characterizations employed in this research work are described in chapter 3.

Chapter 4

The results and the discussion of the research experiment will be discussed in this chapter. The characterization of semiconductor material will be tabulated and discuss for further understanding. DSSC ability (photochemical characteristics and impedance) will be reviewed and compared with to open literature.

Chapter 5

Chapter 5 summarizes the conclusion of the study as well as several suggestions and recommendations for the future work. Such finding will aid in building the fundamentals of graphene film modification within the development of DSSCs system for a sustainable energy system.

CHAPTER 2: LITERATURE REVIEW

2.1 Introduction and Overview

Nowadays, public concern about the environment, climate change and limited fossil fuel resources have given rise to the urgent need of fostering development in the area of renewable energies, which are inexhaustible and non-polluting (Gong et al., 2017). The production of DSSC is one of the most promising prospects for efficient renewable resources . To bring DSSC to the point of commercial readiness and viability in terms of performance and cost, substantial research on the development of highly efficient photoanode for rGO using solar energy is necessary.

Recent studies indicated that graphene-based material has emerged as leading candidate for DSSCs cell because of its unique properties such as high conductivity, high surface area and possess 2D surface which is preferable for electron transfer (Geim, 2009; V. Singh et al., 2011). The high efficiency of graphene-based material as a photoelectrode in a DSSC cell requires a suitable architecture that to be evenly coated with the nanoparticle to improve the transfer path of the electron. In order to further improve the immigration of photo-induced charge carriers, considerable effort has to be exerted to further improve the DSSC performance under solar illumination (Liu et al.; Zhi, Cui, Chen, Xie, & Huang, 2015). Lately, interesting and unique features of TiO_2-rGO thin films have gained much attention and became one of the most favorite research matter among various groups of scientists. The relationship between the rGO on TiO_2 as well as their DSSC performance is still a matter of debate and remains unclear. It was noted that the properties of this nanocomposite photoanode primarily depend on the nature of the preparation method and the role of optimum rGO content incorporated into the TiO_2 nanocomposite. Therefore, the development of efficient solar responsive photoanode photocatalyst remains to be determined.

In the subsequent section, the historical overview, the basic principal, material selection and work done by various researchers with regards to the rGO and TiO_2 applied in DSSC application will be reviewed in detail. This chapter mainly reviews the aspiration of research in solar energy, history and a brief introduction to DSSCs and working principle of DSSCs. Furthermore, the background of each component (eg: reduced graphene oxide properties, material choice of semiconductor oxide background, dye-sensitized, electrolyte and counter electrode) in DSSC was discussed in this chapter for a better understanding about the device.

2.2 Historical overview of solar cell

Over century human are trying to find an alternative way to produce electricity and ensure the availability of the source to producing the electricity (Grätzel, 2005). Energy rules the economic growth as the demands increasing each year and the energy experts predicted by 2050 the world needs 30 TW to maintain the stability of energy production (Asim et al., 2012). The biggest challenge of replacing the ready energy source where energy consumption is predominately rely on fossil fuel (Hemmatzadeh & Mohammadi, 2013). Fossil fuel energy faced a problem with the continuation of consumption will cause the source to depleat and the harmful effect to the environmental plus it is non-renewable energy (S.Anandan, 2007; Wan, 2004). Much alternative and potential energy source being discovered and studied such as nuclear energy, nuclear fission, and solar cell (Wan, 2004). The challenge is to find a sustainable energy that is abundant clean and renewable (Wan, 2004) raw material with low-cost solution (Nazeeruddin et al., 2011).

Solar/Sun energy is the primary energy that is abundantly available and held a tremendous potential for the survival of the future generation especially in Malaysia. Therefore, photovoltaic cell is developed where it can harnessing power from the sun and producing electrical energy (Nazeeruddin et al., 2011). First silicon solar cells were produced in 1954 by Bell Lab and were known as first generation solar cell which refers to p-n junction photovoltaic. The photovoltaic (PV) were made from mono- and poly-crystalline silicon doped with other materials. The mono-crystalline silicon recorded the highest efficiency for the first generation solar cell but this cell is not consumer efficient as it has high fabrication cost and composition (Ludin et al., 2014). In 1954, Hoffman develops a method to increase the PV cell efficiency by using amorphous polycrystalline compound semiconductors such as amorphous silicon (A-Si), cadmium telluride (CdTe) and copper indium gallium selenide (CIGS) which were known as second generation PV device (Ludin et al., 2014). Thin film PV cell consists of three types of film cell structure (single junction, twin junction, and multiple junctions) where it is differentiated by the number of p-i-n junction. To increase the efficiency of thin solar cell, several processes involves in depositing thin-film material which will make the fabrication and device production cost more expensive (Al-Alwani, Mohamad, Ludin, Kadhum, & Sopian, 2016; Ludin et al., 2014). CdTe thin film PV is known as the most expensive thin film candidates. Both the first and second generation solar cell was fundamentally derived from semiconductor materials. Then, third generation solar cell was introduced with the aim to optimize device efficiency and particularly to reduce the device production cost.

The first solar cell is created in 1839 by Antoine – Cesar Becquerel (Chandrasekaran et al., 2011) in 1839 by the photovoltaic effect of a solid electrode in the electrolyte solution when he observes a voltage develop when light strikes to the electrode (Chandrasekaran et al., 2011). Photovoltaic cell holds attractive features such as do not contribute secondary environment pollution, do not contribute to nuclear waste by-products, inexhaustible and no greenhouse by-product waste(Su'ait et al., 2015). Albert Einstein won a noble prize in 1921 by reported photon absorption generate a photoelectric effect in early 1905(Ludin et al., 2014). The solar cell has been the cleanest and abundant energy besides its advantages as the renewable energy and its already 3rd generation study of the solar cell. The 1st generation solar cell is made and based on silicon material (Hemmatzadeh & Mohammadi, 2013). Furthermore, the 2nd generation of the solar cell is made of thin film material such an example is cadmium telluride and copper indium selenide (Hemmatzadeh & Mohammadi, 2013). Basically, dye-sensitized solar cell (DSSCs) is the 3rd generation solar cell where it is more focused on the environmental comparison of electricity generation from DSSCs system (Hemmatzadeh & Mohammadi, 2013). The generation of the solar cell is classified in below Fig. 2.1;

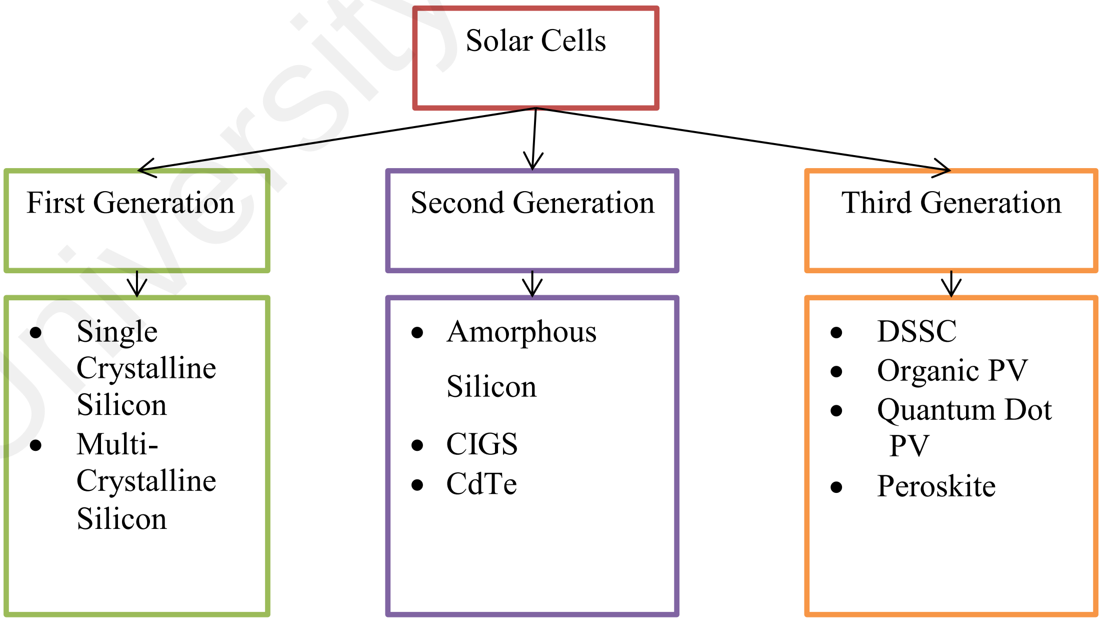

Figure 2.1: Solar Cell history and generations.

DSSC first developed by Michael Gratzel and Brian O'Regan in 1991 (de Souza et al., 2013; Narayan, 2012) by the combination of nanostructures electrode and efficient charge inject dyes (Narayan, 2012). By using thin nanocrystalline mesoporous TiO_2 film and intensify the light absorbed by the sponge-like structure for photoanode it increases the intensity of light absorption by 11% efficiency. The TiO_2 was soaked with dye-sensitized and by the investigation, the conversion of sunlight from the chemical reaction in DSSC resemble the photosynthesis process and known as artificial photosynthesis. The conversion of sunlight into electrical energy gives out the principle of photoelectrochemical (de Souza et al., 2013). The discovery that the energy of sunlight can be captured and converting into electric power had brought out lots of great ideas for scientists and researchers, who seek alternative energy sources.

Renewable solar cell energy source is a key component in sustainable energy development which is considered to be practically inexhaustible and non-polluting to the environment. Taking this fact into consideration, plenty of research works has been done to generate the green and renewable energy from the natural resources with the aim to create a sustainable environment that is in harmony with nature and to enhance the quality of life. Nevertheless, turning sunlight into electricity as the renewable sources which is more controllable and useful energy form while keeping the cost low still remains one of the biggest challenges.

In general, dye sensitizer and photoanode are two major essential parts in DSSCs, in which the sensitizer absorbs light to excite electrons; the electrons migrate to an electrode which produces a current; the photoanode is the path for the electron transport. In recent years, natural resources have been extensively studied as the possible inexpensive and eco-friendly alternatives to the conventional material. The dye-sensitized and photoanode structure is one of the most crucial tasks to be considered as it contributes to the efficiency of the device. In semiconductor oxide photoanode, the study of nanocomposite and the effect of the crystallinity as it affects the semiconductor properties of the chosen material (Asim et al., 2012).

Lately, rGO which is inexpensive and abundance has attracted tremendous research interest in the DSSC field and will be applied as photoanode enhancer in this study. In order to bring the renewable solar energy to the point of commercial readiness, substantial research efforts towards the development of hybrid semiconductor/photoelectrode for highly-efficient solar cell, particularly DSSCs, have been widely developed in recent years. Basically, in the present study, the N719 commercialize dye, red anthocyanin dye and green chlorophyll dye were used as photo-sensitizer for DSSCs. On top of that, dyes derived from natural sources such as the anthocyanin and chlorophyll photo-sensitizer for DSSCs have been extensively studied associated with their high light-harvesting efficiency, large absorption coefficient, low cost and environmental friendliness (Seigo Ito et al., 2008; S. Ito et al., 2010; Maurya et al., 2016). This breakthrough has triggered the subsequent interests in modifying semiconductor oxide research by scientists and researchers from all over the world on TiO_2/rGO and made photoanode as an important component in DSSC applications.

2.3 Dye-sensitized Solar Cell Structure and Working Operation

DSSC is a photovoltaic device that the performances depending on the physical process and the chemical construction which is different from the conventional photovoltaic cell. It combines the operation of liquid and solid phase material to produce current-voltage density. In real life, DSSCs working principle is like an analogous to photosynthesis where it absorbed light to gain energy and excite electrons. DSSCs consists of layer component that being sandwiched together by two conductive transparent glass (mainly ITO/FTO glass) (Wan, 2004). As shown in Fig. 2.2, a typical

DSSC consists of a transparent cathode (e.g., fluorine-doped tin oxide [FTO]), a highly porous semiconductor (Gr-composited with TiO_2 nanocrystals) layer with a soaked layer of dye (e.g. ruthenium polypyridine dye/organic dye), an electrolyte solution containing redox pairs (e.g., iodine/triiodide), and a counter electrode (e.g., platinum sheet) (Al-Alwani et al., 2016; Wan, 2004). For the semiconductor, TiO_2 acts as the electron acceptor, the electrolyte process of redox reaction (electron donor and oxidation) iodide/triiodide (I^-/I_3^-) resemble the water and oxygen in photosynthesis. At the same time, the multilayer structure DSSCs function together to enhance the light absorption and electron collection efficiency, which is same as the thylakoid membrane in photosynthesis (Narayan, 2012). The operational process of DSSC is divided into charge separation process and charge collection when the device was introduced to the photon from the sunlight/illumination.

A transparent conductive film (TCF) is a transparent electrode to maximize the transparency of the DSSC device to protect the inner layer of material against the harsh chemical and thermal treatments. Normally the industry standard TCF is the Indium tin oxide (ITO). The ITO glass increase R_{sh} of 5Ω/sq. However, indium is a rare earth metal which is not cost effective and ITO glass is not compatible with a strong acid, not stable at high temperature and mechanical brittle (Joseph D. Roy-Mayhew & Aksay, 2014; V. Singh et al., 2011). Fluorine tin oxide (FTO) was used as an alternative due to its properties to overcome the harsh chemical and higher thermal treatments almost at ~700^{o}C. In terms of cost, FTO glass is more cost effective and durable than ITO (Al-Alwani et al., 2016; Joseph D. Roy-Mayhew & Aksay, 2014; Sugathan, John, & Sudhakar, 2015)

The working principle of DSSC is illustrated in Fig. 2.3 and Table 2.1 : (1) Firstly, the dye molecules will harvest the high energy photons from the solar irradiation and then the electrons will release into the conduction band of the Gr-composites with TiO_2 nanocrystals. (2) The injected photo-induced electrons will then move to the transparent anode and, through the external circuit before transporting to the cathode.

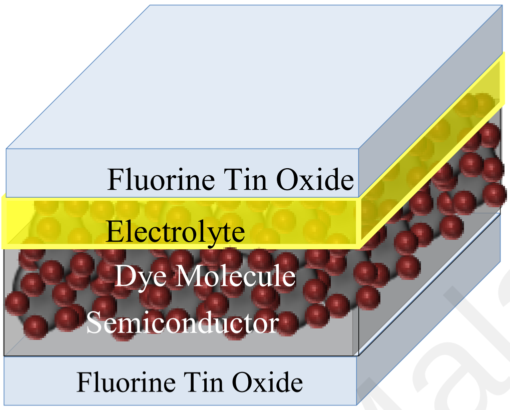

Figure 2.2: Dye-Sensitized Solar Cell Structure Illustration

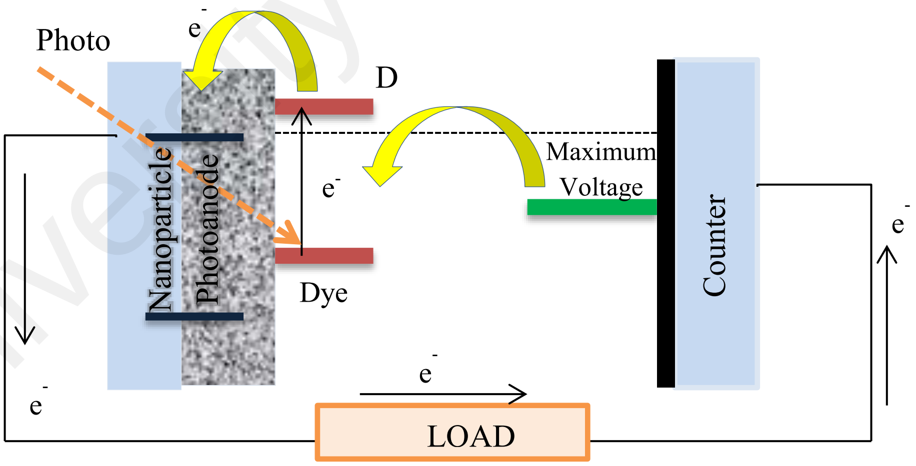

Figure 2.3: Working Operation of Dye-Sensitized Solar Cells (J.Gong, 2012)

Meanwhile, the dye molecules strip one electron from iodine in the electrolyte by oxidizing it to triiodide (redox reaction) (Grätzel, 2003; Narayan, 2012). (3) The triiodide then recovers its missing electron from the one circle of electron migration through the external circuit by diffusing to the counter electrode (i.e., cathode) (O'regan & Grfitzeli, 1991). (4) The counter electrode of a DSSC catalyzes the reduction of redox pairs after electron injection. (5) Voltage generates by the cell is depend on the illumination and show the difference in the Fermi level of the electron and the redox potential in the electrolyte (Grätzel, 2003; Narayan, 2012). (6) By complete this cycle, the device is generating power from the light without undergoing any permanent chemical transformation (Grätzel, 2003; Narayan, 2012). This proposed project will demonstrate a novel approach to enhance DSSC photovoltaic performance by applying modified photoanode of TiO_2 nanocomposite rGO nanocrystals. From the study, photovoltaic performance in DSSC will be addressed with physical and chemical properties of TiO_2 nanocrystals on rGO. Furthermore, the detail kinetic mechanism regarding TiO_2 nanocomposite rGO nanocrystals was established in this proposed project.

Semiconductor oxide has the ability to absorb dye molecule due to the indispensable large surface area. The dye molecules contain the electron to effectively absorb the photon. The device absorbs photon that strikes into the photoanode and the process lead to the excitation of the dye to electronically excited state (S*) and making the electron lies energetically above the conduction band of semiconductor oxide. The above state of semiconductor oxide is known as Lower Unoccupied Molecular Orbital (LUMO). In the excited state, dye-sensitizer collects photons & produced excited electron (S*) from HOMO to LUMO and the energy difference between HOMO level and LUMO level of the photosensitizer generates the amount of photocurrent in DSSCs.

When the excited electron injects to the conduction band it leaves hole/oxidation of photosensitizer. The dye-sensitizer LUMO need to exceed conduction band of semiconductor oxide due to the excited electron to be kinetically favorable to the conduction band of semiconductor oxide where the LUMO energy needs to be sufficiently negative. To ensure the effectiveness of electron injection, the substantial electronic coupling of the conduction band of semiconductor oxide level and LUMO of dye-sensitized level need to have strong electronic interaction with special anchoring group. The morphology of the semiconductor oxide plays an important role as it smoothens the electron transfer in the device and the connectivity of the particles. One of the important steps is the regeneration of the iodide (I^-) to replacing the oxide dye that excites to the LUMO. For the continuation of the current generation, the dye that excited to the conduction band of the semiconductor will be reduced back to the ground state when it lost the energy to the surrounding. Electrolyte acts as the bridge to connect the counter electrode and semiconductor oxide photoelectrode. I ion redox to replace the loss electron in the oxidizes dye.

Table 2.1: Detail equation the working principle in DSSCs (Al-Alwani et al., 2016; Lai et al., 2015; Shalini, Prabhu, Prasanna, Mallick, & Senthilarasu, 2015; E. Singh & Nalwa, 2015)

S + Photon (hv) $\rightarrow$ S*	(Light absorption)
$S^* \rightarrow S^+ + e^-$ TiO_2	(Electron Injection)
$S^+ + I^- \rightarrow S$	(Dye Regeneration)
I_3^- + $2e^-$ (counter electrode) $\rightarrow 3I^-$	(Redox Mediator Reduction)

In DSSC the charge transfers have a large contribution where it occurs in (1) nanocrystalline structure and (2) hole transfer in the electrolyte. The charge transfer in the electrolyte was represented by the redox reaction by tri-iodide and iodide. When the electron travels through the conducting oxide layer to the external load by electrically connects and reaches to the counter electrode. The electron from the counter electrode will flow to the electrolyte where the I_3^- ions float around until the electrolyte will compensate the missing electrons. By regeneration process, the I_3^- reduce back into I^- by the migration of electron from the catalyzed in counter electrode through the external load. The finalization process is the generation of voltage by the illumination corresponds to the Fermi level of the electron in semiconductor oxide and the electrolyte redox potential(Al-Alwani et al., 2016; J.Gong, 2012; Lai et al., 2015; Shalini et al., 2015).

Electron recombination is the main issue in any semiconductor device including DSSC. There is a probability of recombination process or back reaction in the DSSC reaction mainly in the charge separation and electron injection process. The back reaction may occur in the excitation of dye from the HOMO level to the LUMO level where the dye will decay or the energy loss resultant the dye to the surroundings. Next, the probability of recombination occurs in the electron injection from dye excited state to the conduction band and thus electrolyte is needed to overcome this problem. The speed of dye regeneration needs to be maintained in *ns* to lower down the recombination process of the DSSC.

2.4 Material selection for Semiconductor film electrode

Taking into account of the processes involved in the DSSCs on particulate photocatalysts under solar irradiation, the materials used as semiconductor film electrode must satisfy several functional requirements with respect to DSSC properties as shown below:

i. Band-gap: The electronic band gap should be low for most of the solar light spectrum so that can be used for photoexcitation

ii. Transportation of charge carriers: Charge carriers should be transported with minimal losses from the bulk oxide material to the counter electrode for a highly efficient photovoltaic characteristic of DSSC.

iii. Stability: The photocatalyst must be stable against photocorrosion in the electrolyte.

In this research, rGO/TiO_2 is a potential material as the photoanode for DSSC and the combination of these materials will be a great exploration in terms to enhance the conductivity, simplify the transfer path, increasing the active area for the attachments of the dye-sensitizer and reduce the interface resistance of the materials.

A typical photoanode film is made from a glass sheet with transparent glass that has a side of the conductive oxide and known as transparent conductive oxide (TCO). The glass used in DSSC is mainly fluorine tin oxide (FTO) glass or indium tin oxide (ITO) glass. The characteristic of the substrate is needed to allow the light to enter the solar cell. The semiconductor oxide is deposited to the conductive surface to allow the electron travels from the film to the external load and entering the counter electrode. The ideal semiconductor oxide must satisfy these characteristics to improve the performance of DSSC, i) transparency to increase the light absorption of dye, ii) high surface area with uniform nanostructured mesoscopic film to maximize the dye absorption, iii) porous surface for electrolyte accessible and iv) fast electron transport against the semiconductor grain (Raj & Prasanth, 2016).

2.4.1 Titanium Dioxide (TiO_2)

The semiconductor material is the main components that act as a photoanode in DSSCs. Mainly, a mesoporous oxide film is used to cater the photoanode characteristic to able the dye-sensitized attach to the surface of the mesoporous semiconductor. The mesoporous material as the main structure for the semiconductor oxide materials.

Basically, the material is nanometer crystal arrays with mesoscopic pores which act as dye attachments site (active area) and electron transfer passage through the DSSC. The examples of materials used as the semiconductor oxide are metal oxides such as Titanium Dioxide (TiO_2), Zinc Oxide (ZnO) or Tin Oxide (SnO_2) and inorganic material; carbon nanotube, graphene or graphite (Al-Alwani et al., 2016; Joseph D. Roy-Mayhew & Aksay, 2014; Sengupta, Das, Mondal, & Mukherjee, 2016; E. Singh & Nalwa, 2015). In 1990, M.Gratzel and co-workers had a large exploration in DSSC history where successfully combining TiO_2 nanoparticle, charge injection dye and electrodes to produce the 3rd generation solar cell. In order to bring renewable solar energy to the point of commercial readiness, substantial research on the development of hybrid semiconductor/photoelectrode for the highly efficient solar cell has been developed lately and it shows positive impact towards the performances of DSSCs.

Regards to the nanoparticle semiconductor small size, it has the ability to provide a large surface area and the relatively high porosity (Qu & Lai, 2013). Fig.2.4 provides the FESEM image of TiO_2 nanoparticle film semiconductor has a surface 10µm thick, porosity about 50% and the area surface that extremely good for dye absorption. Semiconductor plays an important variability factor for the performance of the dye-sensitized solar cell for electron recombination rate when obtained the electron diffusion coefficient. The semiconductor material also needs to be easy to access the dye and the electrolyte redox couple for the closed circuit system of the dye-sensitized solar cell (Chergui, Nehaoua, & Mekki). Through the study, nanoparticle dye-sensitized solar cell depends on the network of the crystallography of the crystalline and lattice where usually the pattern of the crystal is random plus it would affect or sway the electron or light scattering (Qu & Lai, 2013). The crystal structure can cause limitation of the electron transport where it will affect the rate to become slower, especially in the bright light that has longer wavelengths. Thus, this condition will increase the recombination process that caused by the electron transporting to take more time to (ms) to the contact (Pagliaro, Palmisano, Ciriminna, & Loddo, 2009).

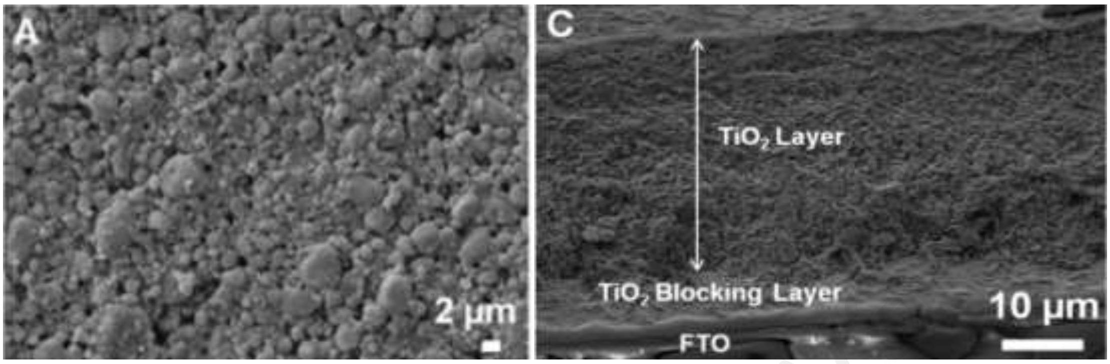

Figure 2.4: FESEM image of TiO_2 nanoparticle deposited on FTO glass (A) TiO_2 morphology (Low magnification) (C) TiO_2 nanoparticle on FTO cross section (Tripathi et al., 2014).

The nanocrystals of TiO_2 are divided into few types of crystal phase; anatase, rutile, and brookite. For the dye-sensitized solar cell, anatase and rutile both are the most common types used as semiconductor oxide. Anatase crystalline form at low temperature, has a pyramid like crystal and stable at low temperatures. Meanwhile, rutile crystal occurs like needle shape, crystal only forms in the high-temperature process (Al-Alwani et al., 2016). The band gap for anatase is slightly higher than those in rutile, but in terms of recombination rate, anatase has lower recombination rate compared to rutile phase (Lai et al., 2015) In dye-sensitized solar cell, the anatase TiO_2 polymorph is more efficient as semiconductor oxide to cater the charge transport and charge separation process compared to rutile. It is proven that TiO_2 anatase phase is a remarkable material for DSSCs as it has a higher electric conductivity that is favorable to transport electron for production of energy (Lai et al., 2015). TiO_2 photoanode usually preferred in anatase phase over rutile phase due to anatase exhibit photocatalytic degradation of organic compound under UV radiation while rutile phase of TiO_2 only absorb 4% of incident light in near UV range and bandgap excitation generated holes reduced the stability of DSSCs which is not favourable (Shalini et al., 2015).

TiO_2 was chosen as one of the best photoanode for the sensitized photoelectrochemistry due to its properties. One of the advantages of TiO_2 is a stable photoelectrode where it has good chemical stability under irradiation, eco-friendly, cheap and widely available (Al-Alwani et al., 2016). With a high dielectric constant (c= 80 for anatase phase), TiO_2 has the properties to lower down the recombination process when the electron excited are injected from dye by providing electrostatic shielding. The high refractive index of TiO_2 (anatase reflective index = 2.5) helps in the efficient diffuse scattering of sunlight in the semiconductor. The porosity of the semiconductor TiO_2 is a crucial characteristic whereby it holds the dye molecules that will make the semiconductor surface electron-rich surface. The dye molecule used as sensitizer and coated to nanocrystalline TiO_2 film that will convert the photons into the excited electron and produce current flow in the device.

Normally, a DSSCs photoanode consist of thick TiO_2 nanoparticles (~10-15µm) that forming a mesoporous network. The thick mesoporous structure (Fig. 3) provide a large surface area that acts as an anchoring site for dye molecules to absorb in the photoanode. In the past research, titanium dioxide (TiO_2) alone have been recorded a remarkable photocurrent-density efficiency for DSSCs, but due to its large band gap, it leads to fast recombination rate. The morphology (particle size, porosity, pore size and nanostructure) of photoanode plays significant roles to modulate the photovoltaic characteristics. The physical properties of each photoanode are determined by the nature of coating such as nature of binder, solvent, viscosity etc. of respective paste.

The recombination occurs due to the injected electron travel in the random colloidal particle matrix and grain boundaries in TiO_2, thus creating a random transfer route which followed by a trap-limited diffusion process (Tang et al., 2010). When photogenerated electrons travel in the random transfer path, it increases the carrier recombination, which contributes to a reduction of photocurrent efficiency in DSSCs. It is favorable to have a highly conductive material as the composite to the semiconductor oxide to enhance the low photocurrent-density voltage. Therefore, reduced graphene oxide (rGO) which is low cost and available in abundance has attracted tremendous research interest. In the dye-sensitized solar cell, the photoanode is an essential part in DSSCs.

2.4.2 Reduced Graphene Oxide (rGO)

Over the past years, the study of DSSCs becomes popular for enhancing the excellent material and structure to boost the efficiency and stability of the DSSCs. The novelty of DSSCs is where it is a molecular device that surpasses form the microelectronic technology to nanotechnology (Narayan, 2012). Each layer has been manipulated to find the suitable material and design for the DSSCs. In order to reduce the cost of solar cell devices, low cost and effective materials are investigated intensively. Therefore, rGO which is low cost and available in abundance has attracted tremendous research interest (Li et al., 2011; J. Wu et al., 2013; Xiang, Yu, & Jaroniec, 2012; Y. Zhu et al., 2010). Dr.Andre Geim and Konstantin Novoselov (Geim, 2009) were first discovered Graphene in 2004 as a result of the duplicate the properties of carbon nanotubes in flat sheets of carbon lattice (Bell).

A tremendous material such as rGO has known as the thinnest and strongest material with a single layer structure of graphite and one atom thick honeycomb-shaped with two-dimensional crystal structure as shown in figure 2.4 (Bell). rGO shows that it 2D carbon-based material has a flat single layer carbon atoms making it is a simple nanostructure material for the nanotechnology application (Dey et al., 2015; Meng, Geng, Liu, Li, & Sun, 2011; E. Singh & Nalwa, 2015; V. Singh et al., 2011; P. Wang, He, Wang, Yu, & Zhao, 2015). rGO has drawn much attention due to its unique properties which have drawn a great deal in various application such as the sensor, photovoltaic, nanoelectronics, and supercapacitor (Shi et al., 2012). In fact, Gr exhibits unique electrical (N. M. Huang, Lim, Chia, Yarmo, & Muhamad, 2011), electrochemical (N. M. Huang et al., 2011) and optical properties (T.-T. Wu & Ting, 2013) as well as incredibly high mobility of charge carriers. Furthermore, rGO possesses the high quality of easy accessibility, good flexibility and transparency property has shown promising potential to be used as the efficient photoelectrode (E. Singh & Nalwa, 2015). The unique combination of high electrical conductivity and optical transparency of rGO has emerged as the leading candidate in photovoltaic solar cell application (C. Huang, Li, & Shi, 2012; Xiang et al., 2012; Y. Zhu et al., 2010).

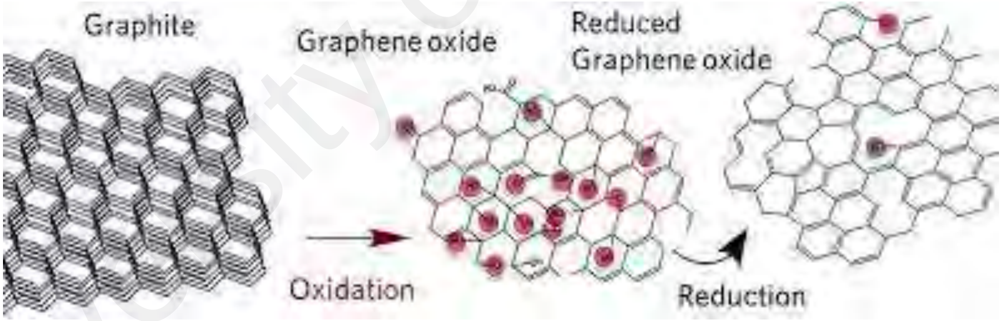

Figure 2.5: Reduction process of Graphite to Reduced Graphene Oxide.

Nowadays, researchers' productions of graphene oxide (GO) form graphite in bulk were developed. In this approach for graphene oxide production, graphite is oxidized with strong oxidants and intercalating compound (eg.KMnO, H_2SO_4, HNO_3, $NaClO_2$). Some researcher uses exfoliation technique through mechanical ultrasonic agitation producing stable suspensions of graphene oxide that demonstrated by Tanaka et al (Joseph D Roy-Mayhew, Bozym, Punckt, & Aksay, 2010; Shearer, Cherevan, & Eder, 2014). Surface functionalization is important for graphene oxide (GO) is important for controlling the surface behavior in order to be used in a different application. Functionalization of GO is needed due to graphene oxide utilizes weak interaction; the π-π interaction, Van der Walls interaction between the GO and molecules. By chemically reduced GO, the rGO is more stable when it is composite and producing functional composite materials (V. Singh et al., 2011; Y. Zhu et al., 2010). The changes from GO to rGO provides structural changes such as electrical conductivity, carrier mobility, optical band gap and thermal stability which beneficial for Gr-based solar cell (E. Singh & Nalwa, 2015).

The rGO electrical and optical properties depend on the spatial distribution of the functional groups and structural defects. Studying the evolution of GO to the rGO functional groups and structural defects are crucial due to obtained desired optical and electrical properties for rGO to perform in the electronic device. Many methods were applied for the production of rGO such as electrochemical, thermal or chemical synthesis. A minimal procedure is held for the reduction of GO to rGO such as chemically reduced graphene oxide. The most frequent method used is by using hydrazine vapor on graphene oxide as a reduction agent. The process path for producing the rGO is crucial and to maintain a simple methodology. However, in practical, rGO films produced via solution processing will contain lattice defects and grain boundaries that act as recombination centers and decrease the electrical conductivity of the material significantly (Blanita & Lazar, 2013; Yang, Feng, Ivanovici, & Müllen, 2010). Besides, rGO only can absorb 2.3% of visible light from the solar illumination (C. Huang et al., 2012; Xiang et al., 2012). Thus, continuous efforts have been exerted to further improve the rGO textural and electronic properties by loading an optimum content of metal oxide photocatalyst for the high photoactive electrode (Yang et al., 2010; Y. Zhu et al., 2010).

2.4.3 Combination of rGO /TiO_2 Nanocomposite

Design and development of the nanostructure of rGO composited TiO_2 assemblies have gained significant scientific interest and become the most studied material as it exhibits promising functional properties. Among the vast number of different metal oxide photocatalysts, TiO_2 is one of the most capable candidates to be coupled with graphene for enhancement in numerous diverse applications, such as solar cell, hydrogen conversion catalyst, water treatment and many more. The reasons mainly attribute to TiO_2 is a stable photocatalyst although it own large energy band gap, have random porosity structure, low cost, non-toxicity, ready availability, strong photocatalytic activity, stability against photo-corrosion, high trap state which favors recombination rate of electron and retard the electron transfer (Al-Alwani et al., 2016; Gong, Liang, & Sumathy, 2012; Gong et al., 2017; Liang, Wang, Casalongue, Chen, & Dai, 2010).

One of the important reason for combining TiO_2 with rGO because TiO_2 alone have a high diffusion coefficient where the structure of TiO_2 consists of random Ti grain that has significant neck size of porosity. When the electron travels on the Ti grain, it might lose their ‘power' due to the random and uncoordinated travel site. Whereby rGO is known as a flat 2D structure with a highly conductive surface that favors the ultrafast electron to travels on the surface of rGO. However, the ability of rGO to trap and absorb light is limited due to they're have a low diffusion coefficient that leads to low absorption of the dye. By combining TiO_2 and rGO, it can meet stability of the material which has tremendous properties. TiO_2 will provide defects on the rGO surface that will increase the material porosity and placeholder for the dye absorption. This will contribute to the enhancement of DSSC J_{SC} and creates travel site for the photogenerated electron (Asim et al., 2012; Gong et al., 2017).

By chemically control reduction process of graphite to GO and to rGO the chemical properties of rGO is improved and create remarkable properties due to its high aspect ratio, so it provides a low percolation threshold (Joseph D. Roy-Mayhew & Aksay, 2014). Gr is one of the carbonaceous materials that has been widely used in solar photovoltaic parts and in this research the implication of rGO into the TiO_2 as photoanodes in DSSC (C. Huang et al., 2012; N. M. Huang et al., 2011). It is noteworthy that the rGO has a matching conduction band with TiO_2 and thereby, a charge transfer could be formed between the rGO and TiO_2 surface. Also, the photo-induced electron can move through rGO bridge where it shuttling electron to the current collector rather than TiO_2 – TiO_2 grain boundary as a result of the diminished charge recombination (L. Chen et al., 2013; Joseph D. Roy-Mayhew & Aksay, 2014). In view of these facts, the combination of TiO_2 and rGO to produce the rGO-TiO_2 composites is an alternative route to improve the conduction pathways and photocurrent-voltage density of DSSC from the point of photoinduced electrons at photoanode to the charge collector electrode. To extend the performance of rGO in photoanode, rGO material should be used which has minimal defects to be effectively coated the dense TiO_2 particle. Many previous studies recorded improvements in terms of increasing photocurrent and elucidate the enhanced mechanism. Below (Table 2.2) recorded the past research of rGO-TiO_2 DSSCs performances as a reference for tailoring the suitable and simple's method to elevate the DSSC performances using RGO. The high efficiency of rGO-composited with TiO_2 as a photoanode in a DSSC requires a suitable architecture that minimizes electron loss at nanostructure connections and maximizes photon absorption (Jo & Kang, 2013; Liang et al., 2010). In order to further improve the immigration of photo-induced charge carriers, considerable effort has to be exerted to increase the photoconversion efficiency of DSSC under visible illumination.

Table 2.2: Past reference of reduced graphene oxide composite Titania dye-sensitized solar cell performances..

Reference	Graphene DSSC	Preparation method	Reference Cell	Graphene DSSC		Reference Cell	
				J_{sc}(mA/cm^{-2})	Ŋ(%)	J_{sc}(mA/cm^{-2})	Ŋ(%)
Chatterjee et al (2013)	PHET with grafted rGO	Molecular grafting	TiO_2	7.50	3.06	5.6	2.66
Sharma et al (2014)	RGO-TiO_2 layer	Hydrothermal method & spin coating	TiO_2 layer	10.95	5.33	9.97	4.18
Sun et al (2010)	P25-Graphene	Heterogeneous coagulation	P25 Electrode	8.38	4.28	5.04	2.70
Kazmi et al. (2016)	Gr-TiO_2(rGO)	Sonication	Pure TiO_2	9.80	-	-	-
Zhang et al. (2015)	TiO_2-G	Synthesis	TiO_2	7.80	1.50	4.06	0.89
(H. Wang, Leonard, & Hu, 2012)	TRGO scaffold layer	Ultrasonication	TiO_2	7.60	2.8	5.0	1.8
(Kim et al., 2012)	Underlayer T-CrGO	solvolthermal	TiO_2	12.90	6.1	5.0	4.4

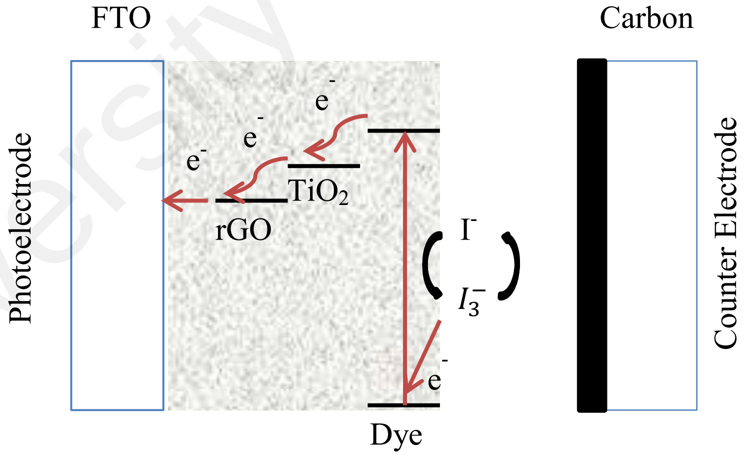

Figure 2.6: Electron flow in the photoanode contains rGO (H. Wang et al., 2012)

From all the previous study in table 2.2, rGO plays the positive role to accelerating the electron transfer in DSSC device where most of the study shows improvement in J_{sc} performances compared to pure TiO_2. From fig 2.6 rGO was reported to be a bridging agent as the incorporation of rGO enhance the conductivity which accelerates the electron transfer from TiO_2 to the FTO glass which will reduce electron-hole recombination (Kim et al., 2012; H. Wang et al., 2012). The incorporation of rGO in TiO_2 will enhance the performance of DSSC, thus a simplified and stable sol method is developed to fulfill the requirement of coating TiO_2 to the rGO sheet efficiently to improve the morphology of the photoanode surface.

2.5 Dye-Sensitizer

In general, dye sensitizer is a major essential part in DSSCs, in which the sensitizer absorbs light to excite electrons; the electrons would then migrate to an electrode which produces a current. In this research, comparison of two types of highly used dye that used in DSSC is being studied to know the suitability to attach to the TiO_2-rGO film. The two highly used dyes in DSSCs are metal complex dye based and dye from natural derivatives. The charge transfer sensitizer that employed is Ru-bipyridyl complexes, crude chlorophyll, and crude anthocyanin. In traditional DSSC, the standard dye was tris (2,2'-bipyridyl-4,4'-carboxylate) ruthenium(II) (N3 dye). Ruthenium complexes (Ru-complexes) is known as the most effective sensitizer due to its high efficiency where we could test the maximum performances of the composite, good photoelectrochemical properties, and intense charge transfer in the wide visible range (Ludin et al., 2014). However, Ru-complexes know with non-environmental friendly due to ruthenium is a heavy metal that is harmful to the environmental (Ludin et al., 2014; Pablo et al., 2016). Furthermore, with the presence of water, Ru-complexes tend to degrade. Ru-complexes has a general formula of $RuL_xL_y'SCN_z$ where the L and L' are polypyridyl ligands and Fig.2.7 shows the N719 Ru metal-based complexes with ligand attachments. The common alteration of the absorption spectrum of a complex π^* level tuning which by using ligands with π^* level energy and introducing methyl or phenyl group to increase the absorption of the metal to ligand charge transfer (MCLT) (Basheer et al., 2014).

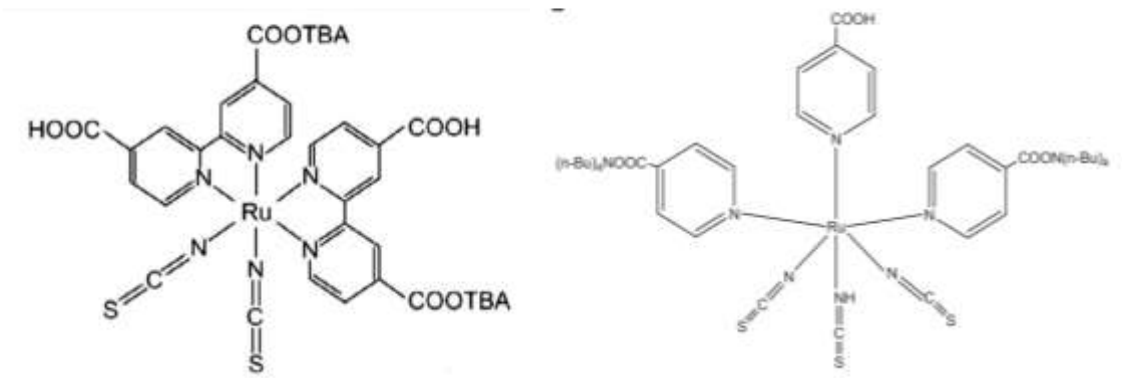

Figure 2.7: Ruthenium metal-based complexes N719 (Basheer et al., 2014; Ludin et al., 2014).

On top of that, dyes derived from natural sources as the photo-sensitizer for DSSCs have been extensively studied associated with their large absorption coefficient, high light-harvesting efficiency, low cost and environmental friendliness (Seigo Ito et al., 2008; S. Ito et al., 2010; Maurya et al., 2016). Natural resources were extensively studied to find the possible substitute of expensive and non-environmental friendly dye compound that previously used in the present study. Many extraction method and source of natural dye pigments or color that can be obtained from natural sources such as flowers, leaves, and bacteria (Shalini et al., 2015). The use of synthetics dye as dye sensitizer in DSSC tends to produce higher efficiency but they suffer from certain limitation such as a tendency to undergo degradation, higher cost, and usage of toxic materials. Due to this limitation of synthetic dye, alternate sensitizer that is natural dye-sensitizer which is biocompatible being introduced. Natural dye implies advantages to the DSSC application such as large absorption coefficient in the visible region, easily obtain, abundant, environmentally friendly and easy preparation (Shalini et al., 2015). Plant pigments have the ability to exhibit electronic structure where it can interact with sunlight and alters the wavelength that transmitted or reflected from the plant tissue. Below table 2.3 show the charts that classify pigments into four different types.

Table 2.3: Type of plant pigments.

Pigments	Common types	Occurrence
Betalains	Betacyanins Betaxanthins	Caryophyllales and some fungi
Carotenoids	Carotenes Xanthophylls	Photosynthetic plants and bacteria Retain from diet by some birds, fish, and crustaceans
Chlorophyll	Chlorophyll	All photosynthetic plant
Flavonoids	Anthocyanins Aurones Chalcones Flavonols Proanthocyanidins	Widespread and common plant including angiosperms, gymnosperms, gymnosperms, ferns, and bryophytes

Accordingly, natural dyes especially cyanine, chlorophyll, anthocyanin, carotene, and flavonoid have been extensively studied as sensitizers in DSSCs. Natural dye is extracted from plant pigments as shown in Fig. 2.6 and each pigment holds different molecular structure and absorption spectrum. Most importantly, the functional group of pigments is necessary to interact with the photoanode surface. In the present study, green chlorophyll extracted from the pandan leaves (*pandanus amarylliforus*) was extracted as the green chlorophyll dye pigment and mulberry (*Morus alba*) was extracted as red anthocyanin dye pigment as in Fig.2.8. Specifically, chlorophyll could be classified as a unique pigment ascribed to its ability to conduct photosynthesis converting the light energy to transduction energy in the plant. Additionally, chlorophyll (a mixture of 2 pigment complexes, namely chlorophyll a and b) is an attractive candidate as the sensitizer in DSSCs attributed to its tendency to absorb blue and red lights. Also, many research works have been focussed on the preparation of porphyrin-type organic dye from chlorophyll due to its low loss, ease of preparation and eco-friendly.

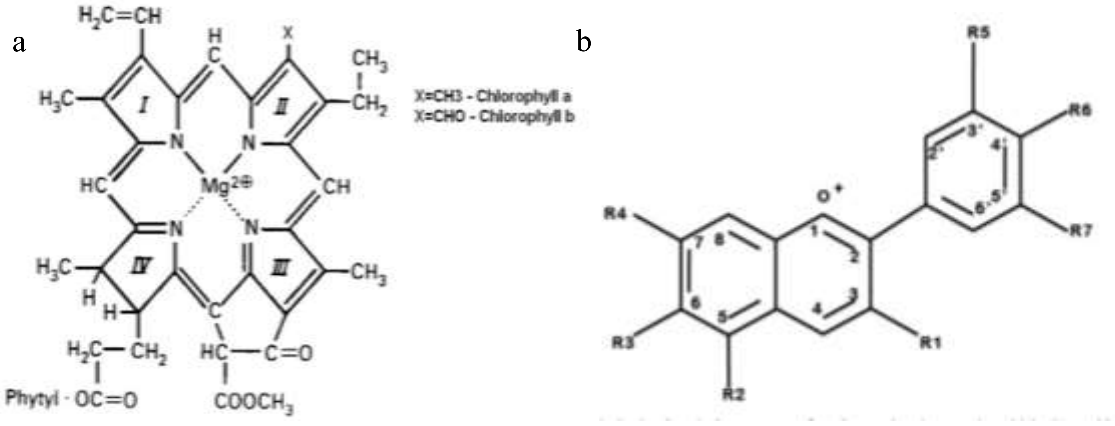

Figure 2.8: a) Chemical structure Chlorophyll ‘a’ and b and b) chemical structure of anthocyanin (Shalini et al., 2015).

Anthocyanin is a red-blue plant pigment which is an abundant type of plant with ~10^9 tonnes/year production (Calogero, Citro, Crupi, & Di Marco, 2014). From the literature, 17 types of anthocyanin have been reported so far and it is classified by per number of sugar molecule such as bioside, monoside, trioside etc. Anthocyanin prevails in the plant at flowers, leaves, fruits, in some type of mosses or ferns etc and the attractive color of anthocyanin ranging from scarlet to blue (Shalini et al., 2015). The anthocyanin counts in a plant determine the modified quantity and quality of light that is incident in the chloroplast. Common anthocyanidins found in a flower are the pelargonidin (orange), cyaniding (orange-red), delphinidin (blue-red), petunidin (blue-red) and malvidin (blue-red). One more advantage of anthocyanin in DSSC is it contains hydroxyl and carbonyl group that can bind to the surface of the semiconductor film, which will alleviate the excitation and transfer of the electron from the anthocyanin molecule to the semiconductor oxide conduction band. The bounding makes the electron transport from anthocyanin molecule to the conduction band of TiO_2. Anthocyanins are being used in organic solar cells due to the ability of light absorbing and convert it into the electron.

Table 2.4: Natural dyes used in DSSCs.

Plant source	Structure	Photoanode area (cm^2)	J_{sc} (mA/cm^{-2})	V_{oc} (mV)	ŋ/FF	Extract method
Rosa xanthia	Anthocyanin	1	0.637	492	-/0.52	Fractionated extract
Black rice	Anthocyanin	1	1.142	551	-/0.52	Fractionated extract
Kelp	Chlorophyll	1	0.433	441	-/0.63	Fractionated extract
Mangosteen pericarp	-	0.2	2.69	686	1.17/0.63	Extract
Spinach	Modified chlorophyll/neoxanthin	-	11.8	550	3.9/0.60	Isolated compounds
Spinach	Modified chlorophyll/β-carotene	-	13.7	530	4.2/0.58	Isolated compounds
Mulberry	-	-	0.86	422	Na/0.61	Extract
Tradescantia Zebrina	Anthocyanin	-	0.63	350	0.23/0.55	Ethanolic extract
Ixora sp.	Anthocyanin	-	6.26	351	0.96/0.44	Ethanolic extract
C.odontrophyllum + Ixora sp.	Anthocyanin	-	6.26	384	1.13/0.47	Mixed ethanolic extract
C.odontophyllum + Ixora sp.	Anthocyanin	-	9.80	343	1.55/0.46	Ethanolic extract in consecutive layers

The natural dyes data that used so far in DSSCs are recorded in table 2.4. The data are obtained by the different research of DSSCs condition and the natural dyes were extracted with a different method. Chlorophyll and anthocyanin as natural photosensitizers are sustainable dye and are available in large amount. In order for commercial readiness, fast extraction methods for purification are necessary for efficient sensitizer. The exploration and modification of natural dye pigments hope to bring out new findings to DSSC community.

2.6 Liquid Electrolyte

The heart of DSSC is a junction that formed between liquid electrolyte for interaction in between the semiconductor electrode and a counter electrode. The catalytic activity in counter electrode need to be efficient in reducing triiodide and continuously helps in regenerating dye molecules (E. Singh & Nalwa, 2015; Su'ait et al., 2015). One of an efficient DSSC requirement is the charge transfer of electrolyte must be faster than that direct electron-hole recombination rate in semiconductor (Bisquert, Fabregat-Santiago, Mora-Sero, Garcia-Belmonte, & Giméń z, 2009). Electrolyte generates the regeneration process in DSSC where it fills in the hole (oxidized state) in the dye sensitizer by donating ground state electron from the redox mediator in an electrolyte. Electrolyte must maintain the process rapidly reduce the oxidized dye and fast diffusion of charge carrier between the counter electrode and semiconductor oxide to sustain energy conversion from light. To remain the highly conducting surface area in any operating conditions, the ionic shielding by cations from a conducting salt that dissolved in liquid phase increases the surface area in the non-porous structure of DSSC. At very high interfacial contact, the charge carrier in the same phase is rapidly separated into different phases (Su'ait et al., 2015).

Liquid electrolyte is chosen due to it offers an effective solution the problem of electroneutrality in DSSC heterogeneous converters. The evolution of liquid electrolyte in DSSC started as metal-salts based liquid electrolyte, then it evolves to ionic liquid and lastly the combination of metal-salts and ionic liquid used as redox couple in DSSC as iodide/triiodide (I^-/I_3^-). The triiodide possess remarkable characteristic in DSSC as a support system to each component in the device system such as i) the regeneration of dye-sensitized hole with unity efficiency by I^-iodide, ii) the back reaction in the TiO_2 to I_3^- is slowed by complicated multielectron transfer mechanism by the liquid electrolyte, iii) I^-/I_3^- has high diffusion coefficient and highly soluble in any solvents due to its small size molecule to allow optimizing concentration for reaching the solubility or diffusion limit, iv) has low light absorbance to reduce competition with dye and v) I^-/I_3^- redox couple is stable and will not decompose under operation conditions (Su'ait et al., 2015).

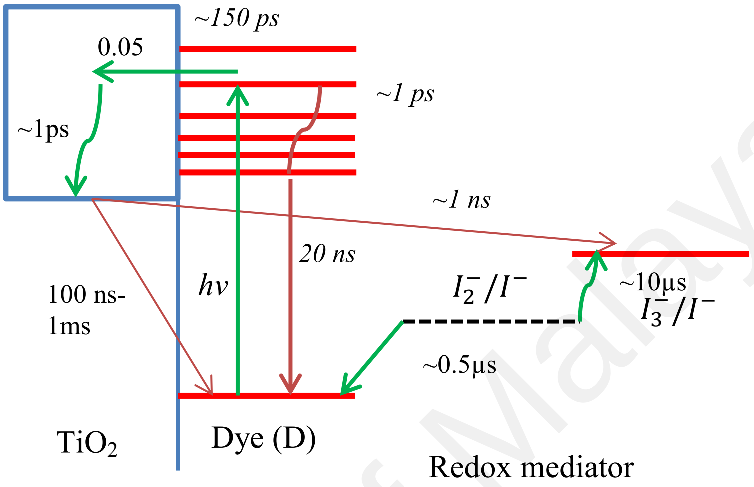

Figure 2.9: Kinetic of the electron in the DSSC with I_3^-/I^- redox mediator (Gong et al., 2012)

From Fig.2.9 it shows the kinetics of the electron the DSSC where the electron injection in the TiO$_2$ conduction band occurs in femtosecond which is faster than electron recombination with I_3^- and the injected electron combining with oxidized dye from the semiconductor react with I^-. The diffusion coefficient of I_3^- ions = 7.6 x 10^{-6} cm^2/s on the porous semiconductor TiO$_2$ oxide(Gong et al., 2012). The difference between quasi-Fermi levels of TiO$_2$ and redox potential in electrolyte determine the maximum voltage generated in DSSC. Corrosion limits the DSSC to obtain higher open circuit voltage, thus additives are added to alter the concentration of iodide been introduced such as 4-tert-butylpyridine (4TBP) (used in the research), quanidiumthiocyanate and methyl benzimidazole (MBI) (Gong et al., 2012). Many research has been dedicated to improving the properties and effectiveness of redox potential such as matching the oxidation potential of dye sensitization with redox potential can minimize the energy loss in the dye regeneration which can strikingly high open-circuit voltage almost to 1V (Gong et al., 2012).

2.7 Cathode Electrode.

The main role of the cathode electrode in DSSC is catalyzing the I^- regeneration from I_3^- in the redox couple to help the regeneration of dye. Nanostructure plays a crucial part in cathode electrode especially the morphological part where it determines the performance of DSSC device. The counter electrode also carries the photocurrent over the width of each solar cell device. Therefore, the counter electrode must be well conducting and exhibiting the low overvoltage. The most common type of cathode electrode is Platinum (Pt) where it i) act as collection center of the electron from the external load to the electrolyte and ii) acts as a catalyst that enhances the regeneration process of redox mediator from I^- to I_3^-.

Pt commonly used due to its good photocatalytic activity and excellent stability towards the I^-/I_3^- electrolyte. By finely dispersing the expensive platinum on a conducting substrate, such as ITO, FTO and $\mathrm{SnO_2}$ coated glass, the required amount has been kept low only about $< 0.1\mathrm{g/m^2}$ Usually, the platinum-loaded fluorine-doped tin oxide (FTO) glass serves as the counter electrode for DSSC. However, the platinum is a rare and high-cost metal in the earth and some of the researcher report that the corrosion of Pt would occur by reacting with triiodide containing the electrolyte form $\mathrm{PtI_4}$ (J. Z. Chen, Yan, & Lin, 2010). The catalytic activity of platinum was found to diminish on exposure of the dye solution, that probably due to blocking of its surface by the adsorbed dye. There is some concern regarding the small amount of platinum that might be dissolved in the electrolyte by oxidation and complex formation with iodide,

I^-/triiodide, I_3^-, an example as H_2PtI_6 (Kay & Grätzel, 1996). However, if a tiny amount of platinum dissolves in the electrolyte, it will slowly redeposit on the TiO_2 layer and short circuit would occur by catalyzing triiodide reduction on the photoelectrode.

Rather than platinum, carbon is an interesting low-cost alternative because of the combination of sufficient conductivity and heat resistance as well as corrosion resistance and electrocatalytic activity for triiodide reduction. Carbonaceous materials contain significant features such as high electronic conductivity, corrosion resistance towards triiodide reduction and low cost which are quite attractive to replace platinum. In 1996, Kay et al report an example of the use of the carbon black as a counter electrode that shows the conversion efficiency of 6,7(Kay & Grätzel, 1996). Since then, the carbonaceous materials such as carbon black, graphite, carbon nanotubes and activated carbon are alternated candidates for counter electrode.

Conductive carbon paste (CC) is an electrically conductive printing ink, made up from non-metal conductive carbon particles and thermoplastics resins. After heat curing, the thin film does not easily oxidized and possesses a good corrosion resistance to acid, alkali, and solvent (Gao et al., 2012). Counter electrodes catalytic activity of triiodide reduction as well as the conductivity considerably enhanced by adding about 20% of carbon black (Kay & Grätzel, 1996). Catalytic activity enhances according to the high surface area of carbon black, while the improvement of conductivity results from the partial filling of large pores between the graphite flakes with smaller carbon black aggregates. Excellent performance and low cost of conductive carbon has been widely applied in printed circuit boards and also membrane switches as a burgeoning electronic paste. Carbon black is cheap in industrial mass production and widely used in printing toners and it can be easily sprayed onto FTO substrates but the conductivity is lower compared to highly oriented carbon materials such as graphite and carbon nanotubes.

The comparison of conversion efficiency for carbon black, carbon nanotube and platinum are listed in Table2.5 based on Chen et.al. (J. Z. Chen et al., 2010).

Table 2.5:Parameters of dye-sensitized solar cells for Carbon black counter electrode and Carbon black nanotube counter electrodes (J. Z. Chen et al., 2010)

Electrodes	$\mathbf{V_{oc}}$	$\mathbf{J_{sc}}$ $(\mathbf{mAcm^{-2}})$	FF	$\boldsymbol{\eta}$(%)
Carbon Black	0.71	9.44	0.57	3.97
Carbon Black Nanotube	0.72	12.69	0.61	5.57
Platinum	0.73	12.63	0.67	6.13

From the table 2.5, carbon black shows a comparable performance to Pt with 9.44 $\mathrm{mAcm^{-2}}$current density for carbon black and carbon black nanotube with 12.63$\mathrm{mAcm^{-2}}$ current density. This phenomenon was attributed to the addition of carbon nanotubes whose electric conductivity and surface area are large that not only reduce the electric resistance and facilitate the electron transfer but also increased the activity of the catalytic site. Even though the superior characteristics of carbon nanotubes in DSSCs devices, it was obviously found that the conversion efficiency of CBNT-CE was low (5.57%) compared to the pure platinum (6.13%). Therefore, carbon is one of the potential substitute compared to Pt to achieve the low cost and environmental friendly DSSC for future development in solar cell industry.

CHAPTER 3: MATERIALS AND METHODOLOGY

3.1 Introduction

Chapter 3 covers the explanation and discussion of experiment and characterization sections. The first section provides information about the raw material selection, and type of chemicals that were used in this study. The second section elaborates on the experimental procedure and design of experiments to produce TiO_2 nanocomposite rGO by considering the effect of weight percent, nanocomposite synthesis pH and calcination temperature of TrGO nanocomposite film. The third section emphasized on the DSSCs device efficiency with regards to the photoanode parameters (e.g., TrGO-1 to TrGO-5 for weight content, pH1 to pH5 for synthesis pH values and TrGO-1 450 to TrGO-5 450 (400 ^{o}C – 450 ^{o}C) for different calcination temperature). Then, in the fourth section, a comprehensive experimental work and studies were conducted to optimize the morphological parameters. These studies aim to determine the optimum processing parameters to obtain desired anatase crystalline phase of the best DSSC performance by improving the facilitate charge carriers separation as well as photovoltaic chacrateristics. The last section in this chapter outlines the characterization of structural, morphological, optical, electronic and electrochemical properties of the DSSC using various techniques, such as FESEM, EDX, TEM, XRD, Raman, FTIR, Uv-Vis, Uv-DRS (tauc plot) and PL analysis. This covers a brief explanation on the characterization equipment, operating principles and sample preparation.

3.2 Materials

Table 3.1 listed the chemical that used in this project. The chemicals were purchased from Sigma Aldrich, Merck Milipore, Dyesol and R&M Chemical.

Table 1.1: Chemical List

Chemicals	**Chemical Formula**	**Supplier**	**Purity**	**Functions**
Titanium (IV) Isopropoxide	TTIP	Aldrich	97%	Titanium precursor
Ethanol (Ethyl Alcohol)	EtOH	R&M	95%	Solution
Ethanol (Ethyl Alcohol)	EtOH	R&M	99%	Solution
Hydrochloric Acid	HCl	R&M	37%	Buffer Solution
Pluronic F127	F127	Aldrich	-	Polymer Co-block
Natural graphite powder (<20μm)	C	Aldrich	-	Graphene raw material
Analytical sulphuric acid	H_2SO_4	R&M	95-98%	Synthesis solution
Potassium permanganate	$KmNO_4$	Merck	-	
Hydrogen peroxide	H_2O_2	Merck	30%	Etch
Hydrazine solution		Aldrich	37%	Reducing solution
Phosphoric acid	H_3PO_4	R&M	85%	Synthesis solution
Fluorine tin oxide conducting glass slide	FTO	Aldrich	7Ω/sq	Anode/cathode glass
Triton X-100	-	Aldrich	-	Binding solution
Ruthenizer 535-bis TBA	N719	Aldrich	0.5mM	Commercial Dye
Electrolyte EL-HPE	KI	Dyesol	-	DSSC electrolyte
Mulberry	-	-	-	Raw anthocyanin
Pandan leaves	-	-	-	Raw chlorophyll

3.3 Experimental Methodology

3.3.1 Synthesis of Titanium Dioxide (TiO_2)

For this project, TiO_2 nanoparticle was synthesized using sol precipitation technique. 0.25g of pulronic F127 was added into the mixture solution of ethanol and deioinized water. The oxidizing solution pH was adjusted with hydrochloric acid (HCl) until the solution pH becomes 3.5. Then, 11mL of titanium (IV) isopropoxide (TTIP) 97% was diluted with 12ml of ethanol and dropped in the oxidizing solution under constant stirring (300rpm). The sol was aging at 60 ^{o}C for 16hours. The sol was collected by centrifugation (7000rpm) and washed several times until it reaches pH 7. The nanoparticle sol was dried at 80 ^{o}C in an oven to obtain the nanopowder. Lastly, TiO_2 nanoparticle was calcined at 400 ^{o}C to increase the crystallization of TiO_2 nanoparticle.

3.3.2 Synthesis of graphene oxide (GO) & reduced graphene oxide (rGO)

The GO was synthesized by simplified Hummers method using natural graphite flakes as starting material. The conversion of graphite flakes to GO achieved by treating graphite flakes in a mixture of phosphoric acid (H_3PO_4) /sulfuric acid (H_2SO_4) and potassium permanganate ($KMnO_4$). This solution will be stirred for 3 days at room temperature. The resultant graphene oxide (GO) suspension obtained from the centrifuge process and dried in the oven at 100 ˚C in order to form a homogenous GO dispersion. The pH of the homogenous GO suspension was adjusted by ammonia solution up to pH 10. Then, the GO dispersion incorporates as reducing agent of hydrazine monohydrate ($H_4N_2{\bullet}H_2O$: GO= 1:2 in weight) to produce a black rGO dispersion. The precipitate was filtered and dried in 60 ^{as} to produce reduced graphene oxide (rGO).

3.3.3 Synthesis of titanium dioxide nanocomposite reduced graphene oxide (TiO2-rGO)

The synthesized method was similar to the TiO_2 procedure, but with the addition of rGO powder into the oxidizing solution. Variable parameters were being optimized such as precipitating agent concentration, weight of rGO, final pH of sol and calcination temperature were studied to obtain the best nanoparticle properties to obtain the desired properties to elevate the DSSCs performance in terms of enhancement of photovoltaic characteristics and electron transport against the device. The weights of rGO were varied 0.01g, 0.02g, 0.03g, 0.04g and 0.05g into the nanocomposite. Meanwhile, for pH of the sol was varied from pH 1, pH 2, pH 3, pH4 and pH5. The reason for the pH range in acidic condition was due to TiO_2 anatase phase of shows high photocatalytic actives works the best in acidic condition where the crystalline forms in anatase phase. The calcination temperature (eg; 400 ^oC and 450 ^oC) determines the crystallinity (the nanocomposite maintain in anatase phase without any rutile in the composition of crystal) of the nanocomposite without oxidizing the rGO from the nanocomposite. The best nanocomposites were determined by the performance of DSSC and EIS analysis.

3.3.4 Extraction of natural dye

For this project, the natural dyes used are from the natural sources and extracted by using soxhlet extraction method. The natural dye that used was pandanus amaryllifolius (*pandan* leaves) and morus plant (mulberry fruits). Both of plants were weight to 10g and was cuts into small pieces. The crude were wrap with a piece of cotton cloth and inserted in soxhlet column. A quantity of 250ml of ethanol was used as the solvent for the soxhlet system. The soxhlet was let run overnight to extract all the dye pigment. The collected dye pigment was placed in a rotary evaporator to make it into gel form before use as dye-sensitizer.

3.3.5 Preparation of conventional N719 dye

Ruthenizer 535-bis TBA was used as the conventional N719 dye. The dye was purchased from Sigma Aldrich and the powder was diluted. The N719 was diluted using ethanol 99.5% into 0.5mM dye solution. The diluted dye was freshly prepared (Fig. 3.1) and used to soak the photoanode to provide more electrons in the semiconductor surface.

Figure 3.1: (a) N719 commercialize dye, (b) natural green chlorophyll dye, and (c) red anthocyanin dye.

3.3.6 Preparation of TiO_2 and TiO_2 nanocomposite rGO paste

The whole project was summarized in the flowchart Fig.3.2. Fluorine-doped tin oxide covered glass (FTO) were employed as the substrate for the semiconductor oxide photoanode. FTO glass was soaked in acetone and cleaned in ultrasonic bath for 15 minutes to remove any contaminant from the surface. Then, the glass was rinsed with

DI water and ethanol 95%. The FTO glass was blown with nitrogen to dye. For the paste preparation, 2.0g of the semiconductor oxide powder (TiO_2 or TiO_2 nanocomposite rGO) was diluted with 10ml of absolute ethanol and stirred at room temperature for 1 hour and sonicated for 30 minutes until its formed homogeneous suspension. Then, a drop of Triton-100 was added to the solution. A tape with 10µm thickness was used to make a $1cm^2$ squared area in the middle ad placed on the conductive side of the glass. The photoanode electrode was fabricated on the FTO glass by using Doctor Blade technique, dried at room temperature for about 30 min and placed on a hotplate at 100 ^{o}C for 10 minutes. The semiconductor oxides were subjected to the final thermal sintering process at 450 ^{o}C for 30 minutes to remove any organic substance.

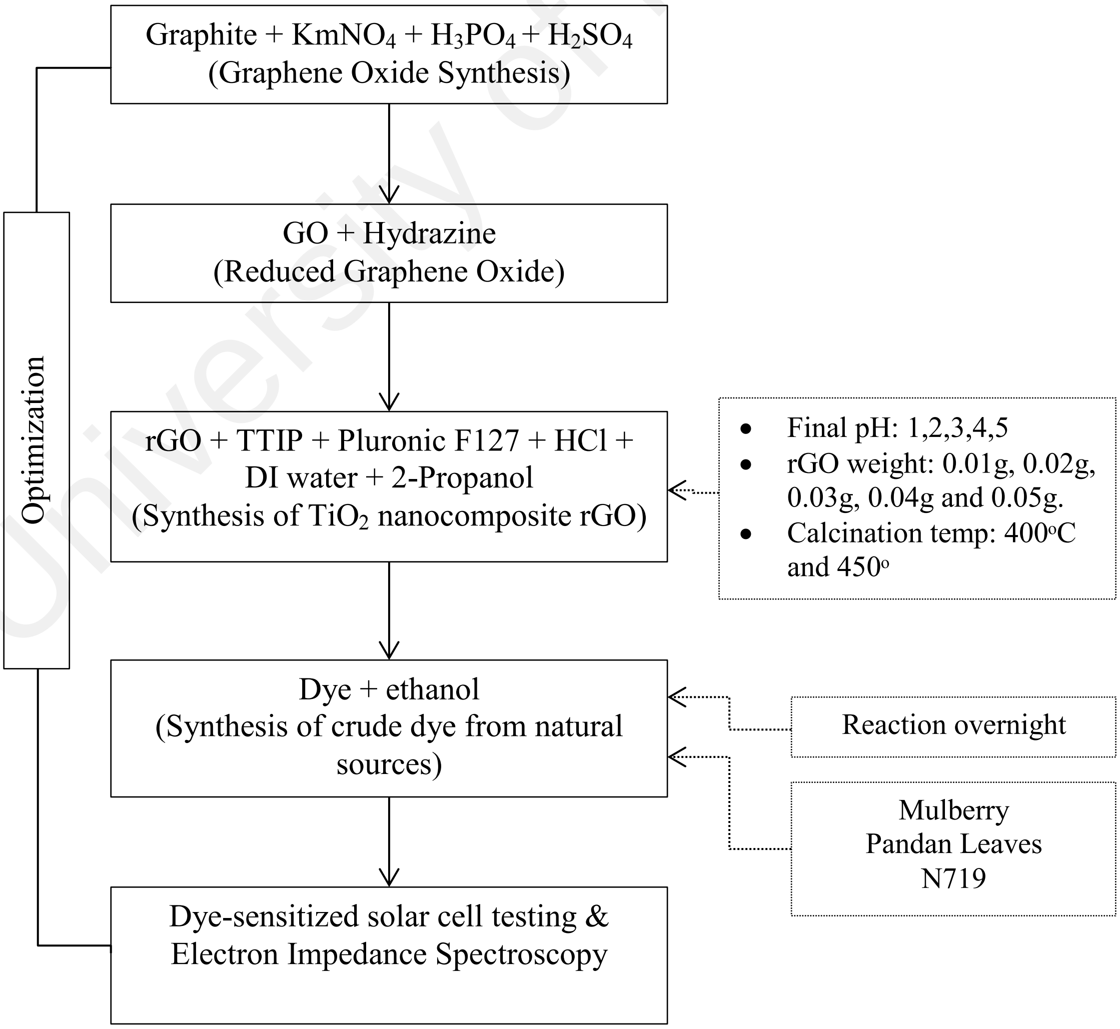

Figure 3.2: Flowchart of synthesis of TiO_2 nanocomposite rGO and the DSSCs testing

3.3.7 Assembling process for dye-sensitized solar cell device.

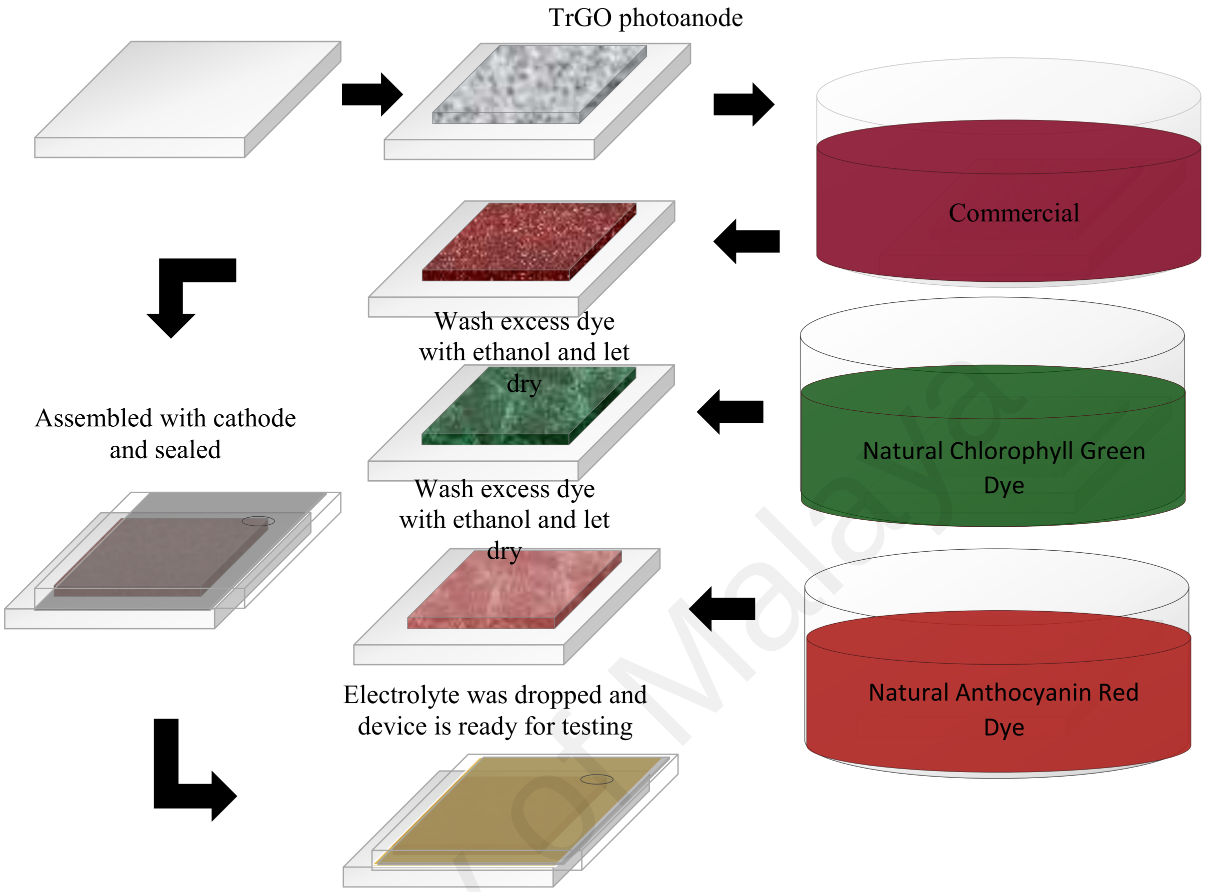

Figure 3.3: Illustration of DSSC assembling method.

The assembling process was simplified in Fig 3.3 to illustrate the whole process to assemble the electrode into the solar cell device. Accordingly, the semiconductor oxide photoanode that was sensitized by soaking the aforementioned electrodes in the dye solution containing 0.5mM N719, natural anthocyanin dye and natural chlorophyll dye overnight. Then, the photoanodes were rinsed with ethanol to remove unabsorbed molecule from the surface and dried. Next, the DSSC was assembled by sandwiching the dye sensitized photoanode and carbon counter electrode. The device was sealed with sealant to prevent any leaking of electrolyte when the device is under testing. After the sealing process, DSSCs were introduced with 6.0µL EL-HPE electrolyte (dyesol) between the electrodes. The device then undergo charaterization of DSSCs current density-voltage (*J*-V) characteristics measured under AM 1,5 stimulated illumination with a power density of 100mW/cm^2.

3.3.8 Characterizations of TiO_2 nanocomposite rGO

All the samples that were prepared in the experimental works were characterized accordingly. The structural, morphological, optical, chemical, electronic properties of TiO_2 nancomposite rGO were characterized via various characterization techniques. The characterization methods used in this experiment are X-Ray Diffraction (XRD), Fourier Transform Infrared Spectroscopy (FTIR), Raman Spectroscopy, Photoluminescence Spectroscopy (PL), High Resolution Transmission Electron Microscopy (HRTEM), Field Emission Scanning Microscopy (FESEM), Uv-Vis Spectroscopy for the dye used in the DSSCs and Uv-Diffuse Reflection Spectroscopy (Uv-DRS). In this section, information on the characterization technique, basic principle and sample preparation of such analytical equipment are discussed briefly.

3.3.8.1 X-Ray Diffraction (XRD)

X-Ray Diffraction (XRD) analysis was used to investigate the crystallographic structure and phase of TiO_2 nanocomposite rGO. XRD analyse were carried out using Bruker D8 Advance diffractometer equipped with a quartz mono-chromator and Cu Kα radiation (λ=0.154059 nm). XRD analysis provides information on crystallographic structures, phase transition, and unit cell parameters. The information can be interpreted using XRD pattern and then analyzed through the EVA software and X'Pert Highscore Plus V software. For sample preparation, photoanode with dimension (10 mm x 10 mm) was place onto a specimen holder and then placed in the rotating unit stage of diffractometer system. The data were collected within 2θ of 10° to 90° with a step size of 0.034° at scan time 71.6 sec. The XRD was measured using semiconductor oxide was fabricated on FTO glass and the sample was placed on the sample holder. The testing provides information on structures phase crystalline orientation and structural parameters as crystallinity, strain (phase), the average grain size and crystal defects. The scan rate for the analysis was 0.02deg/sec and a step size of 0.02 degrees. The sample was scanned from 10° until 90° with diffraction angle of 2θ. From the obtained XRD results, the crystallite size can be determined by using Debye Scherrer's equation (refer Equation 3.1)

$$D = \frac{K\lambda}{\beta \cos\theta} \qquad \textbf{(Equation 3.1)}$$

Where D referred to the mean diameter of the ordered domains, K defined as a sharp factor with a value close to unity, λ is the X-ray wavelength, β represent the line boardening at half maximum intensity (FWHM) and θ is the Bragg angle. The estimation of the nanoparticle size can be obtained by the Debye-Scherre equation.

3.3.8.2 Fourier Transform Infrared Spectroscopy (FITR)

Fourier Transform Infrared (FTIR) spectroscopy is a powerful testing to analyzed the molecular absorption and transmission which used to determine the TiO_2 functional group, presence of rGO functional groups and the functional group that links in theTiO_2 nanocomposite rGO. The FTIR was recorded at 400 cm^{-1} until 4000 cm^{-1} range at resolution of 4 cm^{-1}. By using FTIR spectra, IR radiation was absorbed by the sample and some of it passed via transmission. The testing was useful to determine the due to the Ti-O-Ti and Ti-O-C starching and bending vibration for each phase.

3.3.8.3 Raman Spectroscopy

Raman spectroscopy is a powerful technique to determine the molecular vibration on chemical structure, sample identification and quantitation. This test is crucial for the identification of rGO in the nanocomposite. Raman spectra of samples were collected using Renshaw inVia Raman microscope with He Cd laser source [laser excitation source (k = 514.0nm) at room temperature. The frequency range for raman spectroscopy was 100-3000 cm^{-1}. To obtain Raman spectra, 0.05g of TiO_2 nanocomposite rGO was placed into the sample holder and 1 percent of 0.2 mV laser power with 180 second exposure time was chosen. The obtained Raman spectra showed the different phase, presence of rGO band (D & G band) and the I_d/I_g the intensity ratio of rGO to determine the defect in nanocomposite was determined.

3.3.8.4 Photoluminescence Spectroscopy (PL)

Photoluminescence is a derivation from Raman spectroscopy that function to analyze the absorption or emission process between different electronic transition energy levels in a material which is a powerful tool to support Raman data. For this project, the PL spectroscopy was analyzed using Renshaw inVia confocal raman spectroscopy. The PL testing was obtained by placing 0.05g of the nanocomposite powder on the microscope glass slid. The glass slid was placed in the sample holder and the sample was analyzed with He Cd laser source with laser excitation source of 514.0 nm. Electron transition energy in a material and what are the improvements in the electron transport against the material especially semiconductor oxide. The effect of disordered in a material can be analyzed using PL where it provides information of lattice disorder due to chemical composition.

3.3.8.5 Field Emission Scanning Microscopy (FESEM)

The morphology of semiconductor oxide nanocomposite was investigated by using Field Emission Scanning Microscopy (FESEM). FESEM can visualize tiny topographic details on the surface or entire objects. FESEM that used in this research was HITACHI SU 8030. For FESEM, the surface of photoanode semiconductor oxide was analyzed. Sample preparation is important factor to obtain a better resolution micrograph. The photoanode were cut into desired size (5 mm x 5 mm) and place on the sample stage using a carbon tape. In the present study, morphological conditions of the TrGO were characterized at working distances down to 1 mm and extended accelerating voltage ranging from 30 kV down to 100 V. In this case, InLens SE detector was used for the morphological examination due to the higher magnification image with improving spatial resolution and minimizes sample charge charging could be achieved. The geometrical dimension of the nanotube arrays was conducted by taking the average dimension from eight different spots in the sample. The magnification of 10 kX, 30 kX and 50 kX were selected for the detailed characterization.

3.3.8.6 High Resolution Transmission Electron Microscopy (HRTEM)

The morphological and particle imaging was obtained by high resolution transmission electron microscope (HRTEM). The HRTEM analysis was carried out by Jeol JEM- 2100F instrument with accelerating voltage of 200kV to visualize the morphological of the particle of nanocomposite semiconductor oxide. HRTEM was known as powerful characterization tools for nanoparticle where we can confirm the particle in the nano size state and the particle phase can be obtained by HRTEM. Moreover, the determination of material characterization was obtained from the radiation beam produced by electrons accelerated on the sample and HRTEM could extend high magnification up to 1.6 times magnification to observe tiny particle and lattice-fringe spacing. The sample was prepared by dispersed TiO_2 nanocomposite RGO particle in ethanol (95%) and sonicated for 1 hour. The sample was dropped on a 300 mesh, copper grid and left to dry for 5 days before running the HRTEM tests. The copper grid was placed into HRTEM sample holder before inserting into the HRTEM. The image of the TiO_2 nanocomposite RGO nanoparticle was selected and taken at 50000, 100000, 200000 and 800000times magnification. The image that produced was analyzed using a J - image. By using the information that measured in J-image, the particle size distribution was plotted and the lattice-fringe spacing was used to support XRD information.

3.3.8.7 Uv-Vis Spectrophotometer

Uv-Vis that use in this research was Cary 60 UV–visible (UV-Vis) to obtain the absorption spectroscopy for the semiconductor oxide photoanode film and the absorption spectra of dye-sensitized. For the semiconductor oxide film, the sample was clipped to the sample holder. The sample was tested with 200 – 800 nm absorption wavelengths. The semiconductor oxide film was colored because electron in the metal atoms can be excited from one electronic state to another and it effected the presence of ligands in the material. For characterization of dye, the dye was diluted with ethanol to 6mMol^{-1} and filled in the cuvette of Uv-Vis. The cuvette was placed in the sample holder and tested with absorption wavelength 400 – 800 nm. The organic compound is able to absorb light in either UV or visible region due to the pigment that exist in the dye. The pH and solvents affect the absorption of organic compound.

3.3.8.8 Uv-Diffuse Reflection Spectroscopy (Uv-DRS)

Uv-Diffuse Reflection Spectroscopy (Uv-DRS) was used to obtain the reflectance spectroscopy of the semiconductor oxide. It is similar with Uv-Vis spectroscopy which only measures the relative change of transmission of light that passes through the sample while the Uv-DRS measures the relative change in amount of reflected light on a surface. Furthermore, the tauc plot that represents the band gap of the material can be derived from the Uv-DRS

3.3.9 Characterizations of DSSCs devices.

The performance of the semiconductor oxide was tested when it is fabricated as photoanode and assembled as DSSCs. The performance each DSSCs represent the performance of semiconductor and dye when assembled as a device. The electron travels in the device were the main concern as it involves the effectiveness of the semiconductor oxide photoanode and dye working together as a device. The characterization method used were Photoelectrochemical analysis and Electron Impedance Spectroscopy (EIS).

3.3.9.1 Photoelectrochemical analysis

Photoelectrochemical analysis was the most crucial testing in this research. The overall performance of the nanocomposite semiconductor oxide photoanode and dye-sensitizer that assembled into a DSSC device was tested using Metrohm Autolab (PGSTAT100 N). The current density –voltage (*J-V*) characteristics of DSSCs were measured under the illumination of AM 1.5 condition (Newport 91,160, 300 W xenon lamp, USA) with a power density of 100mW/cm^2. The anode and cathode DSSC was connected to the Autolab and the DSSCs liner sweep voltammetry (LSV) was performed. From the analysis, voltage open circuit (Voc), current short circuit (Jsc), fill factor (*ff*) and efficiency (ŋ%) were obtained which represent the photovoltaic properties of DSSC. The equation 3.2 shows the calcutaion for Fill Factor (FF) and equation 3.3 shows photovoltaic efficiency, ŋ%:

$$FF = P_{max} / I_{sc}V_{oc} \qquad \text{(Equation 3.2)}$$

$$ŋ = V_{oc}\, I_{sc}\, FF / P_{in.} \qquad \text{(Equation 3.3)}$$

3.3.9.2 Electron Impedance Spectroscopy (EIS)

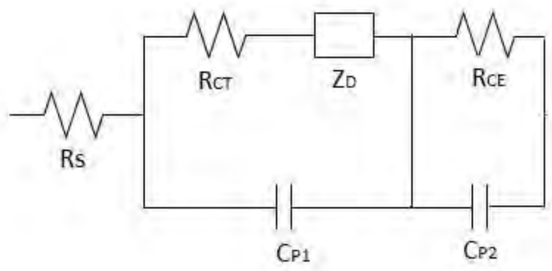

Figure 3.4: Schematic diagram of DSSCs structure that fitting into resistance, capacitance and nyquist.

Electron Impedance Spectroscopy (EIS) is one of powerful tools for semiconductor oxide and photovoltaic testing due to it provides information of interface resistance of DSSC, electron movements in the device and recombination across the device. The EIS analysis of DSSCs was conducted using a Methohm Autolab with frequency range from 0.1 Hz to 100 kHz at the amplitude of 20mV and under open circuit conditions with 100mW/cm^2 irradiation. The EIS uses a simulated model of the internal circuit (Fig. 3.4) of DSSC to identify the resistance of electron charge between each surface material. The EIS analysis will generate a Nyquist plot and Bode plot. The nyquist plot offers a 3 semicircle that represents the series resistance (R_s), the charge transfer resistance between counter electrode/electrolyte (R_{CE}), low frequency resistance towards resistance and the interface hindrance characteristics redox I^{-3}/I^- electrolyte and charge transfer between the intact of photoanode/dye/electrolyte (R_{CT}). The semicircle will be fitted with the internal circuit module to get the value of resistance. Meanwhile, Bode Plot represent the electron lifetime of electronics transfer and recombination of the electron hole in DSScs photoanode-electrolyte interface. By using f_{max} the peak frequency of bode phase, the electron lifetime (τ_n) was obtained from the peak angular frequency using (equation 3.4):

$$\tau_n = \frac{1}{2}\pi f_{max} \qquad \text{(Equation 3.4)}$$

CHAPTER 4: RESULTS AND DISCUSSION

4.1 Introduction to Results

Results and discussion were divided into 4 parts where each part represents the results of each experimental parameter. Each part discussed on the material morphological testing, DSSC performance and EIS performance to evaluate the overall performance of semiconductor oxide and dye performance of the DSSC application. The first parameter was DSSC performance on weight percent of rGO content on rGO nanocomposite TiO_2. The second parameter was the discussion for result DSSC performance on different synthesis pH on the highest rGO content nanocomposite. Moreover, the calcination temperature was tested to obtain either 400^{o}C or 450^{o}C to obtain anatase phase. Lastly, the aging time was tested to obtain the most optimum time for TiO_2 crystal grow on rGO and being tested with DSSC performance.

4.2 Different Weight Content for rGO nanocompositeTiO_2 DSSCs

Different weight contents of rGO and TiO_2 were used in this parameter to achieve the best one step synthesis of TiO_2/rGO (TrGO) composite. Anatase phase crystalline structure of TrGO was the aim in this experiment due to anatase phase was reported as one of the best crystalline structure photoanode film which it is more stable for electron transfer. This characteristic is needed for natural dye to efficiently perform in the device. For this experiment, we are dividing it into two parts which is the photoanode morphology testing and the second one is the DSSCs device performance. The electron lifetime also presented to strengthen the recommendation in this experiment.

4.2.1 Morphological characterization for TrGO different weight.

Fig. 4.1 exhibits the XRD patterns of TiO_2 and TrGO nanocomposites (TrGO-1, TrGO-2, TrgO-3, TrGO-4 and TrGO-5) and to ensure the crystallographic phase. From

Fig.4.1, all (TiO_2 and TrGO) the diffraction peaks can be satisfactorily indexed to anatase. The diffraction spectra for TiO_2 showed peaks of anatase at $2\theta = 25.36^0$, 37.90^0, 48.16^0, 54.05^0, 55.21^0, 62.87^0, 68.98^0, 70.479^0 and 75.28^0 correspond to the (101), (103), (004), (200), (105), (211), (204), (116), (220) and (215) diffraction planes respectively. The TrGO nanocomposites XRD spectra did not show any changes from TiO_2 either. This is presumable by small amount of rGO in the nanocomposites and the rGO peak was overlap due to broad spectrum of rGO at 24^0. For TrGO-5, the peak become more border than all other samples due to less crystallinity characteristics showed in the TrGO-5 sample due to excess of graphene content (Cheng & Stadler, 2015; How, Pandikumar, Ming, & Ngee, 2014; Ling et al., 2013).

From the XRD pattern, TiO_2 and TrGO-3 shows the highest crystallinity due to sharp and intense peak at 25^o peak. The Debye Scherrer Equation has been employed to estimate the average particle size of TiO_2 that synthesized. Only major peak were considered in this experiment. The particle size was estimated at 23 nm for TiO_2, 21nm for TrGO-1, 18 nm for TrGO-2, 15nm for TrGO-3 19 nm for TrGO-4 and 22.6 nm for TrGO-5. This shows that the anchoring of rGO does gives a little influence on the crystallinity and crystallite size of TrGO nanocomposite.

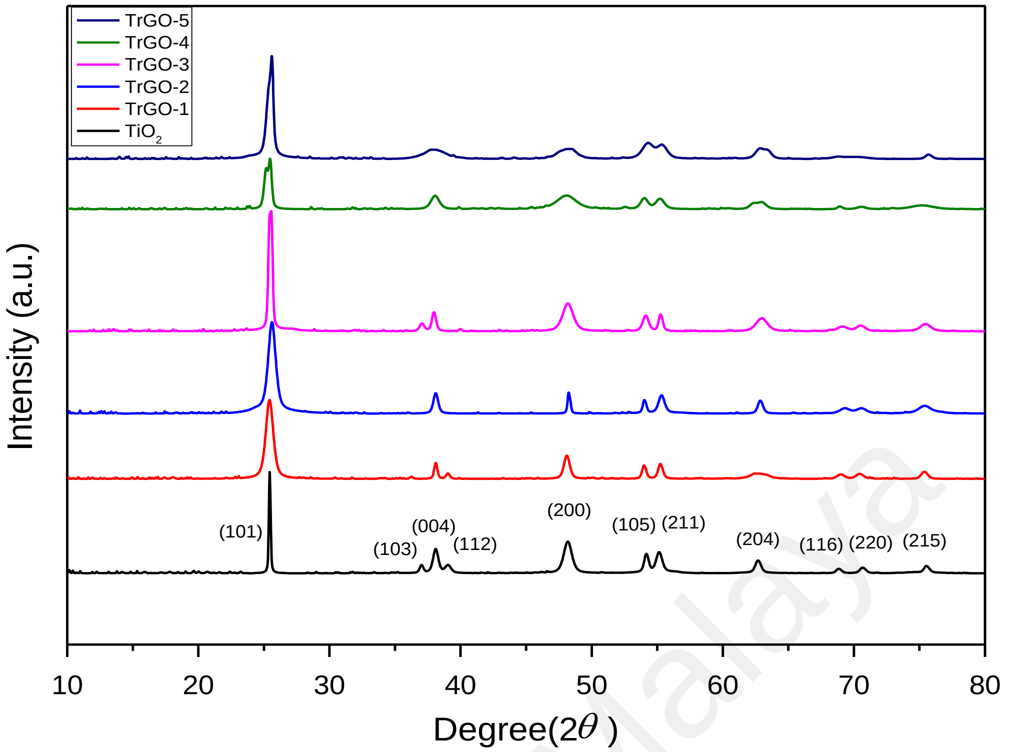

Figure 4.1: X-Ray diffraction (XRD) spectra of pure TiO_2, TrGO-1, TrGO-2, TrGO-3, TrGO-4 and TrGO-5.

FTIR spectroscopy was used in the present study to evaluate the functional groups on TrGO and pure TiO_2. As illustrated in Fig. 4.2, both TiO_2 and TrGO showed a broad band below 1000cm^{-1}, implying Ti-O-Ti and Ti-O-C stretching vibrations within the molecules, respectively (Karimi, Yazdanshenas, Khajavi, Rashidi, & Mirjalili, 2014; Nithya, Rokesh, & Jothivenkatachalam; Yu, Zhang, Zheng, & Zhao, 2003). It was also noted that the stretching peak of C-O at about 1084 cm^{-1}, which appeared in pure TiO_2, disappeared in the TrGO nanocomposites. From Fig. 4.2, it was also observed that TrGO nanocomposite exhibited some characteristic peaks which could be assigned to the C=C stretching (1541 cm^{-1}), C=O stretching (1695 cm^{-1}) and –OH stretching (3440 cm^{-1}) (Karimi et al., 2014). There was also a strong peak located at 2357cm^{-1} assigned to the CO_2 contamination (Zhang, Yuan, & Lu, 2014). Also, as displayed in Fig. 4.2, there were peaks in the region between 3600 and 3900 cm^{-1} corresponding to the formation of oxygen vacancies induced by the formation of Ti^{3+} species (Samsudin, Hamid, Juan, Basirun, & Kandjani, 2015), while the peaks at 3724 and 3845 cm^{-1} were attributed to the Ti^{3+}-OH formation. Moreover, the peak at 3674 cm^{-1} corresponded to the Ti^{4+} in the TiO_2.

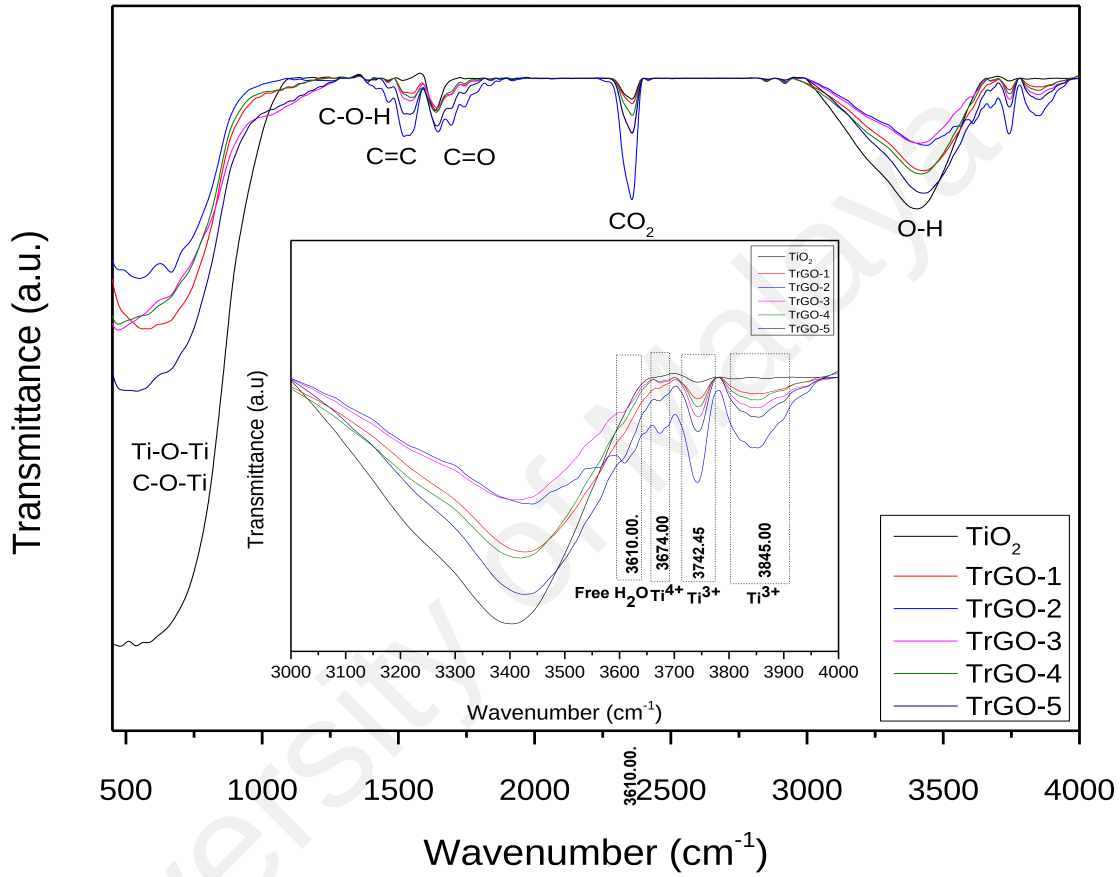

Figure 4.2: Fourier Transform Infrared (FTIR) spectra of pure TiO_2, TrGO-1, TrGO-2, TrGO-3, TrGO-4 and TrGO-5.

Raman spectroscopy was employed in the present study to characterize the structural properties of the graphene materials. Fig. 4.3 shows the Raman spectra of pure TiO_2 and TrGO. It is clear that both the TiO_2 and TrGO possessed the anatase phase consisting of five major vibration peaks at 144 cm^{-1} (E_g), 197 cm^{-1} (E_g), 395 cm^{-1} (B_{1b}), 513 cm^{-1} (A_{1b}), and 635cm^{-1} (E_g). This is in line with the finding reported by Otakar et al. (Frank et al., 2012).

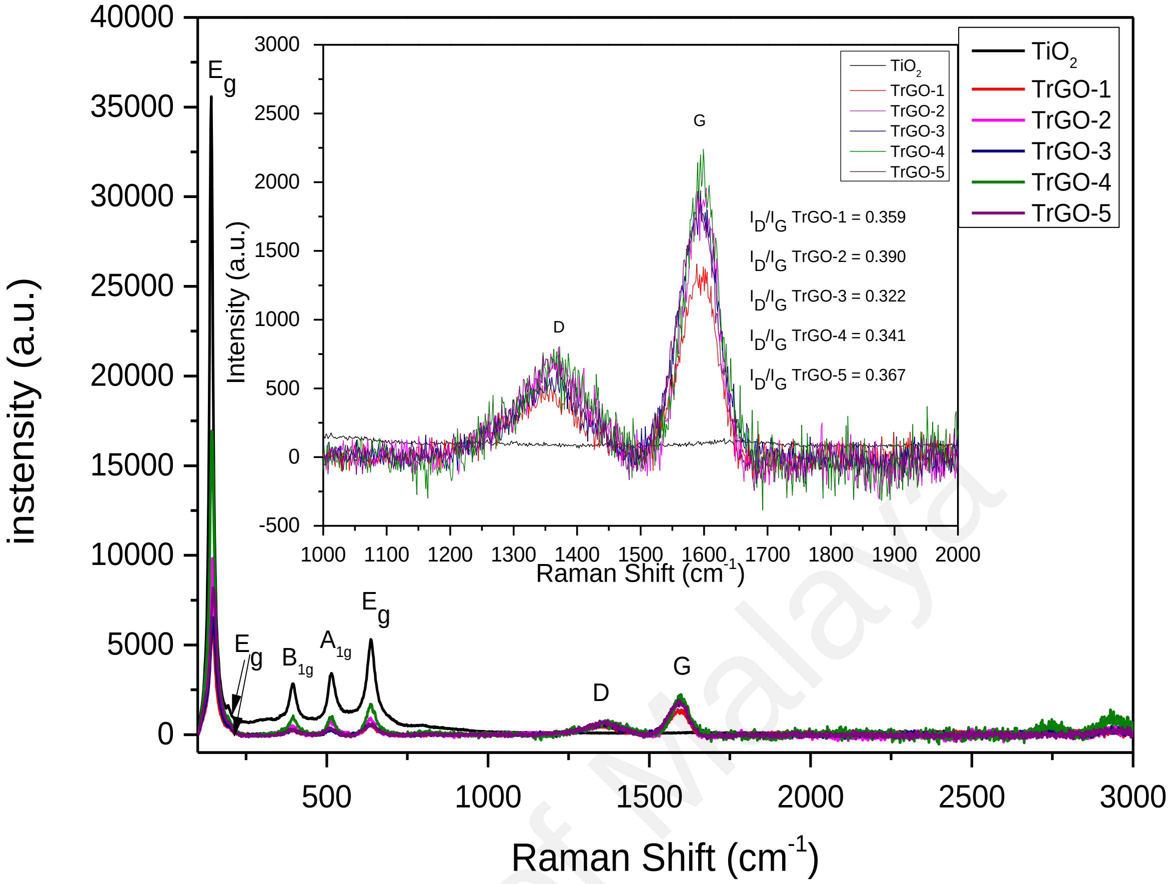

Figure 4.3: Raman spectroscopy of TiO_2, TrGO-1, TrGO-2, TrGO-3 TrGO-4 and TrGO-5.

Also, it is noteworthy that TrGO showed two broad vibration bands within 1200-1700 cm^{-1}, in which the D band (attributed to the breathing mode of A_{1g} symmetry involving phonons near the K zone boundary) appeared at 1309 cm^{-1}, while the G band (originates from sp^2 in-plane vibration mode of carbon atoms) at 1583cm^{-1}. As reported by Ahmed et al. (Ahmad, McCarthy, Baranov, & Gun'ko, 2015), the intensity ratio of D and G bands(I_D/I_G) could represent the structure, defects and size of the graphene. Correspondingly, I_D/I_G of TrGO sample is in between 0.32 to 0.39 and the lowest intensity ratio was TrGO-3 with 0.32. The intsity ratio for nanocompsite indicate most all of the sample suggesting a low level of defect, high crystallinity and small size of rGO in TrGO especially TrGO-3. Additionally, as displayed in Fig. 4.3, Raman 2D band at about 2600 cm^{-1} was detected in TrGO-1 implying the presence of aggregates of some rGO layers in the nanocomposites which might be associated with the restacking of rGO layers during the synthesis process (Amara, Latil, Meunier, Lambin, & Charlier, 2007). The Raman band shifts and broadening in E_g mode (144 cm^{-1}) was also observed in Fig. 4.3. One possible explanation (Samsudin et al., 2015), reported that the peak shifts and broadening might originate from the surface defects such as the presence of oxygen vacancy and peak broadening which roughly show pools of oxygen vacancies.

The PL spectrum was used to identify the behaviour of photo-generated electron and holes in the semiconductor layer of DSSCs. Fig. 4.4 shows the PL spectra of TiO_2 and TrGO nano-composites. The presence of PL peaks in the wavelength range of 450-750nm indicated that TiO_2 and TrGO nanocomposites are the indirect band gap semiconductors.

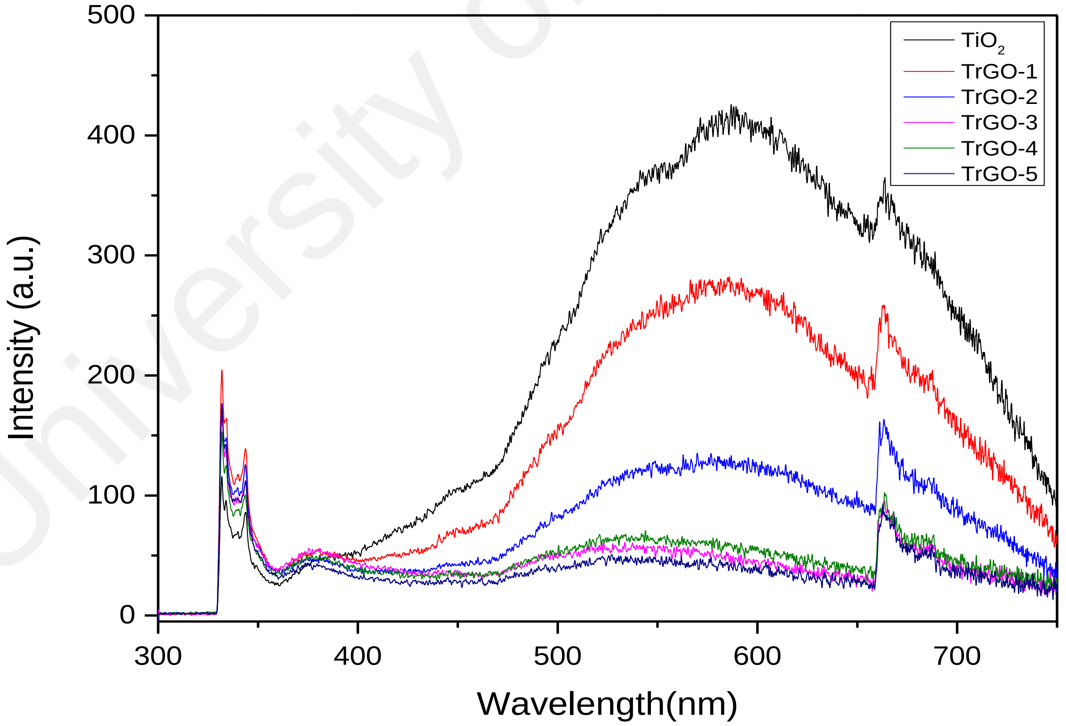

Figure 4.4: Photoluminescence (PL) spectra of pure TiO_2; TrGO-1; TrGO-2; TrGO-3; TrGO-4 and TrGO-5.

It was also determined that the presence of a peak near 330nm was mainly attributed to the ligand to metal charge transfer in TiO_2 (O^{2-} to Ti^{4+}), while the peaks at 380nm, 450nm and 660nm signified the surface oxygen vacancy related defects. Furthermore, all peaks were blue shifted in the Raman peak. This implies the transformation of un-coordinated Ti^{3+} ions to the surface of oxygen vacancy. The green band with peak position at 540nm was also an indication of the surface oxygen vacancy of anatase (101) phase.

According to Liu et al. [19], the red shift of the PL spectra between 600 and 620 nm is attributed to the oxygen-vacancy-related defects as a result of the oxygen atom removal by annealing in an inert argon atmosphere where the removal of the oxygen atom will create electron traps under the conduction band. Specifically, the electron traps usually locate at 0.7 to 1.6 eV below the conduction band edge energy. Ti^{4+} will be reduced to Ti^{3+}considering the removal of oxygen atom can create lone pair of electrons (Jin, Liu, Lei, & Sun, 2015). Furthermore, as shown in Fig. 4.4, pure TiO_2 photoanode displayed higher PL intensity compared to that of TrGO samples. The reduced intensity of PL spectra was in concomitant to the decrease of the weight percent of TiO_2 in the nanocomposite since the PL intensity was mainly influenced by the recombination rate of electron-hole pairs. It has also been reported in literatures that a lower intensity of PL spectra implied an increase in charge separation and a decrease in the rate of electron-hole pair recombination (Gupta, Desai, Jha, Sahoo, & Kirin, 2010; Min et al., 2012; Raghavan, Thangavel, & Venugopal, 2015).

Fig. 4.5 displays the absorption spectra of pure TiO_2 and TrGO-based nanocomposites. Correspondingly, these spectra give the information regarding to the absorption ability of the photoanode and the bandgap of the anatase semiconductor oxide film. From the Uv-Vis spectra, it shows that the intense transition tabulates

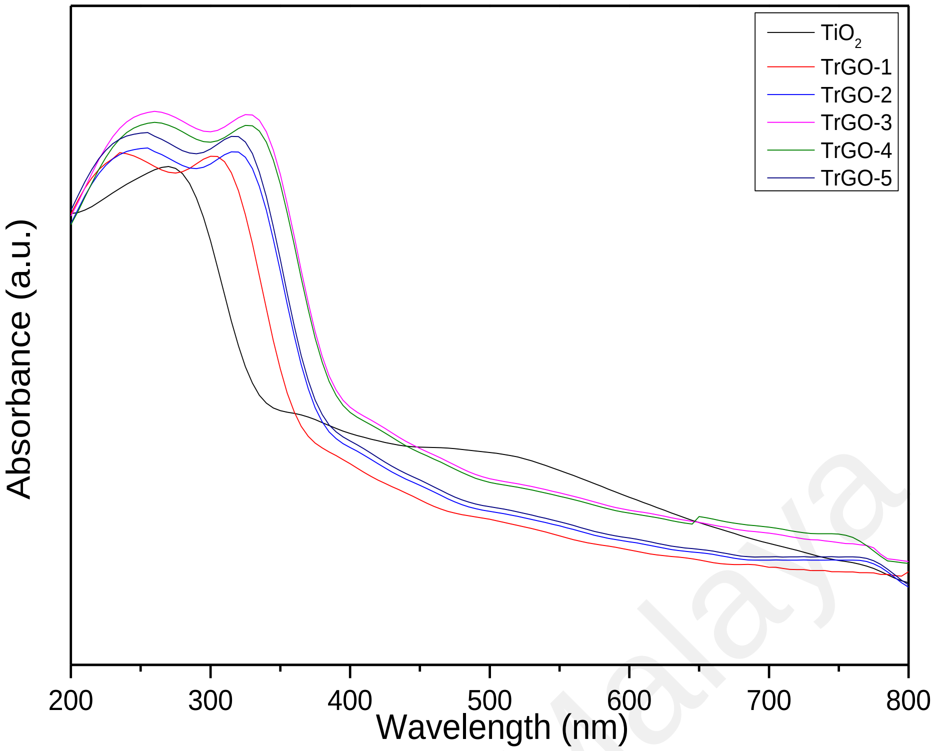

Figure 4.5: Absorption plot of pure TiO_2; TrGO-1; TrGO-2, TrGO-3, TrGO-4 and TrGO-5.

the intrinsic band gap absorption of samples where the electron transited from the valence band (VB) into the conduction band (CB) (O2p-Ti3d). It is noteworthy that the optical absorbance spectrums of all the films was in the range of ~300nm to 430nm. The photon absorption spectrum ability in TrGO was also determined to be higher than that of those pure TiO_2 due to the peak shift towards the blue region. The blue shifting of the absorbance spectra also gives us a hint that the crystalline size of TrGO was smaller than that of TiO_2.

Fig. 4.6 shows the Tauc plot, while Table 4.1 tabulates the energy band gap (from the UV spectra) of pure TiO_2 and TrGO films. It was found that, based on Table 4.1, the optical energy band gap show decrease in energy band gap compared to TrGO samples. The pattern of decrease in energy band gap in TrGO shows a bell pattern where the sample decrease until TrGO-3 but increase a little bit starting on TrGO-4 and obviously on TrGO-5. The smallest band gap was detected to be approximately 2.84eV (TrGO-3). The reduction of band gap was mainly attributed to the enhancement of electron movement to the conduction band induced by rGO in the nanocomposite. The band gap reduction mainly due to TiO_2 nanoparticles acted as potential dopants to create an impurity energy level within the valence band (VB) and conduction band (CB) (O2p – Ti3d). This conclude that TrGO photoanodethe higher visible absorbance and resultant its CB and VB closer to the Fermi level compared to TiO_2 photoanode.

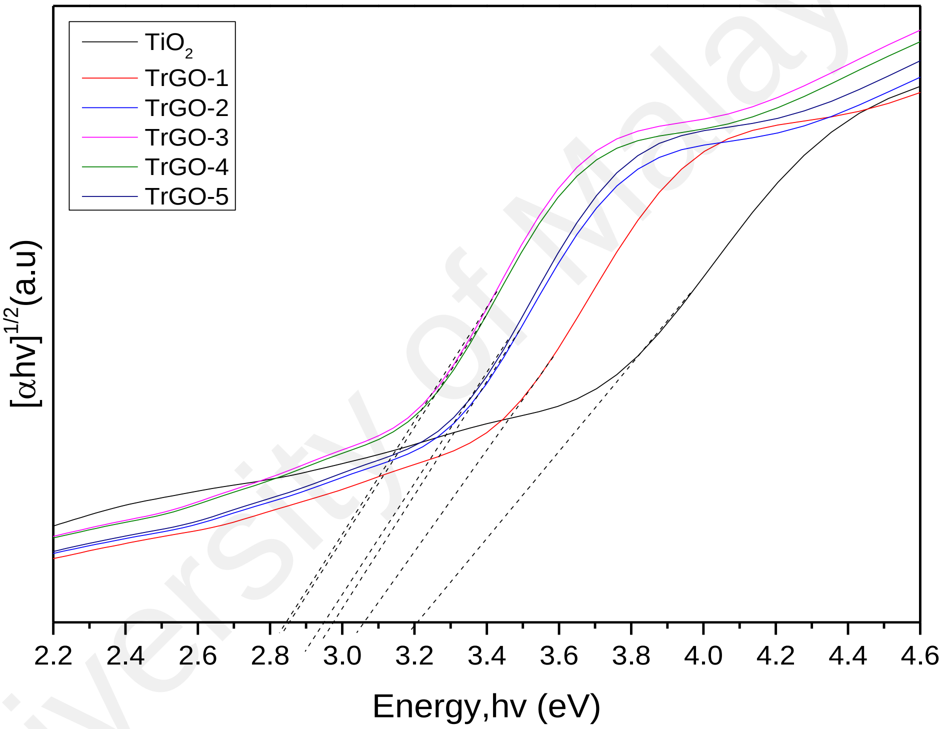

Figure 4.6: Tauc Plot of pure TiO_2; TrGO-1; TrGO-2, TrGO-3, TrGO-4 and TrGO-5.

Table 4.1: Energy band gap from UV spectra.

Sample	Band Gap (eV)
Pure TiO2	3.20
TrGO-1	3.05
TrGO-2	2.97
TrGO-3	2.84
TrGO-4	2.85
TrGO-5	2.94

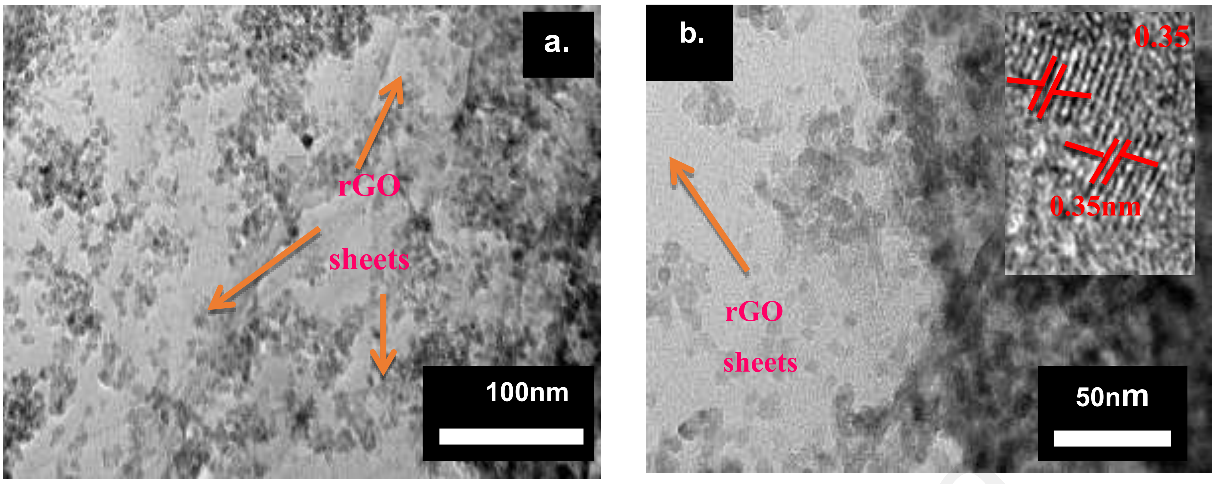

Figure 4.7: HR-TEM images of TrGO-3 (a) 50k magnification(b) 100k magnification.

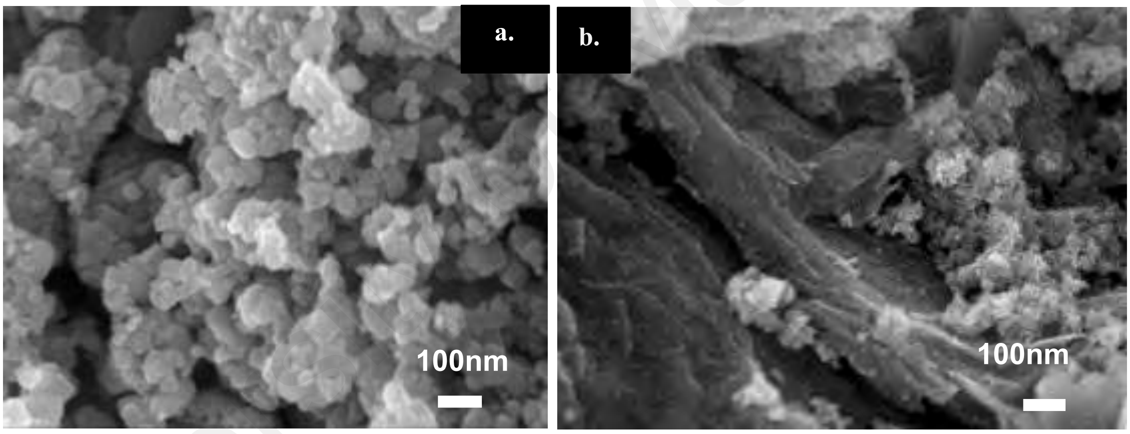

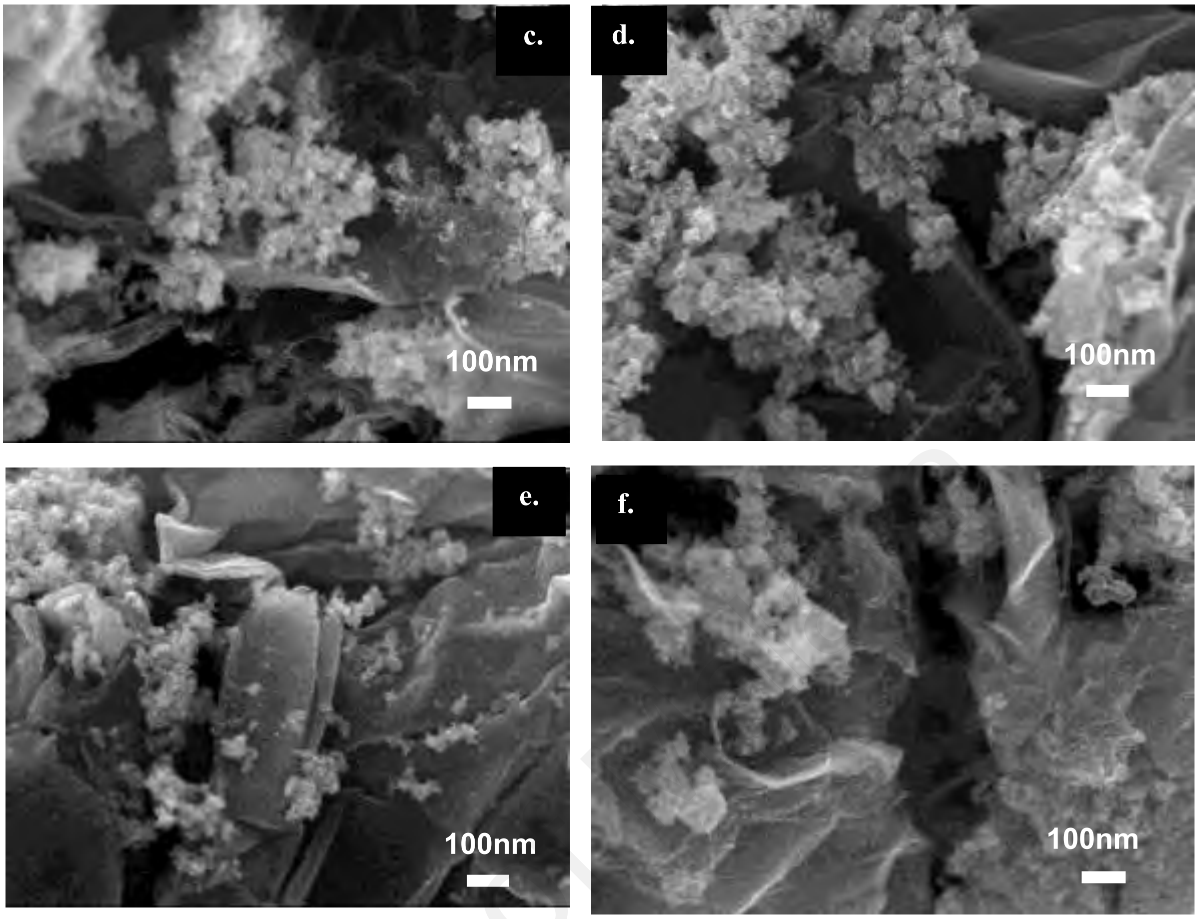

Figure 4.8: FE-SEM images of TiO_2 grow on rGO surface film (i & ii)10µm and 50k magnification (a) TiO_2, (b) TrGO-1, (c) TrGO-2, (d) TrGO-3, (e) TrGO-4 and (f) TrGO-5.

FE-SEM and HR-TEM were used to determine the morphology of the nanocomposites. Based on the surface morphology of TiO_2/rGO (Figs. 4.7 and 4.8), two main conclusions could be drawn: (i) TiO_2 loaded between rGO sheets with little agglomeration; and (ii) the crumpling together of rGO layer sheets with TiO_2 grown on it. On top of that, FE-SEM images (as shown in Fig. 4.8) suggest that the TiO_2 microspheres were encapsulated well in rGO sheets with the increase in rGO content in the TrGO nanocomposite. From HR-TEM images (Fig. 4.7), it was found that the TiO_2 particles with the particle size of ~ 17nm – 28nm were in-situ grown on the surface of rGO during the synthesis of TrGO particle, while the fringe spacing of TiO_2 was estimated to be 0.35nm ensure the presents of (101) anatase. Based on these observations, it is presumable that the TrGO composite possesses enhanced charge transport considering the photo-induced electrons could move through the rGO bridge rather than solely the Ti-Ti grain as a result of the intimate contact between the TiO_2 and rGO. Also, the photoanodes absorption of dye was relatively improved by the addition of rGO ascribed to the larger surface area for dye loading. Considering these facts, it is thereby expected that the photoelectric properties of the DSSCs could be significantly enhanced. The reduction in size for TiO_2 attributed from the pluronic template that gives defect to the rGO sheet and as electron rich material/ surface, rGO attract Ti^{4+} which will reduce the size of TiO_2.

Fig. 4.9 indicates the UV-Vis absorption spectra for green chlorophyll dye (extracted from the Pandan Leaves), red anthocyanin dye (extracted from mulberry) and

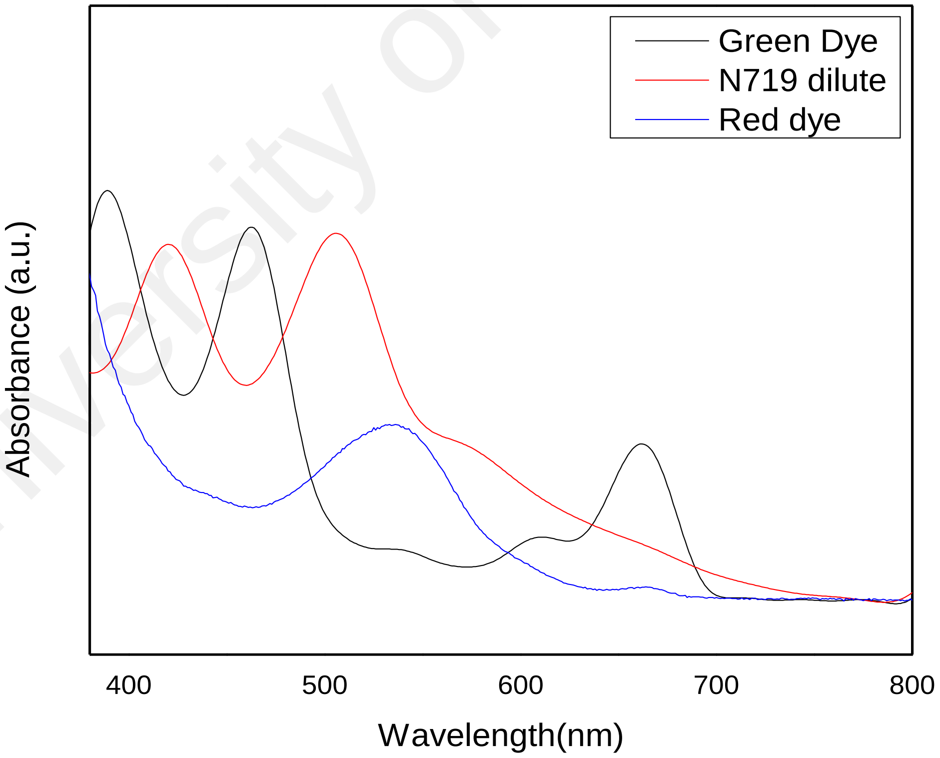

Figure 4.9: UV-Vis Absorbance plot for red anthocyanin dye, green chlorophyll dye and conventional N719.

conventional N719 dye. It has been reported in the previous studies that the absorption range for conventional N719 dye was around 400-600 nm, red anthocyanin dye was around 470-650nm, while the absorption range for green chlorophyll dye was in 400-500 nm with some broad peaks around 520-620nm and 620-700nm. Taking these facts into consideration, it could be concluded that the absorbance of green chlorophyll dye was more efficient than that of the N719 dye in the absorption range of 400-500nm. However, N719 would have a better absorbance performance than the natural green chlorophyll dye at higher absorbance range (such as 500-600nm). Meanwhile, red anthocyanin dye has the highest absorption shift wavelength compared to both N719 and green chlorophyll dye (470-650nm).

4.2.2 Photovoltaic performances of dye sensitized solar cells.

Figs. 4.10, 4.11 and 4.12 show the photocurrent density-voltage (*J*-V) characteristic of the commercialized N719, green chlorophyll and red anthocyanin dyes-sensitized DSSCs under 100mW.cm^{-2} stimulated solar irradiation, while Tables 4.2, 4.3 and 4.4 summarized and tabulated their photoelectrochemical characteristics. Fig.4.13 illustrates the comparison of PCE of DSSCs based on the commercialize N719, green chlorophyll dyes and red anthocyanin dye for different weight rGO nanocomposite. It is noteworthy that the DSSC fabricated with the rGO photoanodes showed an overall better performance than that of those with pure TiO_2. This could be related to the reduction in resistances of each layer, the charge transport and recombination properties. Accordingly, the photocurrent density-voltage curves fill factor (FF) and the overall conversion efficiency (%), maximum power output. I_{sc} and V_{oc} represent short circuit current and open circuit voltage (V_{oc}) and P_{in} is the power of incident light of the overall photovoltic efficiency.

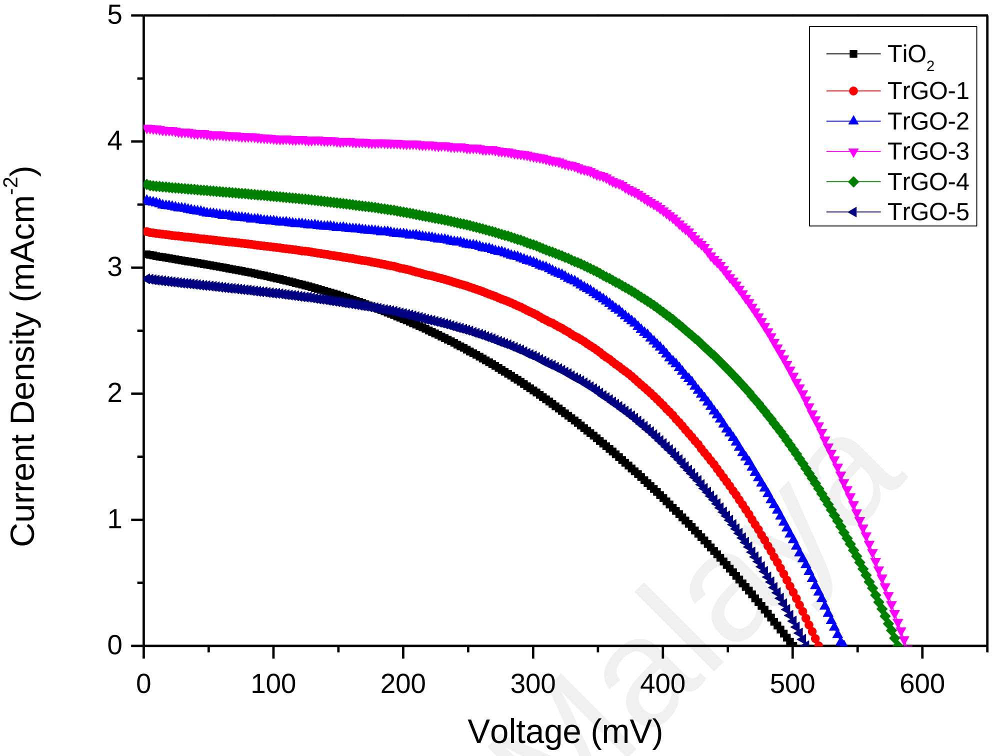

Figure 4.10: Photocurrent density-voltage characteristic of pure TiO_2; TrGO-1; TrGO-2; TrGO-3, TrGO-4 and TrGO-5 using conventional N719 dye.

Table 4.2: Photovoltaic efficiency characteristic DSSCs using conventional N719 dye.

Sample	**Voc(mV)**	***Jsc*(mA cm^{-2})**	**FF(%)**	**ŋ(%)**
Pure TiO_2	671.38	10.91	0.53	3.95
TrGO-1	673.83	10.97	0.53	3.81
TrGO-2	683.59	11.31	0.51	3.98
TrGO-3	695.81	12.98	0.53	4.79
TrGO-4	681.15	11.65	0.49	3.88
TrGO-5	668.95	9.56	0.44	2.93

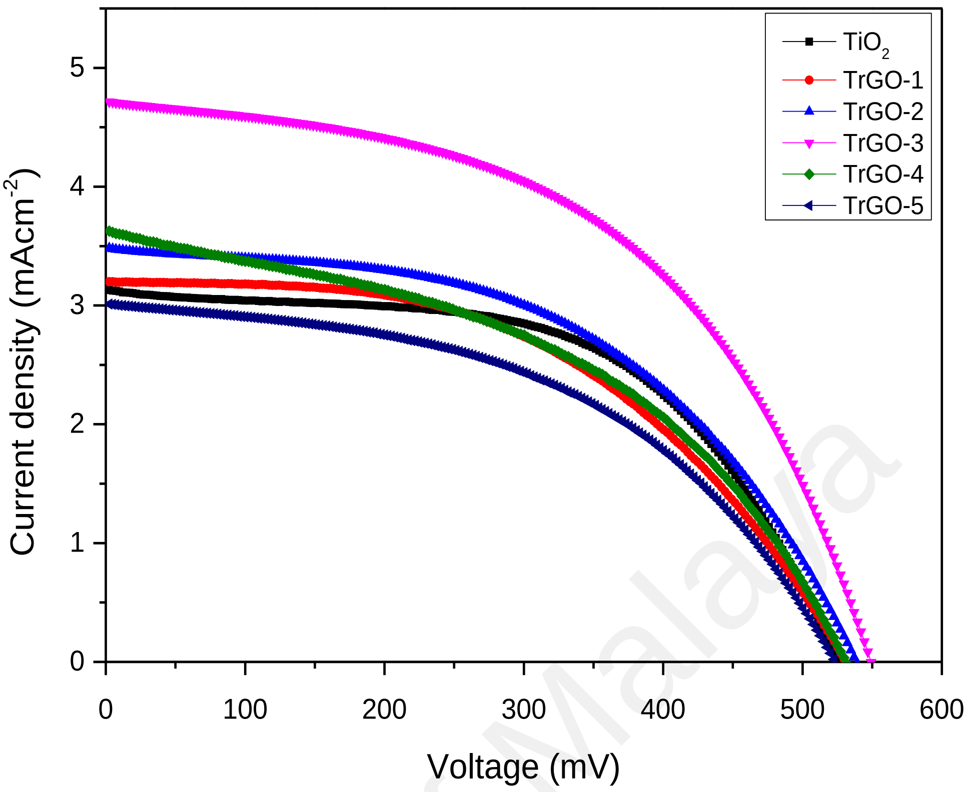

Figure 4.11: Photocurrent density-voltage characteristic of pure TiO$_2$; TrGO-1; TrGO-2; TrGO-3, TrGO-4 and TrGO-5 using Green Chlorophyll dye.

Table 4.3: Photovoltaic efficiency characteristic DSSCs using natural green dye

Sample	**Voc(mV)**	***J*sc(mA cm^{-2})**	**FF(%)**	**ŋ(%)**
Pure TiO$_2$	529.79	3.13	0.56	0.93
TrGO-1	534.67	3.2	0.49	0.84
TrGO-2	541.99	3.48	0.5	0.94
TrGO-3	549.43	4.72	0.51	1.32
TrGO-4	532.27	3.63	0.44	0.84
TrGO-5	522.91	3.01	0.47	0.74

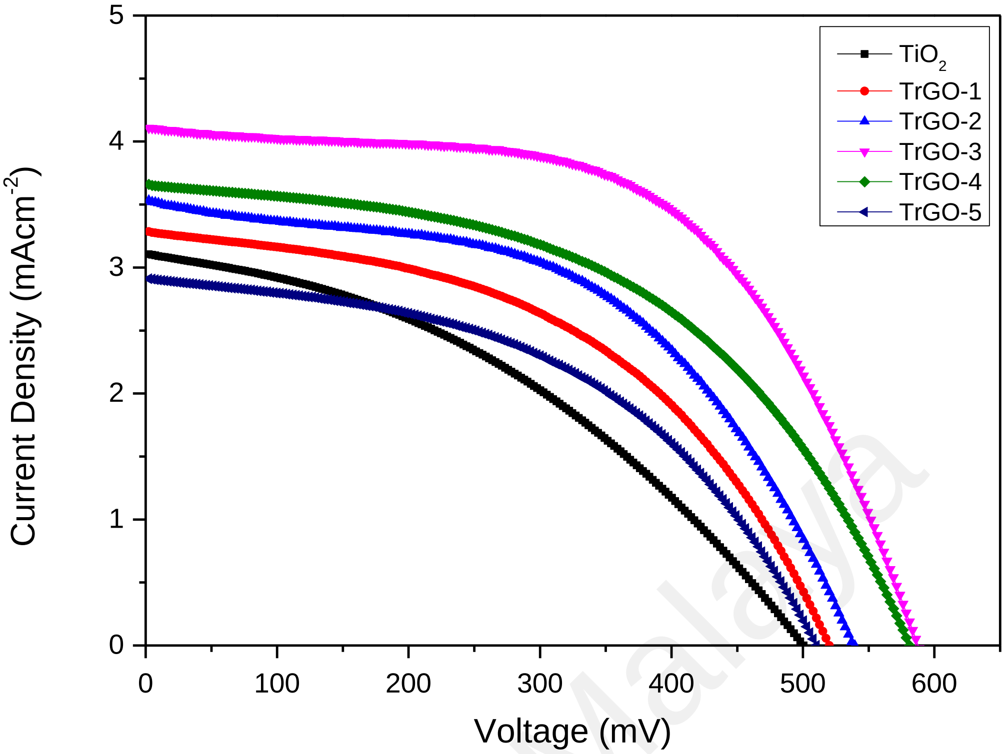

Figure 4.12: Photocurrent density-voltage characteristic of pure TiO_2; TrGO-1; TrGO-2; TrGO-3, TrGO-4 and TrGO-5 using Red Anthocyanin dye.

Table 4.4: Photovoltaic efficiency characteristic DSSCs using red anthocyanin dye

Sample	**Voc(mV)**	***J*sc(mA cm^{-2})**	**FF(%)**	**ŋ(%)**
Pure TiO_2	529.79	3.13	0.36	0.6
TrGO-1	534.67	3.20	0.48	0.82
TrGO-2	541.99	3.48	0.51	0.92
TrGO-3	546.32	4.08	0.61	1.36
TrGO-4	537.11	3.63	0.54	1.05
TrGO-5	522.46	3.01	0.45	0.71

From the *J*-V curves, it is interesting to note that TrGO-3 nanocomposite showed improvement in photocurrent generation regardless of the dye type used compared to TiO_2 DSSCs. The N719 dye-sensitized TrGO-3 illustrated a higher photovoltaic efficiency (4.79%) compared to natural dye of the green chlorophyll dye-sensitized TrGO-3 (1.14%) and red anthocyanin dye (1.36%). It was also found that, in Fig. 4.13, the overall photocurrent efficiency *(η)* of DSSCs improved by the addition of rGO into the photoanode up to 0.03g (i.e., TrGO-3). This is associated with the fact that the addition of rGO enhanced the transfer path for the ultrafast ejected electrons to travel between TiO_2 particle. Additionally, rGO which acts as the protection layer for the photoanode also prevented the liquid electrolyte from reaching the FTO substrate. As a result, these phenomena contributed to an increase in the current density while minimizing/reducing the recombination of electron generation. On top of photocurrent efficiency and current density, TrGO-1, TrGO-2 and TrGO-3 also showed a massive improvement in V_{oc}.

Correspondingly, the V_{oc} improvement led to the reduction in the Fermi level in the photoanode and the Nerst potential of redox couple in the electrolyte when it was under illumination(L. Chen et al., 2013). However, DSSCs containing higher amounts of rGO (i.e., TrGO-4 and TrGO-5) lost its performance as a consequence of the drop in the photovoltaic efficiency. This is mainly due to the antagonistic effect between the rGO and dye molecules to compete for the visible light. In other words, the photon of visible light absorbed by the dye molecules would become less if the rGO content is high considering rGO only absorbed approximately 4% of light [40-41]. This would give rise to less excited electron traveling in the device and eventually lead to a lower current density and photovoltaic efficiency of DSSCs. For anatase semiconductor oxide, there are stable performance between both of the natural dye as the potovoltaic efficiency characteristics of both day were almost similar. This shown that both type of dye can work efficiently on the TrGO nanocomposite film.

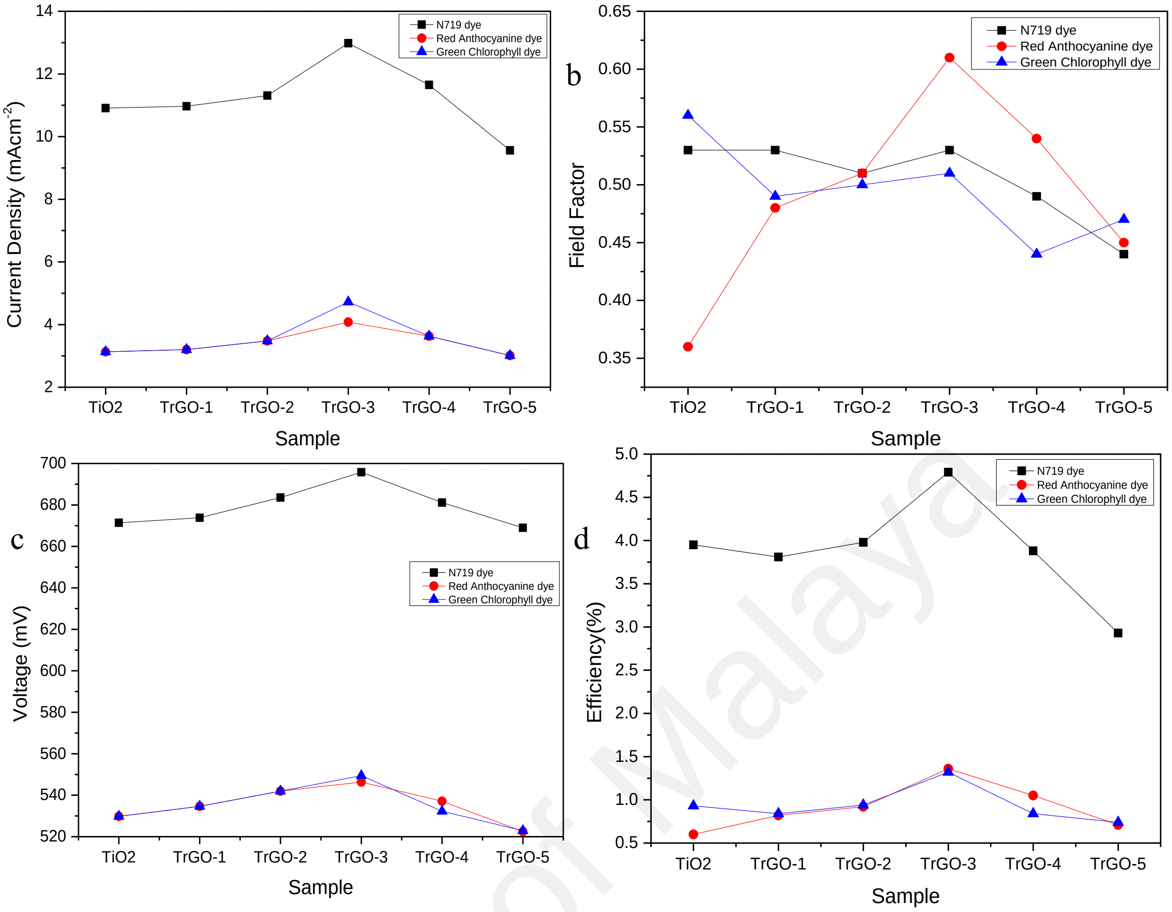

Figure 4.13: DSSCs analysis of all samples; a) current density; b) fill factor; c) voltage short circuit; d) efficiency

Apart from that, as shown in Fig. 4.13, from the pattern of photovoltaic characteristics shows improvments in all characteristics of DSSCs from TrGO-1 to TrGO-3 compared to TiO_2. The positive impact of increment in performance was contribute by the enchoring of TiO_2 on rGO surface. With a balance ratio of rGO and TiO_2 will exhibit a positive improvement in all aspect of DSSC such as bandgap of semiconductor, photovoltaic characteristics and overall efficiency. The DSSCs analysis also showed that ratio TrGO-4 (0.04g) and TrGO-5 (0.05g) DSSC give negative impact to the performance of DSSC where it becomes unstable and decreases in performance. This is due to competitiveness of the semiconductor to absorb and transport light. From the impact of dye on DSSC performance, it is undeniable that conventional N719 dye showed a better performance than the natural dye, but it is strongly believed that a stable and high performance yet enviromentally friendly dye could be prepared by proper altering the R-chains and stabilizing the porphyrin structures of the natural dye. There are potential in natural dye in future as it can work well with material such as rGO/graphene.

Considering the aforementioned facts, it is of great important to optimize the loading of TiO_2 dopants attached to the rGO sheets to maximize the photovoltaic performance. It has been widely accepted that the photon absorption could be significantly improved with a good combination between TiO_2 and rGO; An excessive TiO_2 nanoparticle dopants attached to rGO will cause loss in photons that could have absorbed and eventually lead to electron leakage in the device (Chang et al., 2013). Also, the aim of the present study was to enhance the absorption of the dye via optimizing the ratio of TiO_2 and rGO dopants to maximize the photovoltaic performance by increasing J_{sc} of DSSCs(Sharma et al., 2013; M. Zhu, Li, Liu, & Cui, 2014). Accordingly, the electron transport path can be improved by incorporating rGO into TiO_2 photoanode as rGO could provide path to increase the dye molecule absorption on the photoanode surface. Also, when the surface of photoanode was illuminated with sunlight, the ultrafast electron transport could be enhanced with the support of excellent conductivity of rGO. From the previous study, it was known that the resistance between the grain and path could be minimized by incorporating rGO into TiO_2 as rGO tends to build the bridge between TiO_2 (M. Zhu et al., 2014). This help in enhancing the charge separation, electron collector and transportation of photogenerated electron as well as reducing the probability of charge recombination. This is also beneficial for the photo-generated electron to transfer without suffering from massive resistance (Sharma et al., 2013; Zhao et al., 2013; Zhao, Wu, Zheng, Huo, & Tu, 2015; Zhi et al., 2015).

4.2.3 EIS analysis of dye sensitized solar cells.

Electrochemical impedance spectroscopy (EIS) was employed in the present study to determine the electronic properties behavior and the internal resistance in the DSSCs device. Accordingly, EIS test was conducted under the illumination condition of $100mW/cm^2$ over the frequency range of 100kHz to 0.001Hz at the amplitude of 20mV. The EIS was then analysed using the stimulated model of internal circuit of DSSCs to identify the resistance of electron charge between each surface materials.

From Fig.4.14 (A, B, and C) it shows 3 semicircles where the first semicircle was barely visible due to the large middle frequency semicircle that overlaps the shape of semicircle of the middle frequency, but regardless of that. From Table 4.5, table 4.6 and Table 4.5, 4.6, 4.7 shows the Nyquist plot almost similar value of R_s and R_{CE} where it describes the materials for counter electrode and electrolyte were same for all DSSCs devices for all type of dye. When the first semicircle decreased, it indicted that the fast electron transfer at counter electrode and electrolyte interface. Furthermore, the second semicircle R_{CT} represents the photoanode/dye/electrolyte resistance. For N719 dye, the value or R_{CT} for TiO_2, TrGO-1, TrGO-2, TrGO-3, TrGO-4 and TrGO-5 were 126.0Ω, 92.3Ω, 52.3Ω, 50.2Ω, 129Ω and 138.3Ω respectively. The green dye recorded 351Ω, 199Ω, 132Ω, 284Ω, 132Ω and 288.4Ω for pure TiO_2, TrGO-1, TrGO-2, TrGO-3, TrGO-4 and TrGO-5. Meanwhile, red anthocyanin dye R_{CT} value for TiO_2, TrGO-1, TrGO-2, TrGO-3, TrGO-4 and TrGO-5 were 353Ω, 139Ω, 126Ω, 203Ω and 312 Ω. These values indicate the electrocatalytic activity in the DSSCs where the lowest value of R_{CT} represents the highest electrocatalytic activity then other DSSCs. In this case for red anthocyanin, N719 and natural green chlorophyll dye TrGO-3 recorded highest electrocatalytic activity compared to other DSSCs. In the same time, TrGO-3 had the lowest recombination resistance and lowest electron transmission resistance in the photoanode. When rGO was added into the photoanode, it create new path in the photoanode structure and the generated electron travels quickly to fill the anode surface. Subsequently, rGO helps in acceleration of the interfacial electron transfer which will reduce the electron-hole recombination. With optimized TiO_2 dopants in rGO film, the minimal defect in the photoanode will creating good surface contact for the dye and semiconductor, increased in the performance of DSSCs, supressed the recombination of electron across the semiconductor and enhance the charge transfer between the interfaces of the material (Hu, Zhang, Shen, Li, & He, 2017; Liu et al.; San Esteban & Enriquez, 2013).

Table 4.5 : EIS analysis of N719 dye DSSCs.

Sample	**R_s(Ω)**	**R_{CT}(Ω)**	**R_{CE}(Ω)**	**Bode Peak (Hz)**	**Electron Lifetime τ_n(ms)**
Pure TiO_2	20.9	126.0	38.6	63.096	2.52
TrGO-1	21.5	92.3	37.1	19.953	8.38
TrGO-2	20.9	52.3	38.2	15.849	10.0
TrGO-3	20.0	50.2	37.6	10.000	16.32
TrGO-4	20.9	129.0	36.7	50.119	3.16
TrGO-5	21.7	138.3	37.8	63.096	2.52

Table 4.6: EIS analysis of green chlorophyll dye DSSCs.

Sample	**R_s(Ω)**	**R_{CT}(Ω)**	**R_{CE}(Ω)**	**Bode Peak (Hz)**	**Electron Lifetime τ_n(ms)**
Pure TiO_2	22.0	351.0	39.4	100.00	1.59
TrGO-1	22.6	199.0	38.7	50.119	3.18
TrGO-2	21.3	132.0	38.1	39.811	4.00
TrGO-3	20.3	130.0	37.7	25.119	6.34
TrGO-4	22.6	284.0	40.7	79.433	2.00
TrGO-5	24.4	288.4	39.7	100.00	1.59

Table 4.7: EIS analysis of red anthocyanin dye DSSCs.

Sample	**Rs(Ω)**	**RCT(Ω)**	**RCE(Ω)**	**Bode Peak (Hz)**	**Electron Lifetime τ_n(ms)**
Pure TiO_2	25.7	353.0	35.4	100.00	1.59
TrGO-1	23.9	139.0	34.5	79.443	2.00
TrGO-2	22.4	126.0	30.2	50.119	3.18
TrGO-3	20.6	110.0	30.5	19.953	8.37
TrGO-4	24.7	203.0	31.7	31.623	5.03
TrGO-5	24.7	312.0	36.6	100.00	1.59

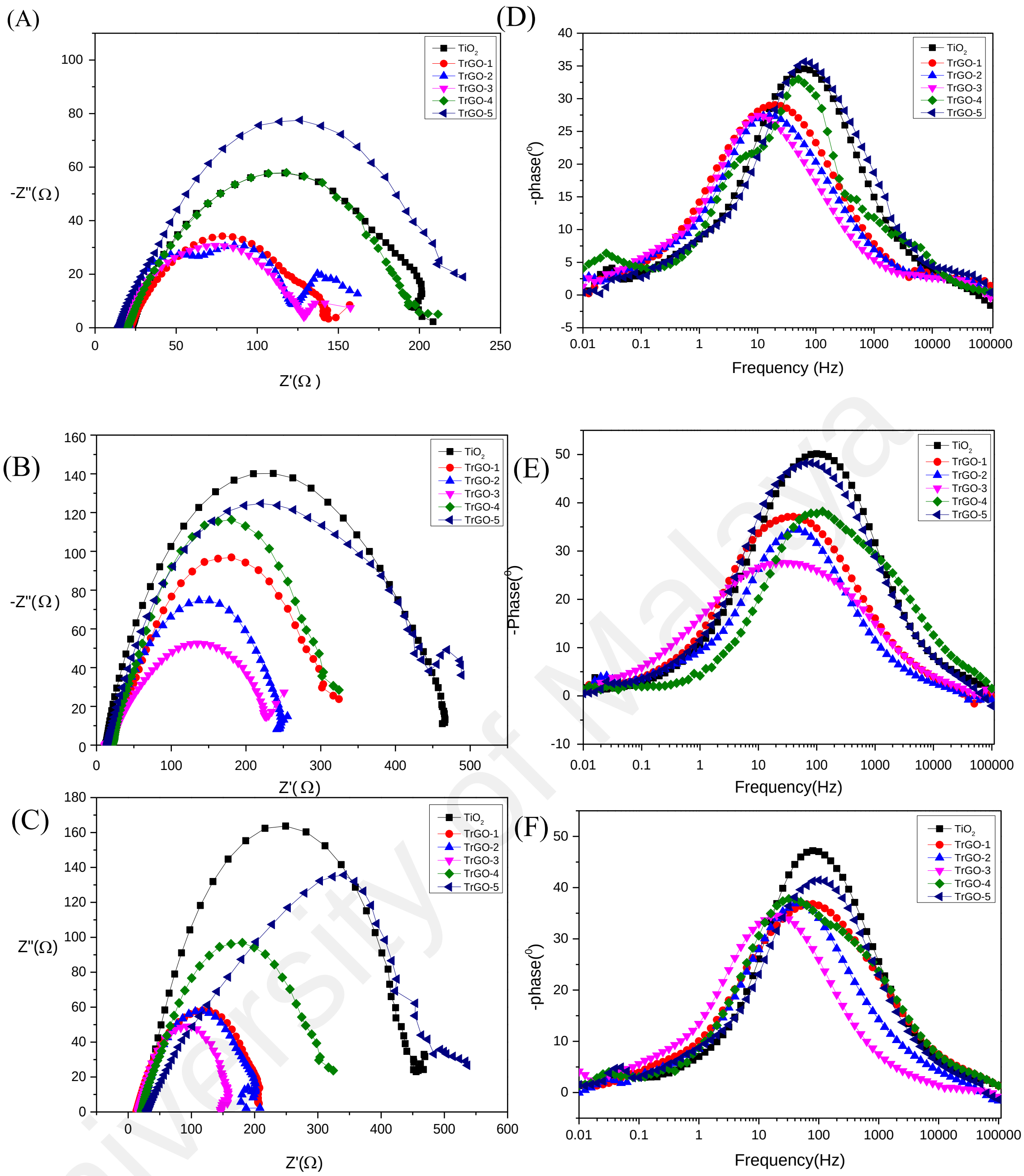

Figure 4.14: EIS analysis (A, B & C) Nyquist plot for commercialize N719 dye, green chlorophyll dye and red anthocyanin dye; (D, E & F) Bode plot for commercialize N719 dye, green chlorophyll dye and red anthocyanin dye.

In order to support the EIS analysis, bode plots (Figs. 4.14 D, E, and F) contribute to the information of electronics transfer and recombination of electron holes lifetime in DSSCs photoanode-electrolyte interface. From the bode plot, electron lifetime (τ_n) could be obtained from the peak angular frequency by using the following equation (3.4):

$$\tau_n = \frac{1}{2}\pi f_{max} \tag{3.4}$$

where f_{max} is the peak frequency of bode phase. As shown in Table 4.5, Table 4.6 and Table 4.7, the recorded electron lifetime for N719 dye were 2.52ms, 8.38ms, 10.00ms, 16.32ms, 3.16ms and 2.52ms. For natural dye, red anthocyanin dye recorded 1.59ms, 2.00ms, 3.18ms, 8.37ms, 5.03ms and 1.59ms electron lifetime while the electron lifetime for green chlorophyll dye were 1.59ms, 3.18ms, 4.00ms, 6.34ms, 2.00ms and 1.59ms. From the bode plot, shifting of the characteristic peak into lower frequency demonstrates with increase in electron transfer. The recombination in the photoanode/dye/electrolyte interface reduced when there is an increase of electron lifetime producing a reduction of recombination (Sharma et al., 2013). From the tables, the increase in electron lifetime was TrGO-3 regardless type of dye which suggests that recombination rate of injected electron has improved and leads to faster diffusion rate, thus increasing J_{sc} and PCE valus (Sacco et al., 2014; Sharma et al., 2013). This explained by Zhao et al (Zhao et al., 2013; Zhao et al., 2015) that graphene reacts as a bridge for the electron transfer in TiO_2 photoanode during the electron photogenerated. This contributes less diffusive hindrance and lowers the charge recombination and back transfer reaction when the electron is photogenerated (Zhao et al., 2013; Zhao et al., 2015).

4.3 Optimum synthesis pH of TrGO-3 DSSCs

One of the main factor in synthesizing TiO_2 is the pH of the catalyst. Optimum synthesis pH gives a main role in crystalline size and shape of the particle growth. In this experiment, synthesizing pH was tested to gain the best shape of particle growth and crystalline size of TrGO nanocomposite.

4.3.1 Morphological characterization of synthesis pH for TrGO-3

Fig. 4.15 exhibits the XRD patterns of TrGO nanocomposites (TrGO-3 pH1, TrGO-3 pH2, TrgO-3 pH3, TrGO-3 pH4 and TrGO-3 pH5) and to ensure the crystallographic phase. From the Fig.4.15, all of the diffraction peaks can be satisfactorily indexed to anatase. The major diffraction spectra for TrGO-3, 25.96^0 showed anatase phase. The XRD peaks obtained shows $2\theta = 25.96^0$, 38.90^0, 48.16^0, 54.05^0, 55.21^0, 63.87^0, 68.98^0, 70.479^0 and 75.28^0 correspond to the (101), (004), (200), (105), (211), (204), (116), (220) and (215) diffraction planes respectively. Th rGO peak is barely visible due to presumable by small amount of rGO in the nanocomposite and the rGO peak was overlap due to broad spectrum of rGO at 24^0. From the XRD pattern, TrGO-3 shows the highest crystallinity due to sharp and intense peak at 25^o peak. For TrGO-3, the main peak have almost the same broadness for all sample although the pH is different. However, the crystallinity was the main concern due to good crystal structure that attached on the rGO will enhance the electron transport in the semiconductor photoanode (Cheng & Stadler, 2015; How et al., 2014; Ling et al., 2013; Senthil, Muthukumarasamy, Agilan, Balasundaraprabhu, & Kumaran, 2013). The Debye Scherrer Equation has been employed to measure the average particle size of TrGO-3 that synthesized with different pH value. Only major peak were considered in this experiment which is 25.96^0. The particle size was estimated at 18.8 nm for TrGO-3 pH1, 15.2 nm for TrGO-3 pH2, 11.2 nm for TrGO-3 pH3, 17.8 nm for TrGO-3 pH4 and

21.5 nm for TrGO-3 pH5. This shows that the pH variation does gives a little influence on the crystallinity and crystallite size of TrGO nanocomposite.

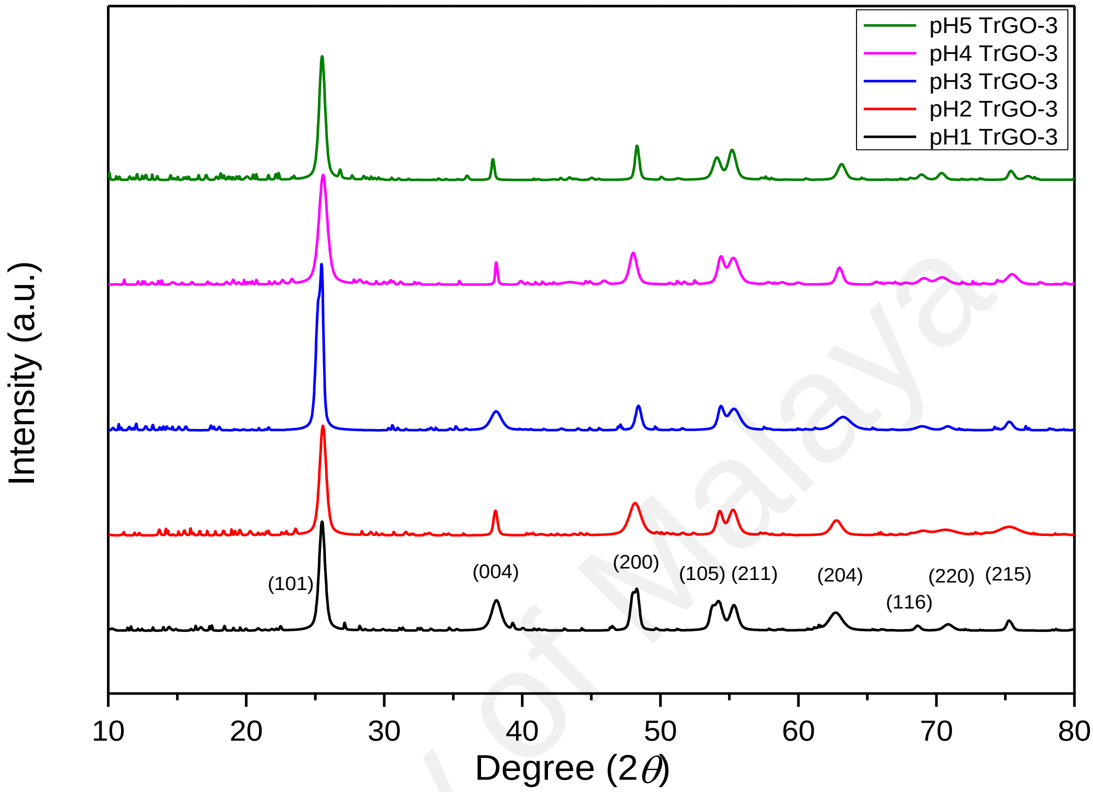

Figure 4.15: X-Ray diffraction (XRD) spectra of pH1 TrGO-3, pH2 TrGO-3, pH3 TrGO-3, pH4 TrGO-3 and pH5 TrGO-3.

FTIR spectroscopy is illustrated in Fig. 4.16, TrGO-3 showed a broad banding below 1000cm^{-1}, implying Ti-O-Ti and Ti-O-C stretching vibrations within the molecules, respectively (Karimi et al., 2014; Nithya et al.; Yu et al., 2003). From Fig. 4.16, it was also observed that TrGO nanocomposite exhibited some characteristic peaks which could be assigned to the C-H stretching (1080 cm^{-1}), C=C stretching (1541 cm^{-1}), C=O stretching (1695 cm^{-1}) and –OH stretching (3440 cm^{-1}) (Karimi et al., 2014). There was also a strong peak located at 2357cm^{-1} assigned to the CO_2 contamination (Zhang et al., 2014). In Fig. 4.16, there were peaks in the region between 3600 and 3900 cm^{-1} corresponding to the formation of oxygen vacancies induced by the formation of Ti^{3+} species (Samsudin et al., 2015), while the peaks at 3724 and 3845 cm^{-1} were attributed to the Ti^{3+}-OH formation. Moreover, the peak at 3674 cm^{-1} corresponded to the Ti^{4+} in the TiO_2.

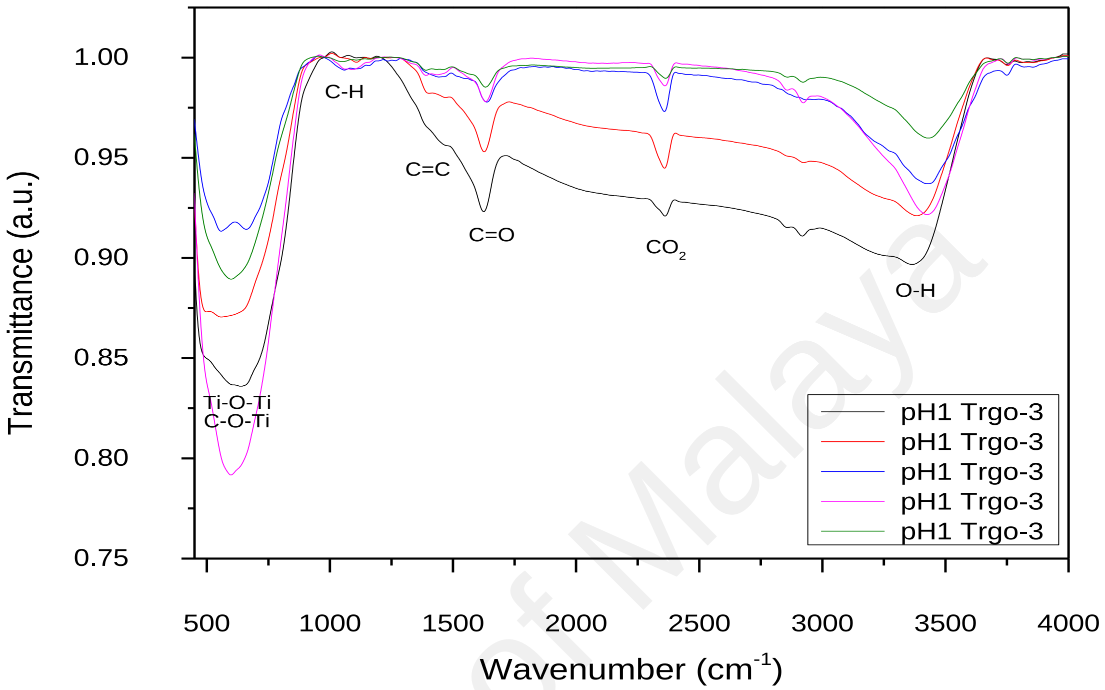

Figure 4.16: Fourier Transform Infrared (FTIR) spectra of pH1 TrGO-3, pH2 TrGO-3, pH3 TrGO-3, pH4 TrGO-3 and pH5 TrGO-3.

Raman spectroscopy was employed in the present study to characterize the structural properties of the graphene materials. Fig. 4.17 shows the Raman spectra of TrGO-3 with different pH value. It is clear that all TrGO-3 with different pH value possessed the anatase phase consisting of five major vibration peaks at 144 cm^{-1} (E_g), 197 cm $^{-1}$ (E_g), 395 cm^{-1} (B_{1b}), 513 cm^{-1} (A_{1b}), and 635cm^{-1} (E_g). This is in line with the finding reported by Otakar et al. (Frank et al., 2012). Also, it is noteworthy that TrGO showed two broad vibration bands within 1200-1700 cm^{-1}, in which the D band (attributed to the breathing mode of A_{1g} symmetry involving phonons near the K zone boundary) appeared at 1309 cm^{-1}, while the G band (originates from sp^2 in-plane vibration mode of carbon atoms) at 1583cm^{-1}.

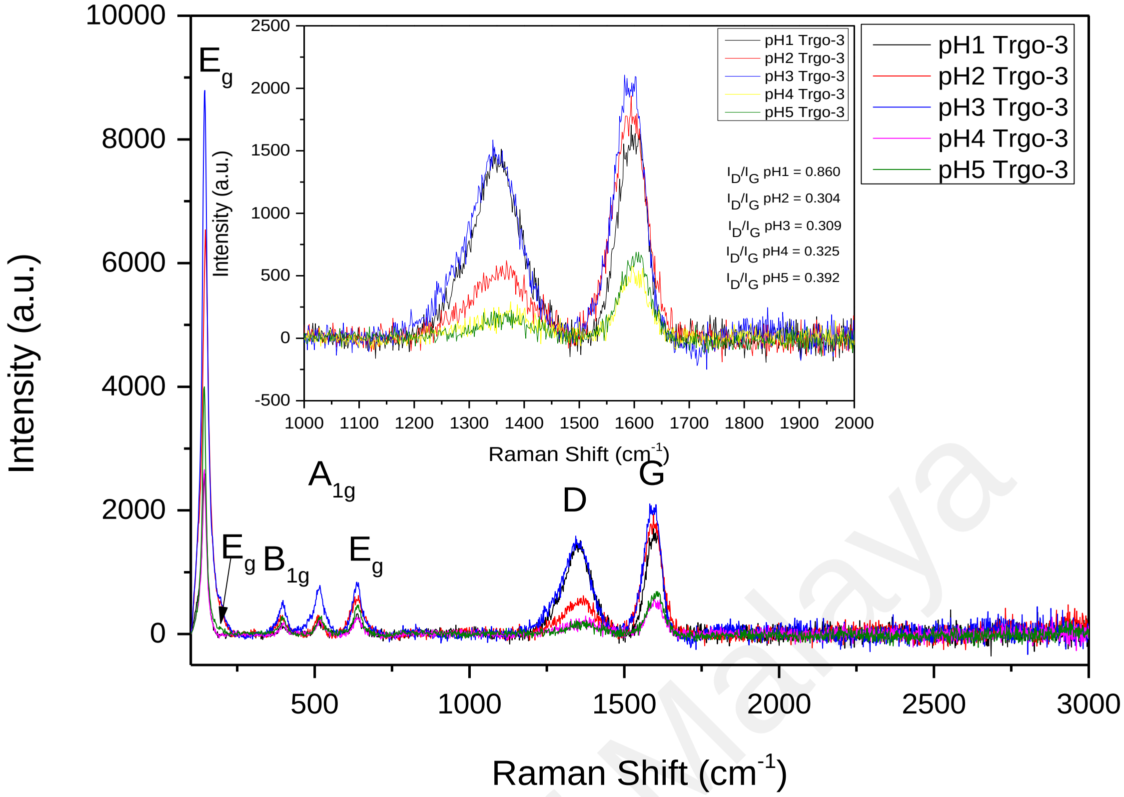

Figure 4.17: Raman spectroscopy of pH1 TrGO-3, pH2 TrGO-3, pH3 TrGO-3, pH4 TrGO-3 and pH5 TrGO-3.

From the Fig. 4.17, from pH 1 to pH 3 showed that the D and G band intensity were higher than in pH 4 and pH 5. As reported by Ahmed et al. (Ahmad et al., 2015), the intensity ratio of D and G bands(I_D/I_G) could represent the structure, defects and size of the graphene. Correspondingly, I_D/I_G of TrGO sample is in between 0.86 to 0.39 and the lowest intensity ratio was TrGO-3 with 0.309. The intensity ratio for nanocompsite indicates most all of the sample suggesting a low level of defect, high crystallinity and small size of rGO in TrGO especially TrGO-3. Additionally, as displayed in Fig. 4.17, Raman 2D band at about 2600 cm^{-1} was detected in TrGO-1 implying the presence of aggregates of some rGO layers in the nanocomposites which might be associated with the restacking of rGO layers during the synthesis process (Amara et al., 2007). The Raman band shifts and broadening in E_g mode (144 cm^{-1}) was also observed in Fig. 4.17. One possible explanation (Samsudin et al., 2015), reported that the peak shifts and broadening might originate from the surface defects such as the presence of oxygen vacancy and peak broadening which roughly show pools of oxygen vacancies.

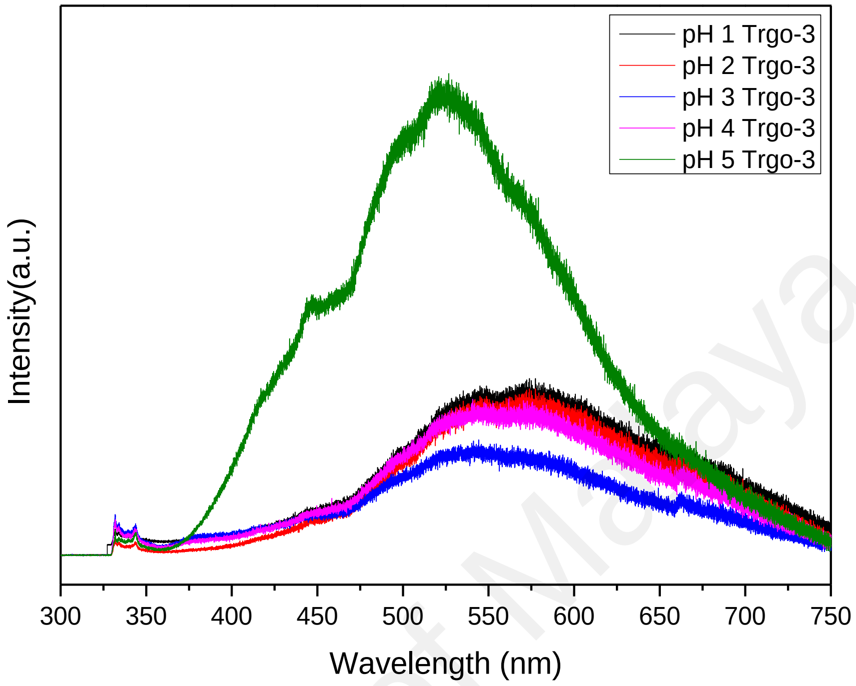

Figure 4.18: Photoluminescence (PL) spectra of pH1 TrGO-3, pH2 TrGO-3, pH3 TrGO-3, pH4 TrGO-3 and pH5 TrGO-3.

Fig. 4.18 shows the PL spectra of TrGO nano-composites. The presence of PL peaks in the wavelength range of 450-750nm indicated that TiO_2 and TrGO nanocomposites are the indirect band gap semiconductors. The presence of small peak near 330nm was mainly attributed to the ligand to metal charge transfer in TiO_2 (O^{2-} to Ti^{4+}), a little bump at 450nm signified the occurance of surface oxygen vacancy related defects. Furthermore, all peaks were blue shifted in the Raman peak. This implies the transformation of un-coordinated Ti^{3+} ions to the surface of oxygen vacancy. The green band with peak position at 540nm was also an indication of the surface oxygen vacancy of anatase (101) phase. According to Liu et al. [19], the oxygen-vacancy-related defects as a result of the oxygen atom removal by annealing in an inert argon atmosphere where the removal of the oxygen atom will create electron traps under the conduction band.

Specifically, the electron traps usually locate at 0.7 to 1.6 eV below the conduction band edge energy. Ti^{4+} will be reduced to Ti^{3+}considering the removal of oxygen atom can create lone pair of electrons (Jin et al., 2015).

In terms of intensity, the intensity of TrGO samples is decreasing from sample pH 1 TrGO-3 to pH 4 TrGO-3 but the intensity increases in pH5 TrGO-3. The lowest PL intensity was pH3 TrGO-3. The reduced intensity of PL spectra in the nanocomposite shows that the PL intensity was mainly influenced by the recombination rate of electron-hole pairs. It has also been reported in literatures that a lower intensity of PL spectra implied an increase in charge separation and a decrease in the rate of electron-hole pair recombination which it suggest pH3 TrGO-3 samples (Gupta et al., 2010; Min et al., 2012; Raghavan et al., 2015).

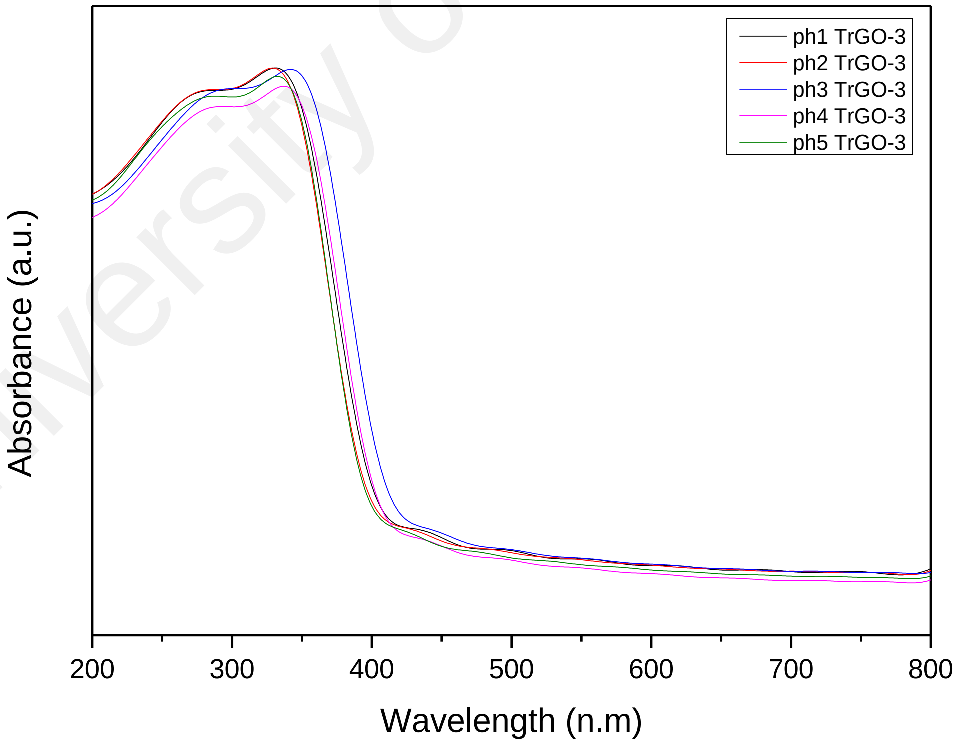

Figure 4.19: Absorption plot of pH1 TrGO-3, pH2 TrGO-3, pH3 TrGO-3, pH4 TrGO-3 and pH5 TrGO-3.

Fig. 4.19 displays the absorption spectra of TrGO-3 nanocomposites with diferrent pH values. Correspondingly, these spectra give the information regarding to the absorption ability of the photoanode and the bandgap of the anatase semiconductor oxide film. It is noteworthy that the optical absorbance specta of all the films were in the range of ~300nm to 430nm. The photon absorption ability in TrGO-3 was approximately to each other although the synthesis pH of nanocomposite was different. Athough the samples have different pH synthesis value, it does not alter the ability of photoanode to absorb the light due to the same quantity of rGO in the photoanode.

Fig. 4.20 shows the Tauc plot, while Table 4.8 tabulates the intrinsic energy band gap (from the UV spectra) TrGO-3 with different pH values films. It was found that, based on Table 4.8, the optical energy band gap indicate between 2.93eV to 2.84eV. The pattern of energy band shows a bell pattern where the sample decrease

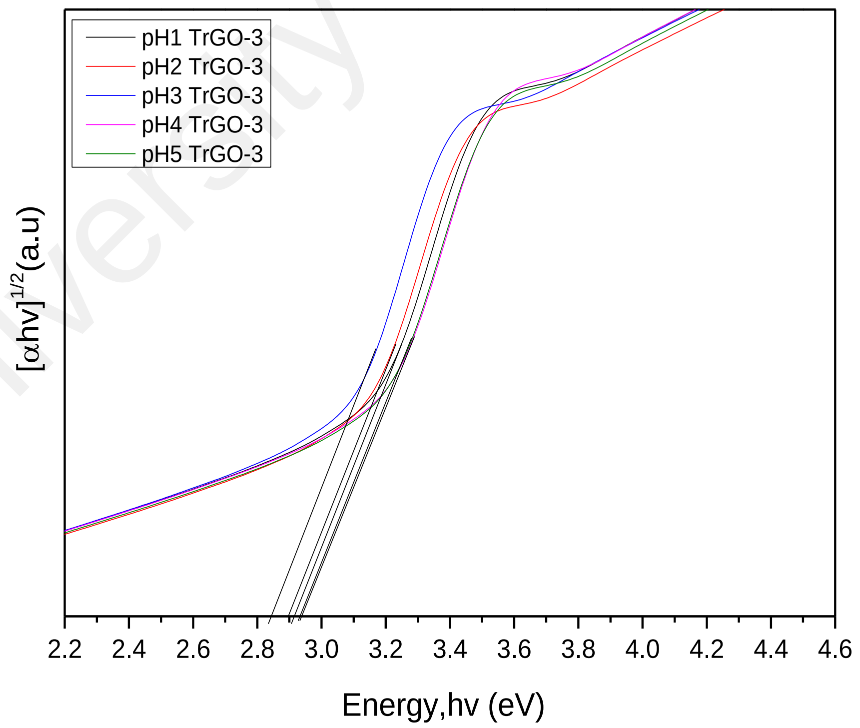

Figure 4.20: Tauc plot of pH1 TrGO-3, pH2 TrGO-3, pH3 TrGO-3, pH4 TrGO-3 and pH5 TrGO-3.

Table 4.8: Energy band gap from UV spectra.

Sample	Band Gap (eV)
pH 1 TrGO-1	2.91
pH 2 TrGO-2	2.89
pH 3 TrGO-3	2.84
pH 4 TrGO-4	2.93
pH 5 TrGO-5	2.93

from gap in pH1 TrGO-3 and pH3 TrGO-3 but slightly increase starting on pH4 TrGO-3 and pH5 TrGO-3. The smallest band gap was detected to be approximately 2.84eV (pH3 TrGO-3 The band gap reduction mainly attributed to the presence of TiO_2 nanoparticles acted as potential dopants to create an impurity energy level within the valence band (VB) and conduction band (CB) (O2p – Ti3d).

FE-SEM and HR-TEM were used to determine the morphology of the nanocomposites. Based on the surface morphology of TiO_2/rGO (Figs. 4.21 and 4.22), two main conclusions could be drawn: (i) TiO_2 loaded between rGO with size of TiO_2 loaded on rGO sheets; and (ii) different pH values shows different crystalline growth of TiO_2 on rGO sheets. On top of that, FE-SEM images (as shown in Fig. 4.21) suggest that the TiO_2 microspheres were encapsulated well in rGO sheets with the increase in rGO content in the TrGO nanocomposite in TrGO-3. From the HRTEM, particle size of the sample was varied according to the samples where TrGO-3 pH1 to pH3 shows size between ~15nm to 27nm while TrGO-3 pH4 and pH5 was about ~17 – 38nm. The size of TrGO nanocomposite still acceptable for DSSC application. The size reduction was contribute from electron rich rGO surface attract the Ti^{4+} contributes to the reduction in TrGO particle size(Samsudin et al., 2015).

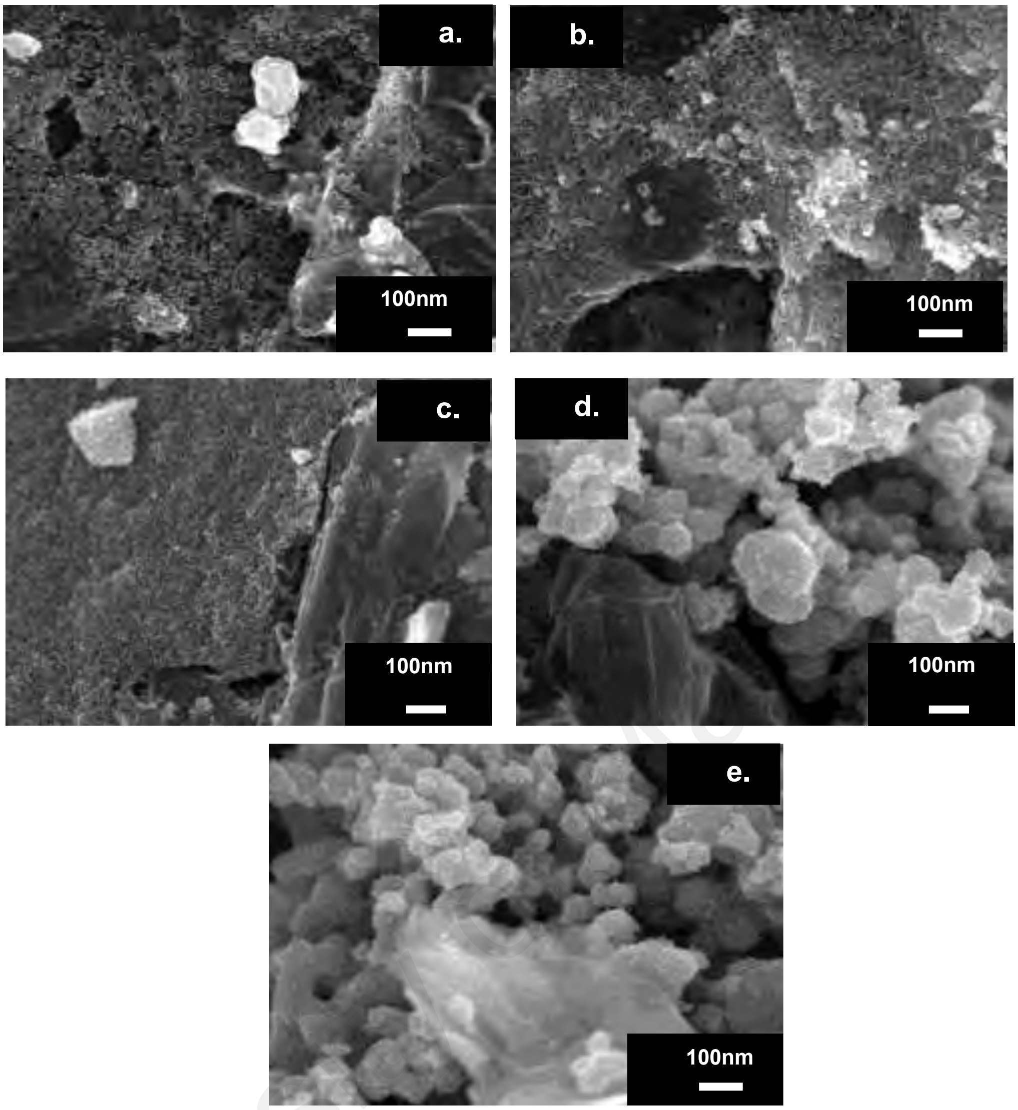

Figure 4.21: FE-SEM images of TiO_2 grow on graphene film on 50k magnification (a) pH1 TrGO-3, (b) pH2 TrGO-3, (c) pH3 TrGO-3, (d) pH4 TrGO-3 and (e) pH5 TrGO-3.

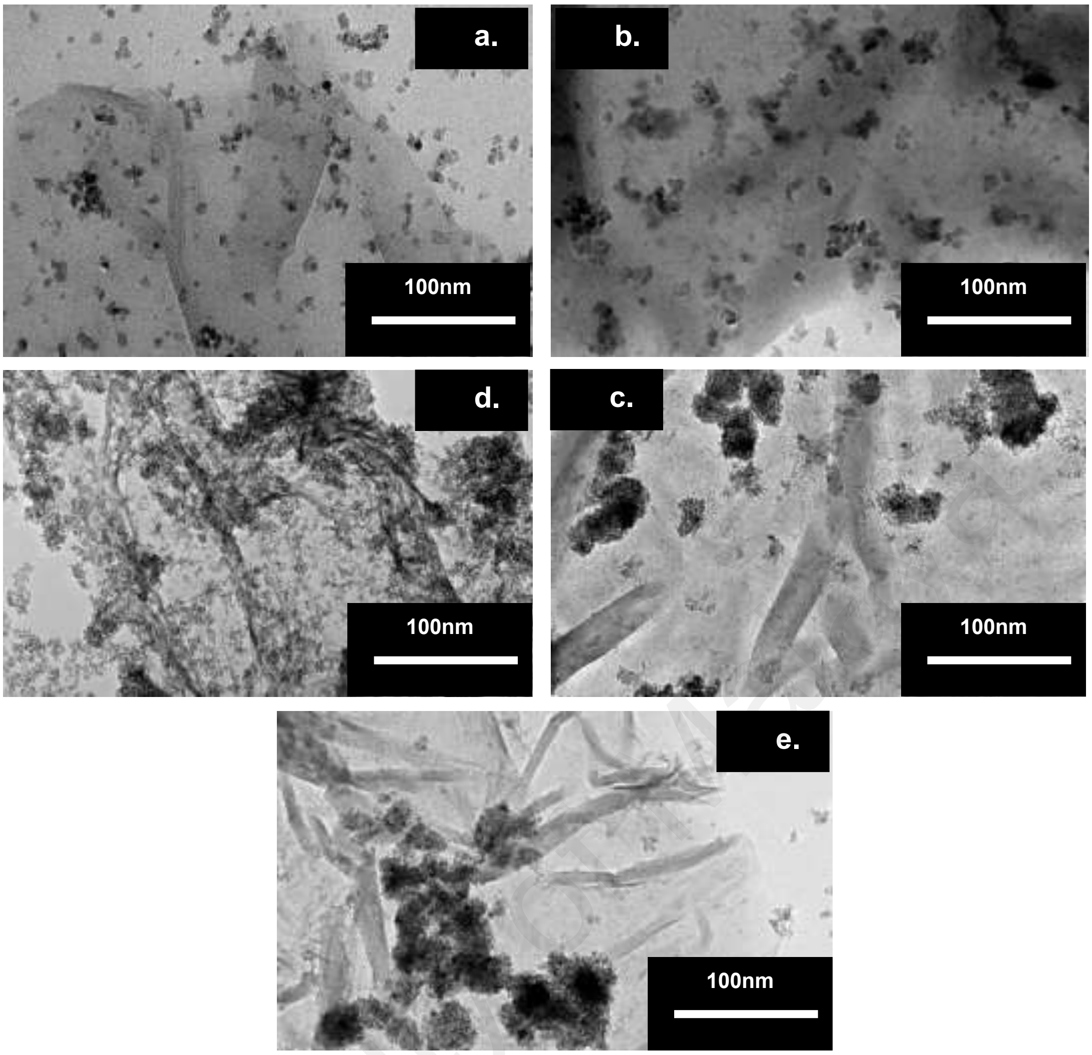

Figure 4.22: HR-TEM images of TiO_2 grow on graphene film on 50k magnification (a) pH1 TrGO-3, (b) pH2 TrGO-3, (c) pH3 TrGO-3, (d) pH4 TrGO-3 and (e) pH5 TrGO-3.

The fringe spacing of TiO_2 particle on rGO was estimated to be 0.35nm ensure the presents of (101) anatase. Based on these observations, it is presumable that the TrGO-3 composite possesses enhanced charge transport considering the photo-induced electrons could move through the rGO bridge rather than solely the Ti-Ti grain as a result of the intimate contact between the TiO_2 and rGO. Also, the photoanodes absorption of dye was relatively improved by the addition of rGO ascribed to the larger surface area for dye loading. Considering these facts, it is thereby expected that the photoelectric properties of the DSSCs could be significantly enhanced.

4.3.2 Photovoltaic performances of dye sensitized solar cells

The photocurrent density-voltage (*J*-V) characteristic of the commercialized N719, green chlorophyll and red anthocyanin dyes-sensitized DSSCs under 100mW.cm^{-2} stimulated solar irradiation were shows in Figs. 4.23, 4.24 and 4.25, while their photoelectrochemical characteristics were presented on Tables 4.9, 4.10 and 4.11. Fig.4.26 illustrates the comparison of PCE of DSSCs based on the commercialize N719, green chlorophyll dyes and red anthocyanin dye for different weight rGO nanocomposite.

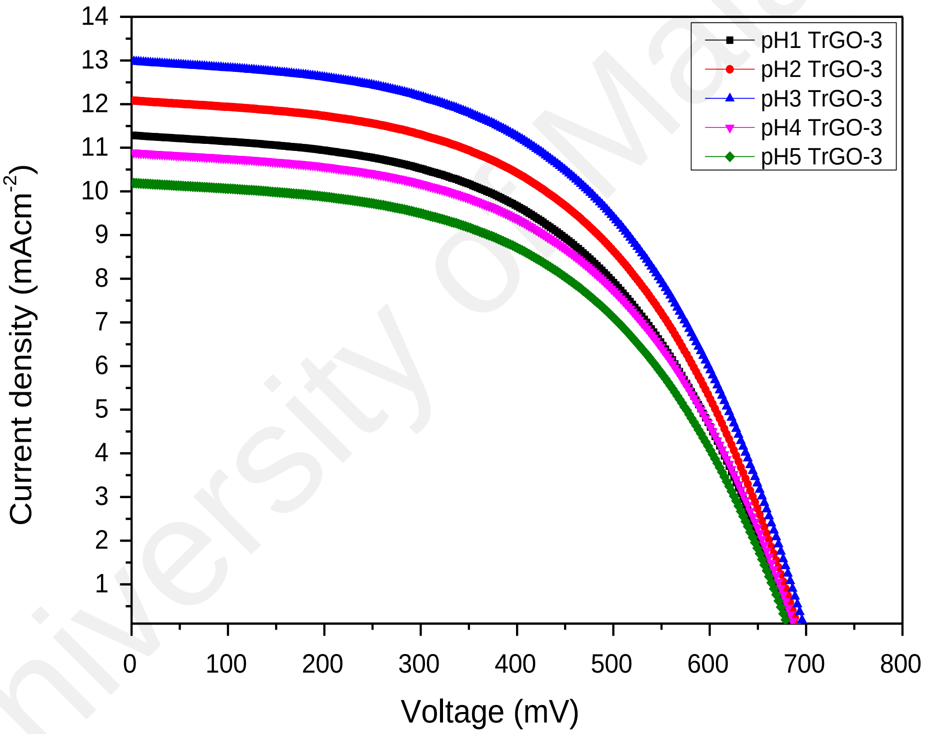

Figure 4.23: Photocurrent density-voltage characteristic of pH1 TrGO-3, pH2 TrGO-3, pH3 TrGO-3, pH4 TrGO-3 and pH5 TrGO-3 using conventional N719 dye.

Table 4.9: Photovoltaic efficiency characteristic DSSCs using conventional N719 dye.

Sample	Voc(mV)	*J*sc(mA cm^{-2})	FF(%)	η(%)
pH1 TrGO-3	683.59	11.28	0.52	4.01
pH2 TrGO-3	690.92	12.08	0.52	4.34
pH3 TrGO-3	695.80	12.976	0.53	4.79
pH4 TrGO-3	686.04	10.89	0.52	3.88
pH5 TrGO-3	678.71	10.19	0.52	3.60

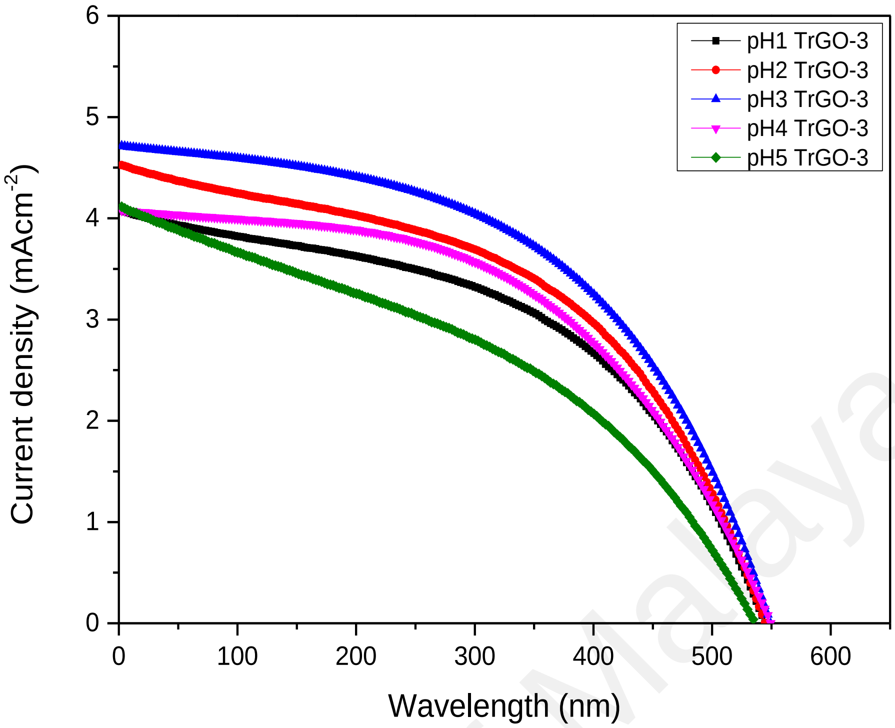

Figure 4.24: Photocurrent density-voltage characteristic of pH1 TrGO-3, pH2 TrGO-3, pH3 TrGO-3, pH4 TrGO-3 and pH5 TrGO-3 using green chlorophyll dye.

Table 4.10: Photovoltaic efficiency characteristic DSSCs using green chlorophyll dye.

Sample	**Voc(mV)**	***J*sc(mA cm^{-2})**	**FF(%)**	**ŋ(%)**
pH1 TrGO-3	544.43	4.07	0.44	0.98
pH2 TrGO-3	549.32	4.52	0.48	1.19
pH3 TrGO-3	549.43	4.72	0.51	1.32
pH4 TrGO-3	549.32	4.07	0.51	1.14
pH5 TrGO-3	539.55	4.11	0.39	0.87

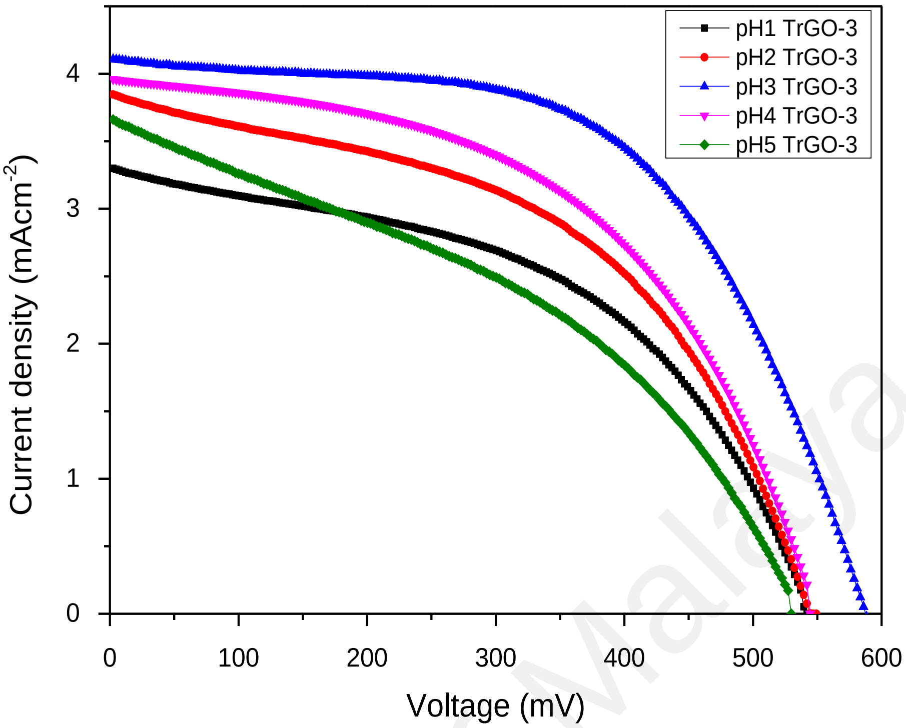

Figure 4.25: Photocurrent density-voltage characteristic of pH1 TrGO-3, pH2 TrGO-3, pH3 TrGO-3, pH4 TrGO-3 and pH5 TrGO-3 using red anthocyanin dye.

Table 4.11: Photovoltaic efficiency characteristic DSSCs using red anthocyanin dye.

Sample	**Voc(mV)**	***J*sc(mA cm^{-2})**	**FF(%)**	**ŋ(%)**
pH1 TrGO-3	541.99	3.29	0.49	0.88
pH2 TrGO-3	549.32	3.85	0.48	1.01
pH3 TrGO-3	546.32	4.08	0.61	1.36
pH4 TrGO-3	544.43	3.96	0.51	1.09
pH5 TrGO-3	529.79	3.66	0.39	0.76

From all of *J*-V curves (Figs. 4.23, 4.24, 4.25) and photovoltaic characteristics (Table 4.9, 4.10, and 4.11) it is interesting to note that TrGO-3 nanocomposite showed improvement in photovoltaic generation with the variation of pH value of nanocomposite regardless of the dye type used DSSCs. The highest samples value for all three dyes are pH3 TrGO-3 with N719 dye-sensitized illustrated photovoltaic efficiency (4.79%) compared to natural dye of the green chlorophyll dye-sensitized TrGO-3 (1.32%) and red anthocyanin dye (1.36%). It was also found that, in Fig. 4.26, the overall photovoltaic efficiency *(η)* of DSSCs improved by the variation of pH towards the nanocomposite rGO. This is associated with the fact that the addition of rGO enhanced the transfer path for the ultrafast ejected electrons to travel between TiO_2 particle.

Apart from that, as shown in Fig. 4.26, from the pattern of photovoltaic characteristics shows improvement in all characteristics of DSSCs from pH1 to pH3. The positive impact of increment in performance was contribute by the improved growth of TiO_2 crystalline on rGO surface. pH plays main role in crystalline growth as it will control the growth of crystal with desired phase. As for this case of DSSC, anatase phase was the most desired phase due to the stability concern of electron travels across the semiconductor and DSSC device(Han, Yu, & Liu, 2013; Isley & Penn, 2008; Lai et al., 2015). The DSSCs analysis also ph4 and pH5 DSSC shows unstability on the performance of DSSC and the overall performance was decreased. From the FESEM, the morphology of both of this samples shows the growth of TiO_2 on the rGO surface become bulky and unevenly distributed on the rGO film. Therefore, it give impact on the electron transfer in the semiconductor where it effect the overall efficiency performance of the DSSC device.

Overall performance shows positive impact accordingly with the support of morphology where with suitable pH the morphology become more supportive to the electron transfer in the semiconductor and improves the charge separation across the device(Tsega & Dejene, 2017). On top of photovoltaic efficiency and current density, the samples shows massive improvement in V_{oc} production in pH1, pH2 and pH3 TrGO-3. Correspondingly, the V_{oc} improvement led to the reduction in the Fermi level in the photoanode and the Nerst potential of redox couple in the electrolyte when it was under illumination (L. Chen et al., 2013). From the PL and absorption spectra, the sample most likely are in blue shift where it shows pools of oxygen vacancy that can contribute to the increment in the ability of the crystal to absorb light(Tsega & Dejene, 2017). However, DSSC with higher pH values (pH 4 and pH 5) shows lost its performance as a consequence of the drop in the conversion efficiency. This is mainly due to the antagonistic effect between the rGO and the uneven growth of TiO_2 crystal makes it hard to compete for the visible light thus contribute to the decrease in performance.

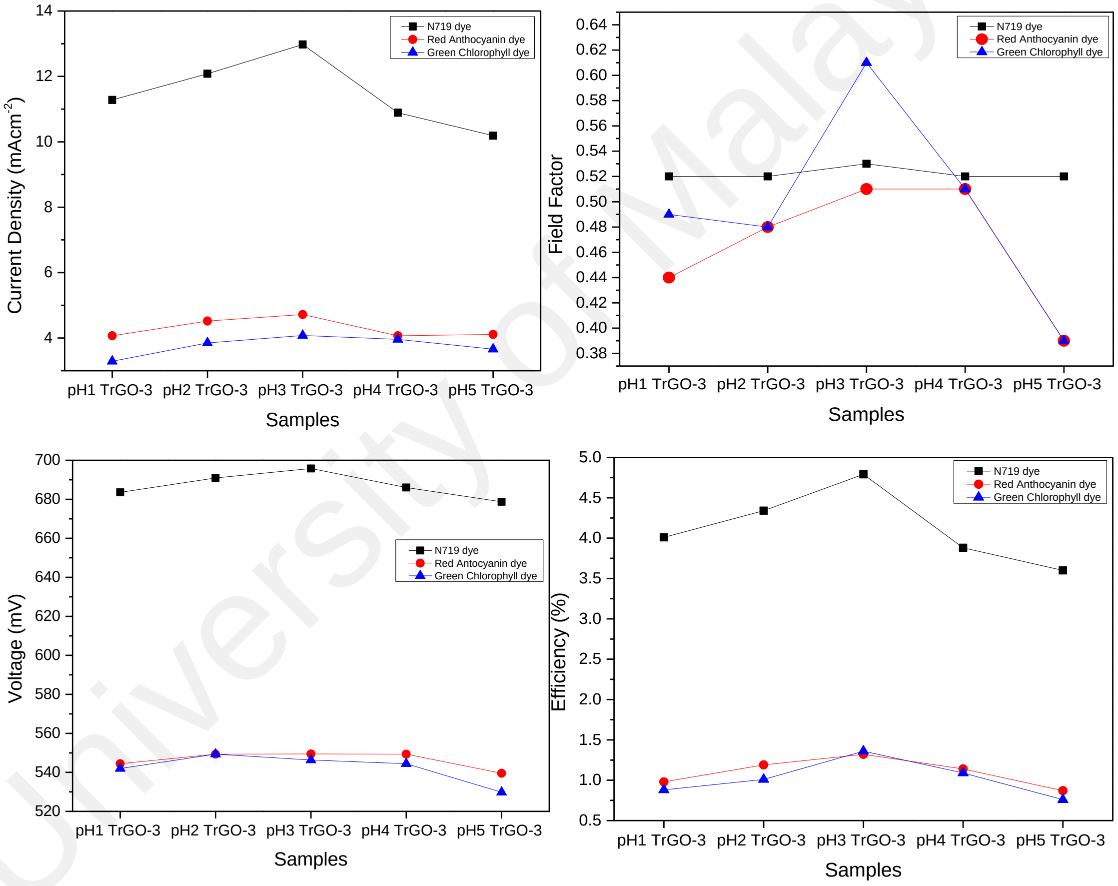

Figure 4.26: DSSCs analysis of all samples; a) current density; b) fill factor; c) voltage short circuit; d) efficiency

It is undeniable that when the surface of photoanode was illuminated with sunlight, the ultrafast electron transport could be enhanced with the support of excellent conductivity of rGO. From the previous study, it was known that the resistance between the grain and path could be minimized by incorporating rGO into TiO_2 as rGO tends to build the bridge between TiO_2 (M. Zhu et al., 2014). This help in enhancing the charge separation, electron collector and transportation of photogenerated electron as well as reducing the probability of charge recombination. This is also beneficial for the photo-generated electron to transfer without suffering from massive resistance (Sharma et al., 2013; Zhao et al., 2013; Zhao et al., 2015; Zhi et al., 2015).

4.3.3 EIS analysis of dye sensitized solar cells.

Electrochemical impedance spectroscopy (EIS) was employed in the present study to determine the electronic properties behavior and the internal resistance in the DSSCs device. The EIS was then analysed using the stimulated model of internal circuit of DSSCs to identify the resistance of electron charge between each surface materials. From Fig.4.27 (A, B & C), it shows 3 semicircles where the first semicircle was barely visible due to the large middle frequency semicircle that overlaps the shape of semicircle of the middle frequency, but regardless of that. From Table 4.11, table 4.12 and Table 4.13, the Nyquist plot show almost similar value of R_s and R_{CE} where it describe the materials for counter electrode and electrolyte were same for all DSSCs devices for all type of dye. When the first semicircle decreased, it indicted that the fast electron transfer at counter electrode and electrolyte interface. Furthermore, the second semicircle R_{CT} represents the photoanode/dye/electrolyte resistance. For N719 dye, the value of R_{CT} for pH1TrGO-3, pH2TrGO-3, pH3TrGO-3, pH4TrGO-3and pH5TrGO-3 were 92.3Ω, 58.3Ω, 50.2Ω, 99.0Ω and 125.3Ω respectively. The red anthocyanin dye recorded 197.0Ω, 152.0Ω, 130.0Ω, 244.0Ω and 268.4Ω for pH1TrGO-3, pH2TrGO-3, pH3TrGO-3, pH4TrGO-3and pH5TrGO-3. Meanwhile, green chlorophyll dye R_{CT} value for pH1TrGO-3, pH2TrGO-3, pH3TrGO-3, pH4TrGO-3and pH5TrGO-3 were189.0Ω, 142.0Ω, 130.0Ω, 254.0Ω and 298.0Ω.

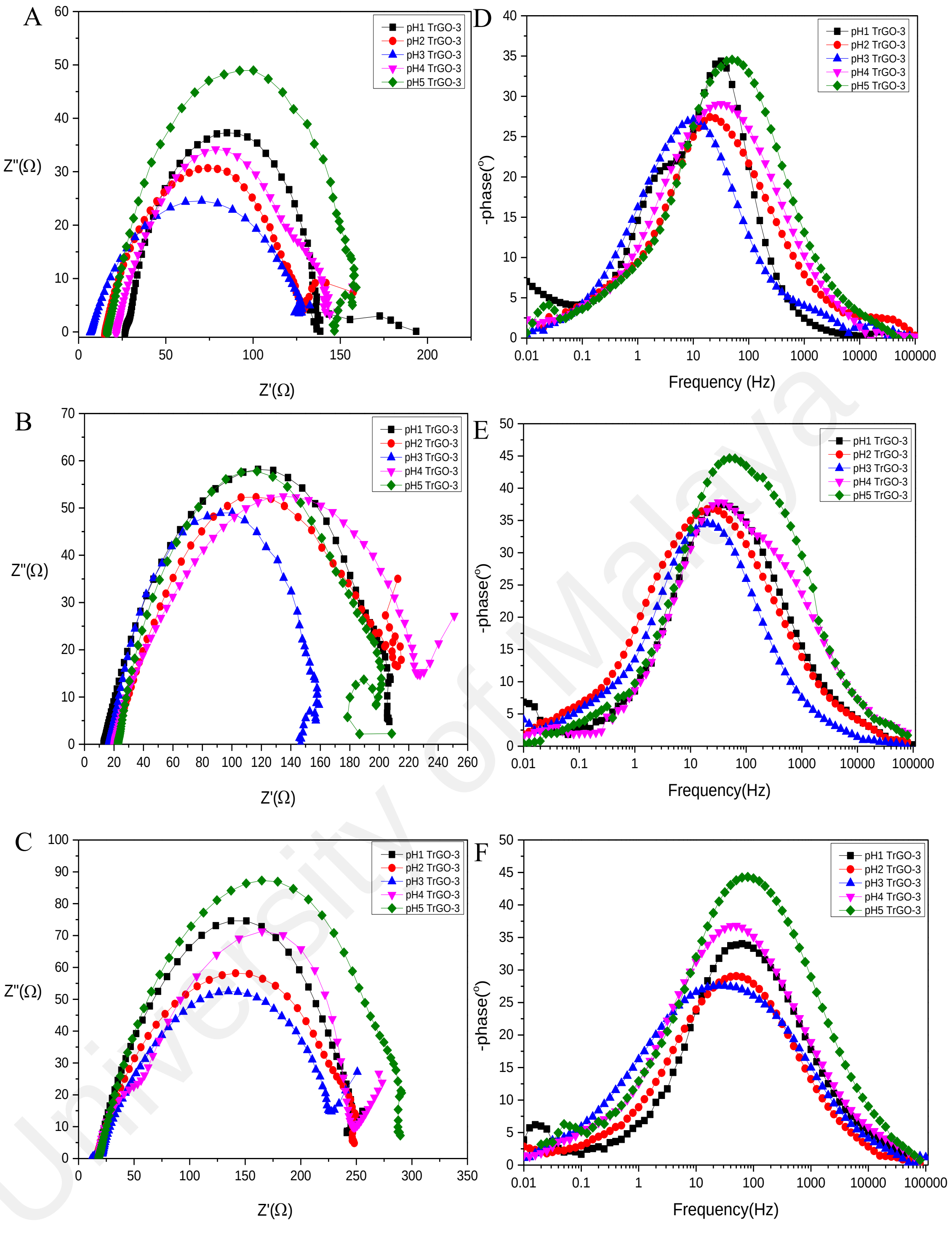

Figure 4.27: EIS analysis (A, B & C) Nyquist plot for commercialize N719 dye, green chlorophyll dye and red anthocyanin dye; (D, E & F) Bode plot for commercialize N719 dye, green chlorophyll dye and red anthocyanin dye.

These values indicate the electrocatalytic activity in the DSSCs where the lowest value of R_{CT} represents the highest electrocatalytic activity then other DSSCs. In this case, for red anthocyanin, N719 and natural green chlorophyll dye TrGO-3 recorded highest electrocatalytic activity compared to other DSSCs. In the same time, TrGO-3 had the lowest recombination resistance and lowest electron transmission resistance in the photoanode. From the previous study, rGO create new path in the photoanode structure and the generated electron travels quickly to fill the anode surface. Subsequently, rGO helps in acceleration of the interfacial electron transfer which will reduce the electron-hole recombination with the aid of good crystalline structure. With optimized pH for the growth of TiO_2 dopants on rGO film will creating good surface contact for the dye and semiconductor, increased in the performance of DSSCs, supressed the recombination of electron across the semiconductor and enhance the charge transfer between the interfaces of the material(Hu et al., 2017; Liu et al.; San Esteban & Enriquez, 2013).

Table 4.12: EIS analysis of N719 dye DSSCs.

Sample	R_s(Ω)	R_{CT}(Ω)	R_{CE}(Ω)	Bode Peak (Hz)	Electron Lifetime τ_n(ms)
pH1 TrGO-3	21.5	92.3	37.1	25.119	6.34
pH2 TrGO-3	20.9	58.3	38.2	15.849	8.38
pH3TrGO-3	20.0	50.2	37.6	10.000	16.32
pH4TrGO-3	20.9	99.0	36.7	31.623	5.03
pH5 TrGO-3	21.7	125.3	37.8	50.119	3.18

Table 4.13: EIS analysis of red anthocyanine dye DSSCs.

Sample	R_s(Ω)	R_{CT}(Ω)	R_{CE}(Ω)	Bode Peak (Hz)	Electron Lifetime τ_n(ms)
pH1 TrGO-3	22.6	197.0	38.7	39.811	4.00
pH2 TrGO-3	21.3	152.0	38.1	25.119	6.34
pH3TrGO-3	20.3	130.0	37.7	19.953	8.37
pH4TrGO-3	22.6	244.0	40.7	31.623	5.03
pH5 TrGO-3	24.4	268.4	39.7	50.119	3.18

Table 4.14: EIS analysis of green chlorophyll dye DSSCs.

Sample	**$R_s(\Omega)$**	**$R_{CT}(\Omega)$**	**$R_{CE}(\Omega)$**	**Bode Peak (Hz)**	**Electron Lifetime τ_n(ms)**
pH1 TrGO-3	22.6	189.0	38.7	39.811	4.00
pH2 TrGO-3	21.3	142.0	38.1	25.119	6.34
pH3TrGO-3	20.3	130.0	37.7	19.953	8.37
pH4TrGO-3	22.6	254.0	40.7	31.623	5.03
pH5 TrGO-3	24.4	298.4	39.7	63.096	2.52

In order to support the EIS analysis (Figs. 4.27 (D, E & F)), bode plots contribute to the information of electronics transfer and recombination of electron holes lifetime in DSSCs photoanode-electrolyte interface. From the bode plot, electron lifetime (τ_n) could be obtained from the peak angular frequency by using the following equation (3.4):

$$\tau_n = \frac{1}{2}\pi f_{max} \qquad (3.4)$$

where f_{max} is the peak frequency of bode phase. As shown in table 4.5, table 4.6 and table 4.7, the recorded electron lifetime for N719 dye were 6.34ms, 8.38ms, 16.32ms, 5.03ms and 3.18ms. For natural dye, red anthocyanin dye recorded 4.00ms, 6.34ms, 8.37ms, 5.03ms and 3.18ms electron lifetime while the electron lifetime for green chlorophyll dye were 4.00ms, 6.34ms, 8.37ms, 5.03ms and 2.52ms. From the bode plot, shifting of the characteristic peak into lower frequency demonstrate with increase in electron transfer. The recombination in the photoanode/dye/electrolyte interface reduced when there is an increase of electron lifetime producing a reduction of recombination (Sharma et al., 2013). From the tables, the increase in electron lifetime was TrGO-3 regardless type of dye which suggests the recombination rate of injected electron have improved and leads to faster diffusion rate, thus increasing J_{sc} and PCE valus (Sacco et al., 2014; Sharma et al., 2013).

4.4 Different calcination temperature for Anatase phase rGO nanocomposite TiO_2 DSSCs

Calcination is a process to enhance the crystalline structure of a nanoparticle especially Titanium Dioxide. TiO_2 crystalline structure are dependent on the calcination temperature due to it will change phase in different temperature. In this case we are tailoring anatase phase. The previous sample we calcine the sample with 400 ^oC but for this parameter we calcine the photoanode to 450 ^oC. As this nanocomposite was synthesized, no higher temperature was used as it will completely turns the sample into rutile phase as synthesized TiO_2 have lower calcination range temperature. To enhance the electron transfer across nanocomposite structure. The crystalline that attached on the rGO film need to possess the best morphology structure to enhance the electron transport across the semiconductor photoanode film. The first testing to verified the crystalline phase of the sample was XRD.

4.4.1 Morphological characterization for different calcination temperature

Fig. 4.28 exhibits the XRD patterns of TrGO nanocomposite (TrGO-1, TrGO-2, TrgO-3, TrGO-4 and TrGO-5) on 450^oC calcination temperature. From Fig. 4.28, all the diffraction peaks can be satisfactorily indexed to anatase and some shows small amount of rutile appearance. The diffraction spectra for TiO_2 showed peaks of anatase at 2θ = 25.36^0, 37.90^0, 48.16^0, 54.05^0, 55.21^0, 62.87^0, 68.98^0, 70.479^0 and 75.28^0 correspond to the (101), (103), (004), (200), (105), (211), (204), (116), (220) and (215) diffraction planes respectively. For small amount of rutile can be viewed at 26.83^o with (110) diffraction plane. The rGO peak was overlap due to broad spectrum of rGO at 24^0.

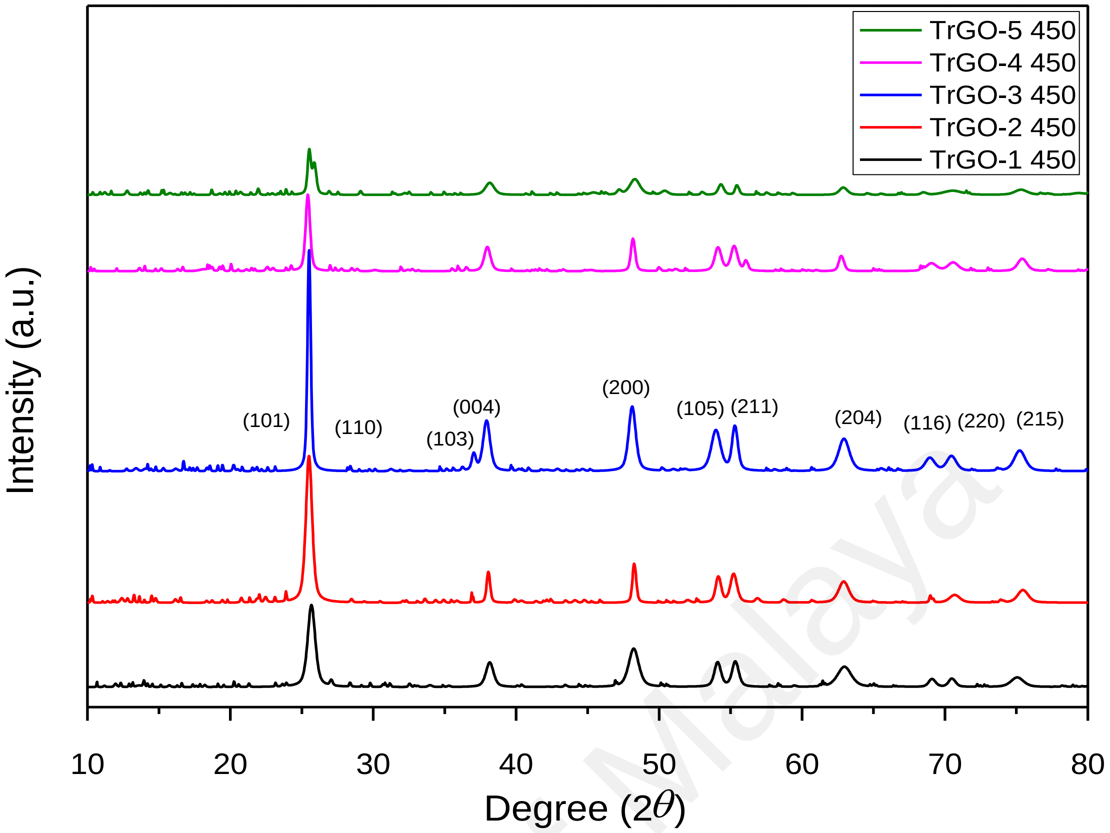

Figure 4.28: X-Ray diffraction (XRD) spectra of TrGO-1 450, TrGO-2 450, TrGO-3 450, TrGO-4 450 and TrGO-5 450.

For TrGO-5 450, the peak intensity become lower and become more border than all other samples due to less crystallinity characteristics showed in the TrGO-5 450 sample due to excess of graphene content (Cheng & Stadler, 2015; How et al., 2014; Ling et al., 2013). From the XRD pattern, TrGO-3 450 and TrGO-4 450 shows the highest crystallinity due to sharp and intense peak at 25° peak. The Debye Scherrer Equation has been employed to measure the average particle size of TiO_2 that synthesized. The particle size was estimated at 31.8 nm for TrGO-1 450, 22.6 nm for TrGO-2 450, 13.5 nm for TrGO-3 450, 22.7 nm for TrGO-4 450 and 35.6 nm for TrGO-5 450. This shows that the anchoring of rGO does gives a little influence on the crystallinity and crystallite size of TrGO nanocomposite. Mixed phase between anatase and rutile were found in TrGO-3 450 but not utterly visible as one of main peak.

FTIR spectroscopy was used in the present study to evaluate the functional groups on TrGO 450 nanocomposite. As illustrated in Fig. 4.29, TrGO showed Ti-O-Ti and Ti-O-C stretching vibrations within the broad band below 1000cm^{-1} respectively From Fig. 4.29, it was also observed that TrGO nanocomposite exhibited some characteristic peaks which could be assigned to the C=C stretching (1541 cm^{-1}), C=O stretching (1695 cm^{-1}) and –OH stretching (3440 cm^{-1}) (Karimi et al., 2014). There was also a strong peak located at 2357cm^{-1} assigned to the CO_2 contamination (Zhang et al., 2014). In Fig. 4.2, there were peaks in the region between 3600 and 3900 cm^{-1} corresponding to the formation of oxygen vacancies induced by the formation of Ti^{3+} species (Samsudin et al., 2015), while the peaks at 3724 and 3845 cm^{-1} were attributed to the Ti^{3+}-OH formation. Moreover, the peak at 3674 cm^{-1} corresponded to the formation of Ti^{4+} in the TiO_2.

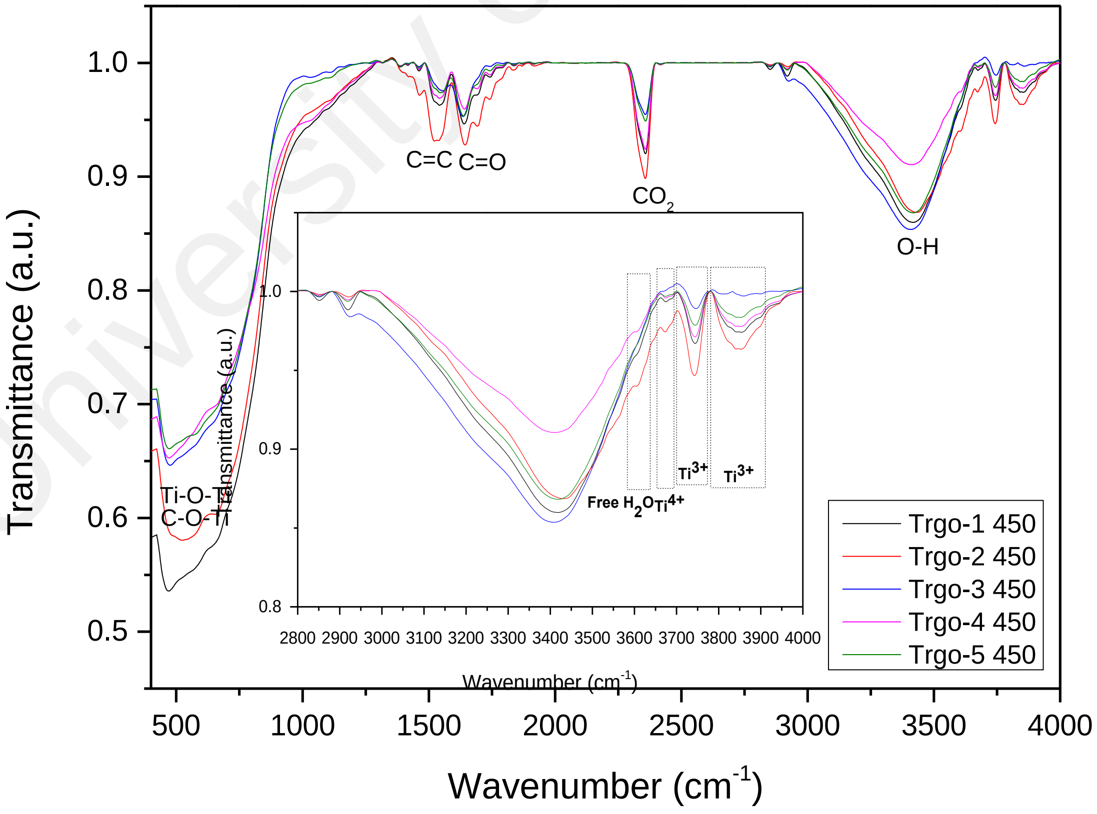

Figure 4.29: Fourier Transform Infrared (FTIR) TrGO-1 450, TrGO-2 450, TrGO-3 450, TrGO-4 450 and TrGO-5 450.

Next, Raman spectroscopy was employed in the present study to characterize the structural properties of the graphene materials. Fig. 4.30 shows the Raman of TrGO 450 spectra. It is clear that all TrGO 450 possessed the anatase phase consisting of five major vibration peaks as reported previously by Otakar et al. (Frank et al., 2012) at 144 cm^{-1} (E$_g$), 197 cm $^{-1}$ (E$_g$), 395 cm^{-1} (B$_{1b}$), 513 cm^{-1} (A$_{1b}$), and 635cm^{-1} (E$_g$) while no major peak of rutile appeared in Raman spectroscopy.

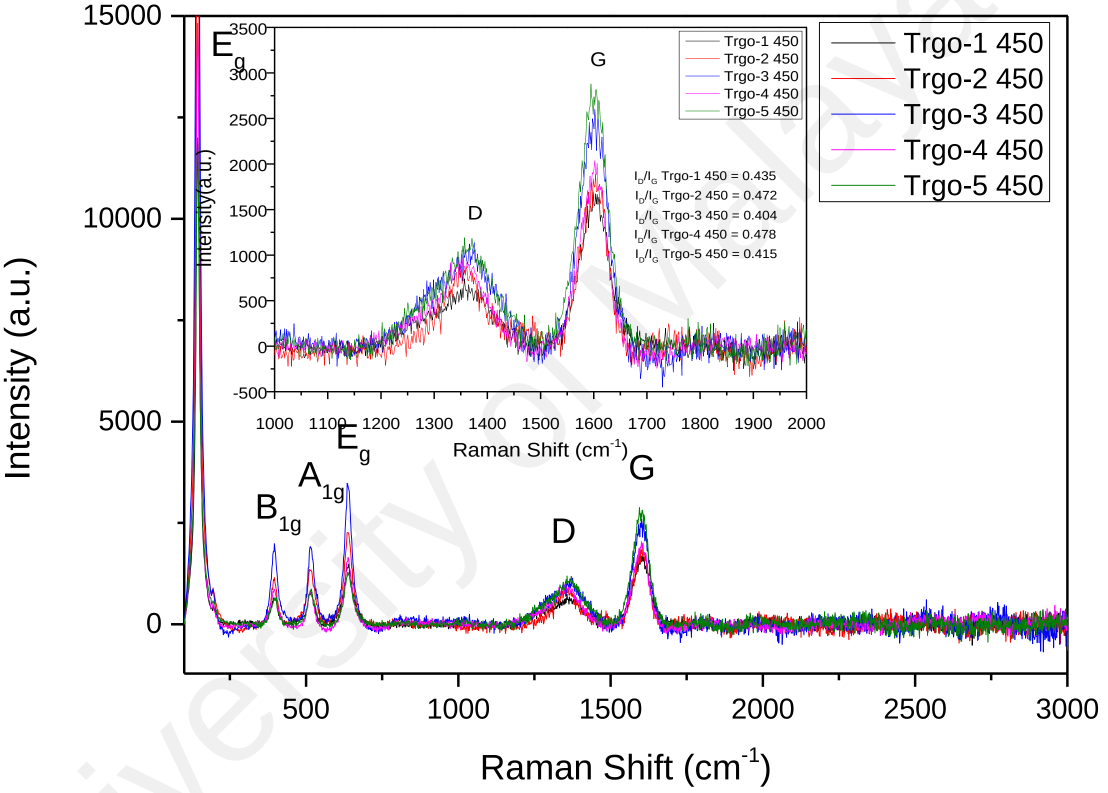

Figure 4.30: Raman spectroscopy TrGO-1 450, TrGO-2 450, TrGO-3 450, TrGO-4 450 and TrGO-5 450.

The intensity of TrGO-3 450 is the highest compared to other parameter. Moreover, all TrGO 450 showed two broad vibration bands within 1200-1700 cm^{-1}, in which the D band (attributed to the breathing mode of A$_{1g}$ symmetry involving phonons near the K zone boundary) appeared at 1309 cm^{-1}, while the G band (originates from sp^2 in-plane vibration mode of carbon atoms) at 1583cm^{-1}. As reported by Ahmed et al. (Ahmad et al., 2015), the intensity ratio of D and G bands(I_D/I_G) could represent the structure, defects and size of the graphene. Correspondingly, I_D/I_G of TrGO sample is in between 0.400 to 0.472 and the lowest intensity ratio was TrGO-3 with 0.402. The intensity ratio for nanocomposites indicates most all of the sample suggesting a low level of defect, high crystallinity and small size of rGO in TrGO especially TrGO-3.

The PL spectrum was used to identify the behaviour of photo-generated electron and holes in the semiconductor layer of DSSCs. Fig. 4.31 shows the PL spectra TrGOs 450 nanocomposites. The presence of PL peaks in the wavelength range of 450-750nm indicated that TrGO nanocomposites are the indirect band gap semiconductors. It was also determined that the presence of a peak near 330nm was mainly attributed to the ligand to metal charge transfer in TiO_2 (O^{2-} to Ti^{4+}), while the peaks at 450nm and 660nm signified the surface oxygen vacancy related defects. Furthermore, all peaks were blue shifted in the Raman peak. This implies the transformation of un-coordinated

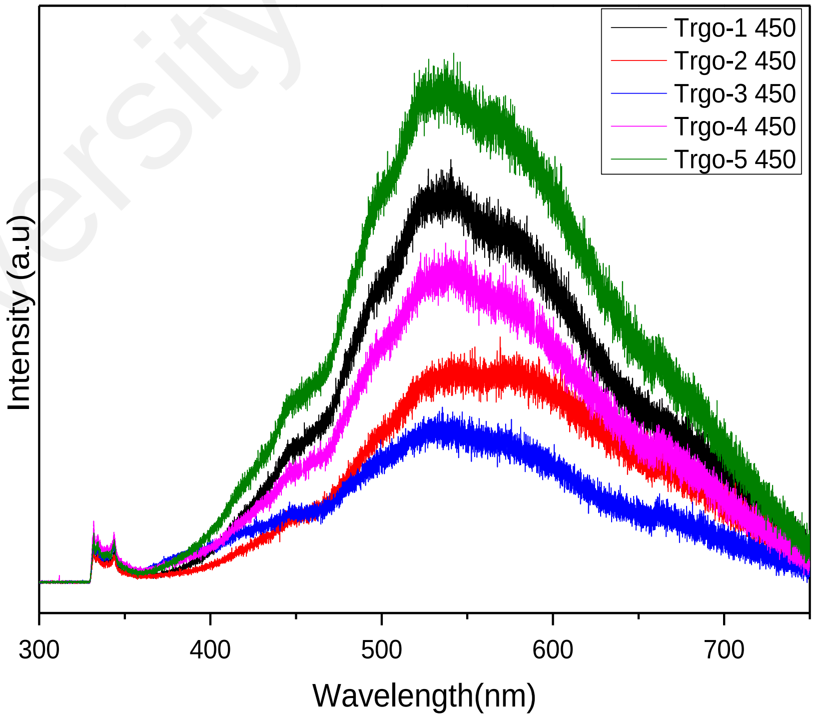

Figure 4.31: Photoluminescence (PL) spectra of TrGO-1 450, TrGO-2 450, TrGO-3 450, TrGO-4 450 and TrGO-5 450.

Ti^{3+} ions to the surface of oxygen vacancy. The green band with peak position at 540nm was also an indication of the surface oxygen vacancy of anatase (101) phase.

According to Liu et al. [19], the red shift of the PL spectra between 600 and 620 nm is attributed to the oxygen-vacancy-related defects as a result of the oxygen atom removal by annealing in an inert argon atmosphere where the removal of the oxygen atom will create electron traps under the conduction band. Specifically, the electron traps usually locate at 0.7 to 1.6 eV below the conduction band edge energy. Ti^{4+} will be reduced to Ti^{3+}considering the removal of oxygen atom can create lone pair of electrons (Jin et al., 2015).

Furthermore, as shown in Fig. 4.31, TrGO-5 450 photoanode displayed higher PL intensity while TrGO-3 450 shows lower PL intensity. The PL intensity was mainly influenced by the recombination rate of electron-hole pairs. It has also been reported in literatures that a lower intensity of PL spectra implied an increase in charge separation and a decrease in the rate of electron-hole pair recombination (Gupta et al., 2010; Min et al., 2012; Raghavan et al., 2015). Which means TrGO-3 450 and TrGO-2 450 possessed low recombination rate compared to others sample of TrGO 450. A negative kickback was showed in sample TrGO-5 450 where the intensity was the highest maybe due to less crystallinity in the morphology of the sample. To explore more on the morphology state of the nanocomposite film, absorption spectra and tauc plot were study to know ability of light absorption and energy gap of the semiconductor nanocomposite film.

Fig. 4.32 displays the absorption spectra of all TrGO 450 nanocomposites. Correspondingly, UV-Vis spectra give the information regarding to the absorption ability of the photoanode and the bandgap of the anatase semiconductor oxide film. It is noteworthy that the optical absorbance spectrums of all the films were in the range of

~300nm to 430nm. The photon absorption ability of all TrGO 450 samples peak shifts towards the blue region. The blue shifting of the absorbance spectra also gives us a hint that the crystalline size of TrGO was smaller.

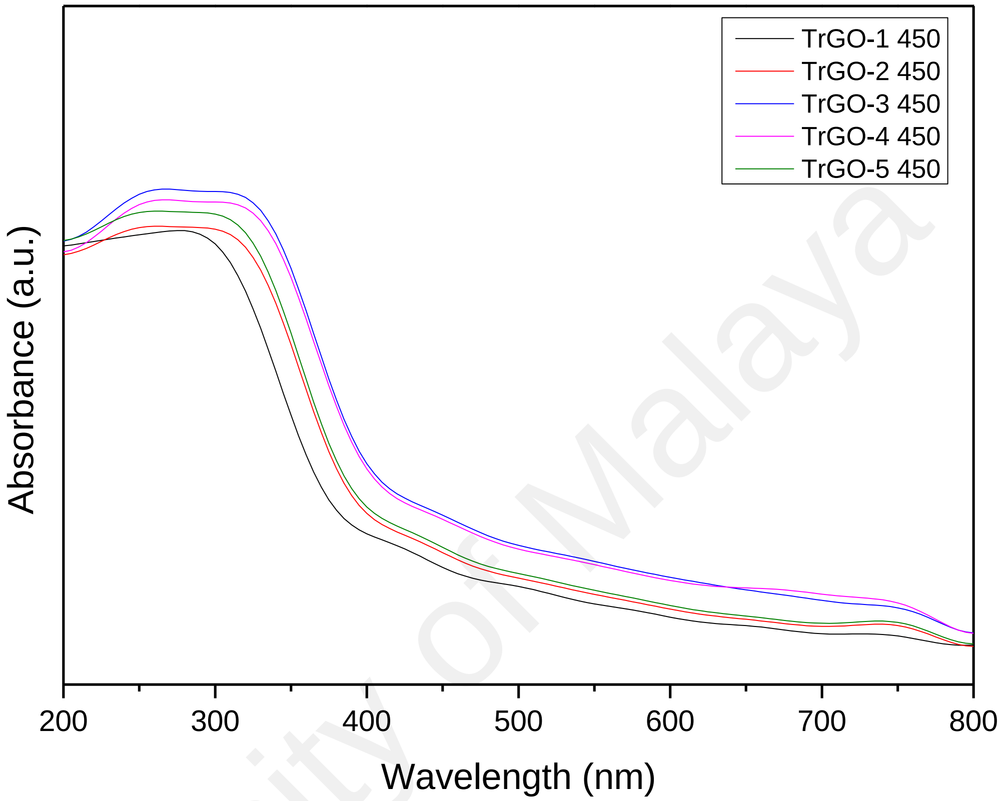

Figure 4.32: Absorption plot of TrGO-1 450, TrGO-2 450, TrGO-3 450, TrGO-4 450 and TrGO-5 450.

Fig. 4.33 shows the Tauc plot, while Table 4.14 tabulates the energy band gap (from the UV spectra) TrGO-3 with calcination temperature 450°C. It was found that, based on Table 4.14, the optical energy band gap indicated the bandgap of samples were narrow from 2.93eV to 2.72eV. The pattern of energy band shows a bell pattern where the sample narrowing the band gap fromTrGO-1 450 and TrGO-3 450 but slightly increases starting on TrGO-4 450 and TrGO-5 450. The smallest band gap was detected to be approximately 2.72eV (TrGO-3 450). The band gap reduction mainly attributed to

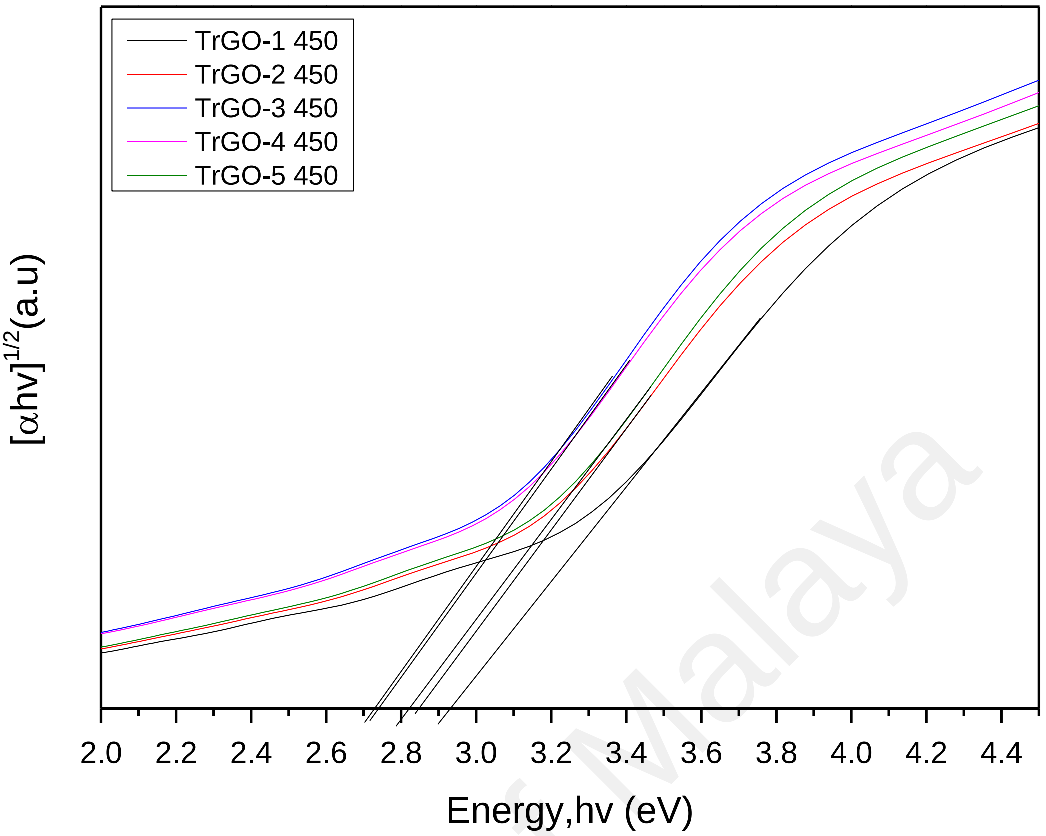

Figure 4.33: Tauc plot of TrGO-1 450, TrGO-2 450, TrGO-3 450, TrGO-4 450 and TrGO-5 450.

Table 4.15: Energy band gap from UV spectra.

Sample	Band Gap (eV)
TrGO-1 450	2.93
TrGO-2 450	2.84
TrGO-3 450	2.72
TrGO-4 450	2.73
TrGO-5 450	2.81

the presence of TiO_2 nanoparticles acted as potential dopants to rGO surface where it creates an impurity energy level within the valence band (VB) and conduction band (CB) (O2p – Ti3d). This statement was convinced with the reduction of intensity in the PL spectra of the nanocomposite. The bandgap of TrGO 450 is lower than the TrGO nanocomposite due to a little occurrence of rutile will lower down the energy band gap of nanocomposite.

FE-SEM and HR-TEM were used to determine the morphology of the nanocomposites. Based on the surface morphology of TrGO (Figs. 4.34 and 4.35), two main conclusions could be drawn: (i) TiO_2 loaded between rGO with different shape of crystalline; and (ii) the rGO layer sheets looks like rock mountain with TiO_2 grown on it. On top of that, FE-SEM images (as shown in Fig. 4.34) suggest that the TiO_2 microspheres were encapsulated well in rGO sheets with the increase in rGO content in the TrGO nanocomposite.

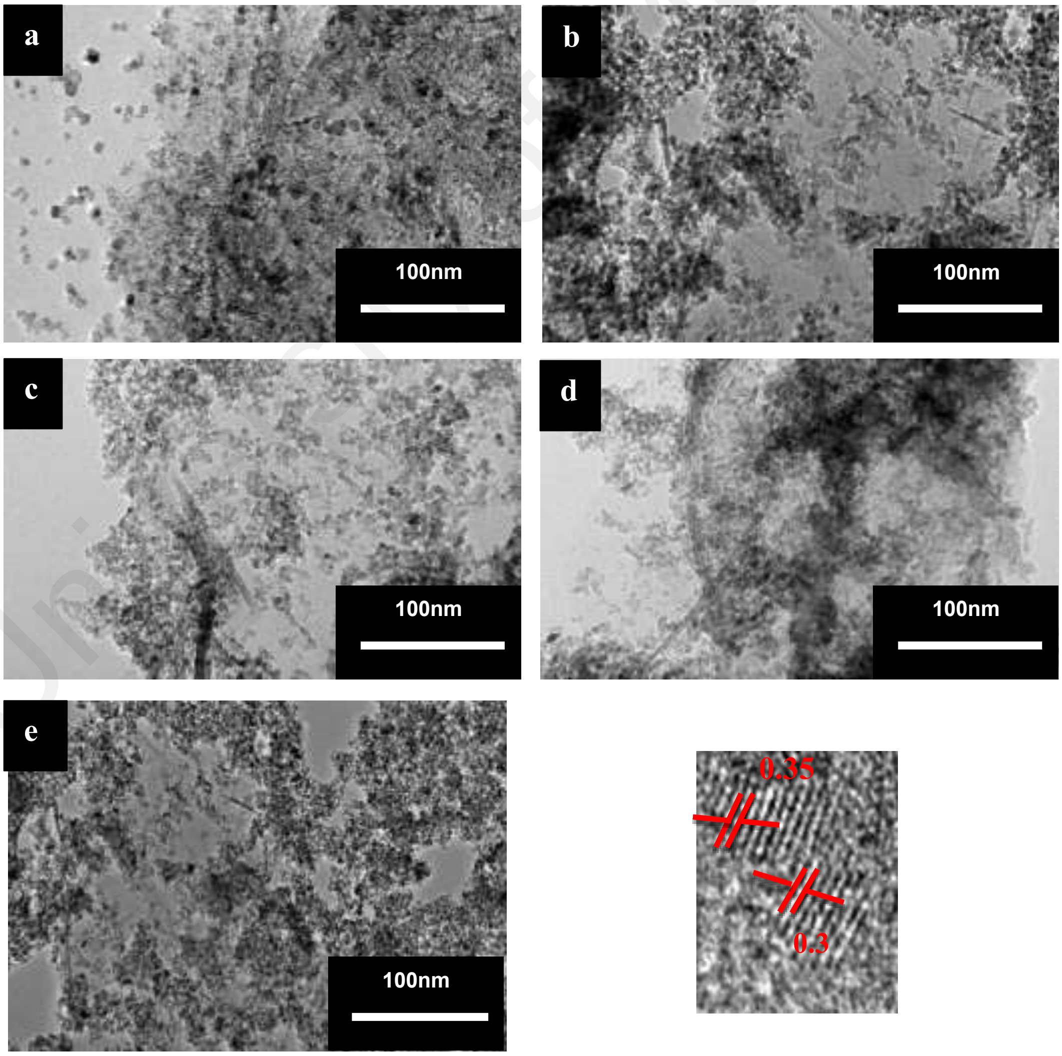

Figure 4.34: HR-TEM images of TrGO film on 50k magnification (a) TrGO-1 450, (b) TrGO-2 450, (c) TrGO-3 450, (d) TrGO-4 450 and (e) TrGO-5 450.

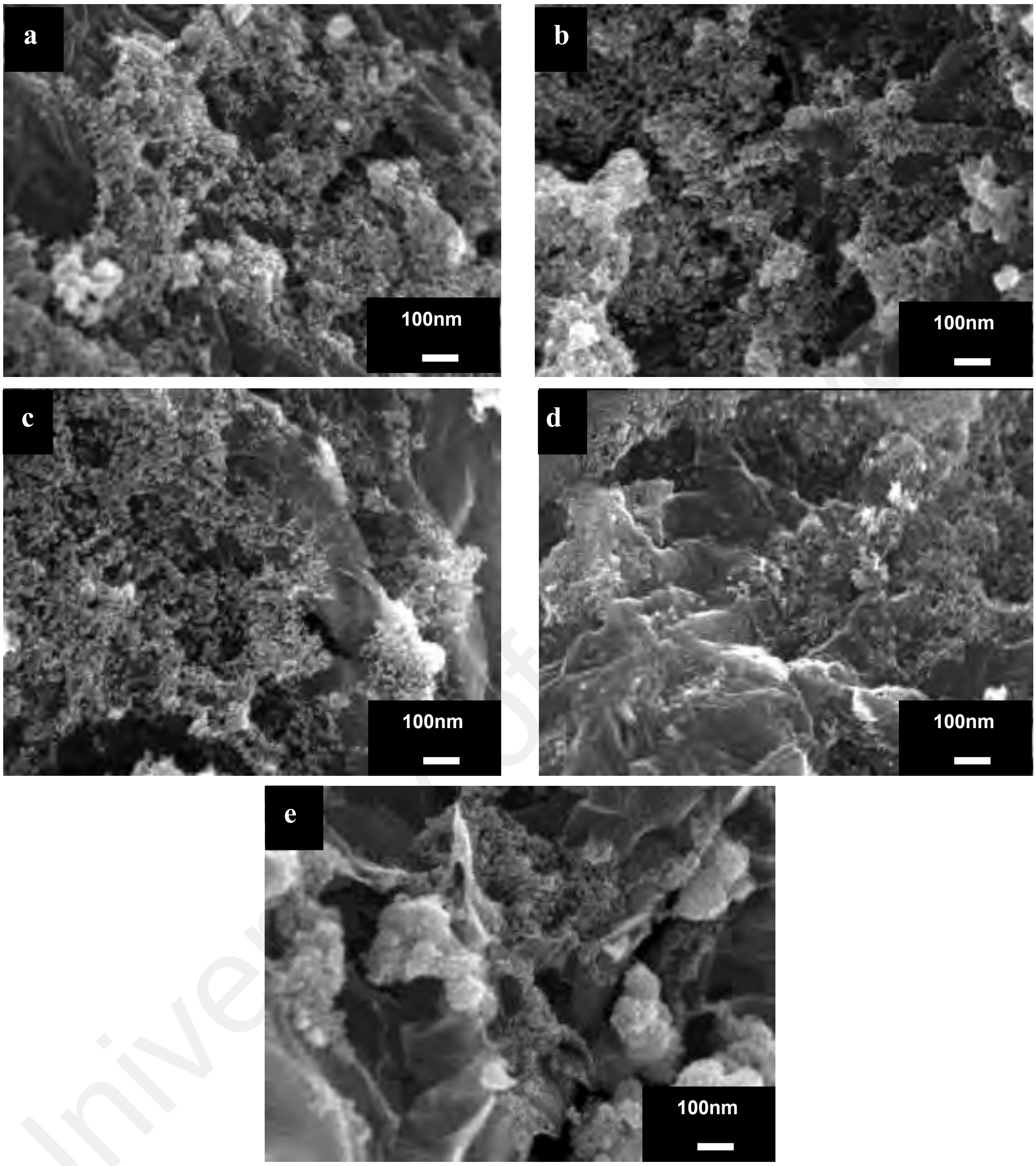

Figure 4.35: FESEM images of TrGO film on 50k (a) TrGO-1 450, (b) TrGO-2 450, (c) TrGO-3 450, (d) TrGO-4 450 and (e) TrGO-5 450.

From the HRTEM image the nanocomposite showed less crumple effect at sample TrGO-3 450 and TrGO-5 450 compared to other nanocomposite samples. From HR-TEM images (Fig. 4.22), it was found that the TiO_2 particles with the particle size of ~ 13nm – 32nm were in-situ grown on the surface of rGO during the synthesis of TrGO particle. The fringe spacing of TiO_2 particle on rGO was estimated to be 0.35nm ensure the presents of (101) anatase. The reduction in size for TiO_2 attribute from the rGO that as it is an electron rich material/ surface where the electron attraction between Ti^{4+} and the rGO surface contributes to reduction in size of TiO_2 (Samsudin et al., 2015) . With the addition of pluronic template, rGO sheet affects more on the pulling of porous template where it increases the porosity and active area for placeholder of dye sensitization.

4.4.2 Photovoltaic performances of dye sensitized solar cells.

Figs. 4.36, 4.37 and 4.38 show the photocurrent density-voltage (*J*-V) characteristic of the commercialized N719, green chlorophyll and red anthocyanin dyes-sensitized DSSCs under $100mW.cm^{-2}$ stimulated solar irradiation, while Tables 4.15, 4.16 and 4.17 summarized and tabulated their photovoltaic characteristics. Fig.4.39 illustrates the comparison of PCE of DSSCs based on the commercialize N719, green chlorophyll dyes and red anthocyanin dye for different weight rGO nanocomposite. From the plotted curves, the improvements of DSSC device influenced by the ability of dye to travel acrossed suitable semiconductor oxide film. Some samples showed astonishing improvements in terms of V_{oc} or J_{sc} and thus influenced the increment in overall photovoltaic efficiency. This could be related to the reduction in resistances of each layer, the charge transport and recombination properties.

.

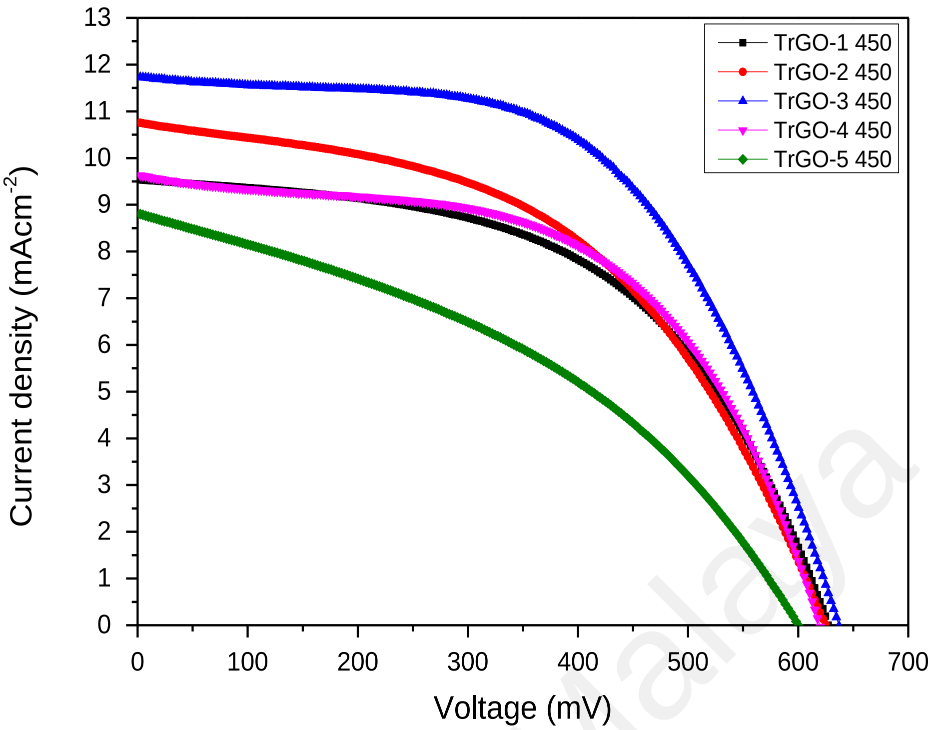

Figure 4.36: Photocurrent density-voltage characteristic of TrGO-1 450, TrGO-2 450, TrGO-3 450, TrGO-4 450 and TrGO-5 450 using conventional N719 dye.

Table 4.16: Photovoltaic efficiency characteristic DSSCs using conventional N719 dye.

Sample	Voc(mV)	*J*sc(mA cm^{-2})	FF(%)	η(%)
TrGO-1 450	627.44	9.53	0.52	3.11
TrGO-2 450	629.88	10.76	0.48	3.25
TrGO-3 450	637.21	11.78	0.55	4.11
TrGO-4 450	620.12	9.63	0.55	3.28
TrGO-5 450	600.59	8.81	0.41	2.11

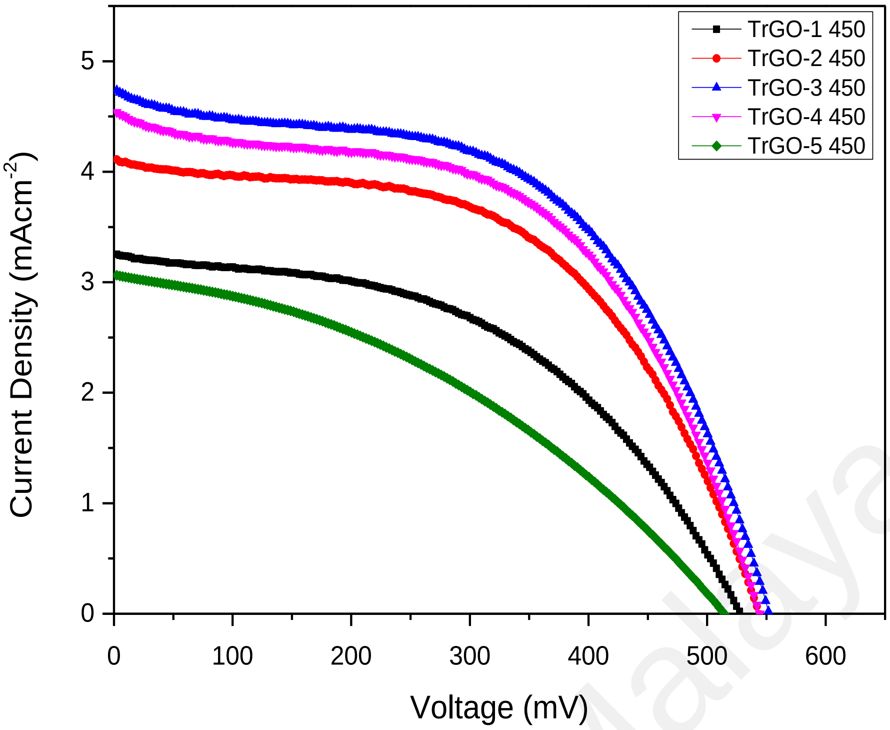

Figure 4.37: Photocurrent density-voltage characteristic of TrGO-1 450, TrGO-2 450, TrGO-3 450, TrGO-4 450 and TrGO-5 450 using green chlorophyll dye.

Table 4.17: Photovoltaic efficiency characteristic DSSCs using green chlorophyll dye.

Sample	Voc(mV)	*J*sc(mA cm^{-2})	FF(%)	ŋ(%)
TrGO-1 450	529.78	3.25	0.48	0.83
TrGO-2 450	544.43	4.11	0.52	1.16
TrGO-3 450	559.08	4.73	0.53	1.40
TrGO-4 450	549.32	4.53	0.52	1.29
TrGO-5 450	515.58	3.66	0.32	0.60

From the *J*-V curves, it is interesting to note that TrGO-3 nanocomposite showed improvement in photovoltaic generation regardless of the dye type used compared to TiO_2 DSSCs. The N719 dye-sensitized TrGO-3 illustrated a higher photovoltaic efficiency (4.11%) compared to natural dye of the green chlorophyll dye-sensitized TrGO-3 (1.40%) and red anthocyanin dye (1.47%). It was also found that, in Fig. 4.39, the overall photovoltaic efficiency *(ŋ)* of DSSCs improved by the addition of rGO into the photoanode up to 0.03g (i.e., TrGO-3).

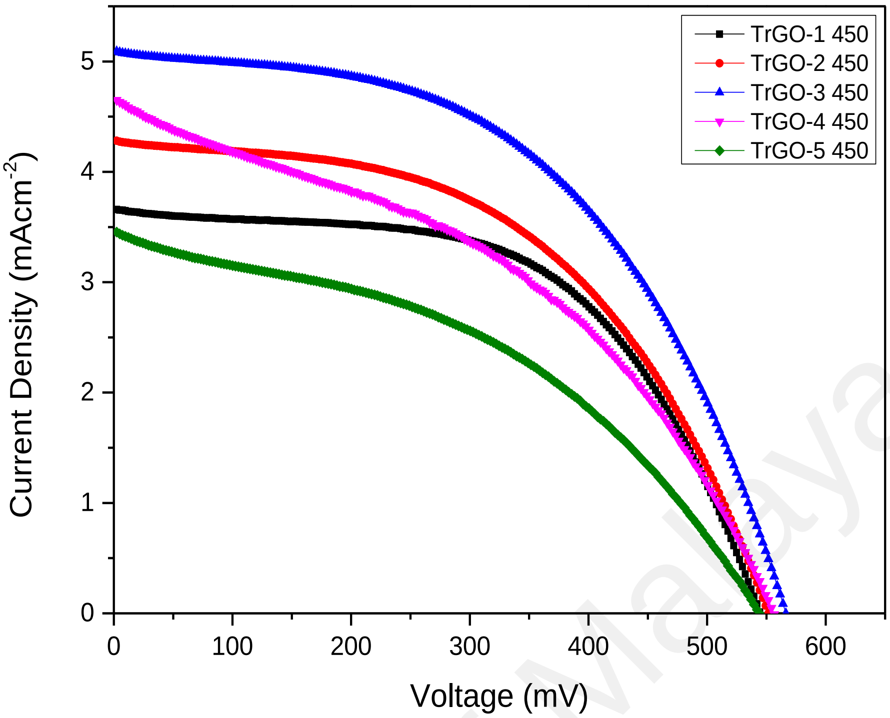

Figure 4.38: Photocurrent density-voltage characteristic TrGO-1 450, TrGO-2 450, TrGO-3 450, TrGO-4 450 and TrGO-5 450 using Red Anthocyanin dye.

Table 4.18: Photovoltaic efficiency characteristic DSSCs using Red Anthocyanin dye

Sample	Voc(mV)	*J*sc(mA cm^{-2})	FF(%)	ŋ(%)
TrGO-1 450	546.88	3.66	0.56	1.12
TrGO-2 450	554.19	4.28	0.51	1.21
TrGO-3 450	566.41	5.09	0.51	1.47
TrGO-4 450	556.64	4.65	0.41	1.06
TrGO-5 450	544.43	3.45	0.42	0.79

This is associated with the fact that the addition of rGO enhanced the transfer path for the ultrafast ejected electrons to travel between TiO_2 particle. As a result, these phenomena contributed to an increase in the current density while minimizing/reducing the recombination of electron generation. On top of photovoltaic efficiency and current density, TrGO-1 450, TrGO-2 450 and TrGO-3 450 also showed improvement in V_{oc}. Correspondingly, the V_{oc} improvement led to the reduction in the Fermi level in the photoanode and the Nerst potential of redox couple in the electrolyte when it was under illumination (L. Chen et al., 2013). However, DSSCs containing higher amounts of rGO (i.e., TrGO-4 450 and TrGO-5 450) lost its performance as a consequence of the drop in the photovoltaic efficiency compared to TrGO-3 450. This is mainly due to the antagonistic effect between the rGO and dye molecules to compete for the visible light. In other words, the photon of visible light absorbed by the dye molecules would become less if the rGO content is high considering rGO only absorbed approximately 4% of light (L. Chen et al., 2013; Fang et al., 2012; Jumeri et al., 2015; Mehmood, Ahmed, Hussein, & Harrabi, 2015; Zhi et al., 2015). This would give rise to less excited electron traveling in the device and eventually lead to a lower current density and photovoltaic efficiency of DSSCs.

Based on these observations, it is presumable that the TrGO-3 450 composite possesses enhanced charge transport considering the photo-induced electrons could move through the rGO bridge rather than solely the Ti-Ti grain as a result of the intimate contact between the TiO_2 and rGO. Also, the photoanodes absorption of dye was relatively improved by the addition of rGO ascribed to the larger surface area for dye loading. Considering these facts, it is thereby expected that the photovoltaic properties of the DSSCs could be significantly enhanced.

Apart from that, as shown in Fig. 4.39, from the pattern of photovoltaic characteristics shows improvements in all characteristics of DSSCs from TrGO-1 450 to TrGO-3 450. The positive impact of increment in performance was contributed by the anchoring of TiO_2 on rGO surface. With a balance ratio of rGO and TiO_2 will exhibit a positive improvement in all aspect of DSSC such as bandgap of semiconductor, photovoltaic characteristics and overall efficiency. From the 4.39 figure, it showed that ratio TrGO-4 450 (0.04g) and TrGO-5 450 (0.05g) DSSC give negative impact on the performance of DSSC where it become unstable and decrease in performance. This is due to competitiveness of the semiconductor to absorb and transport light. For this parameter, red anthocyanin dye shows a better DSSC performance in natural dye compared to green chlorophyll dye.

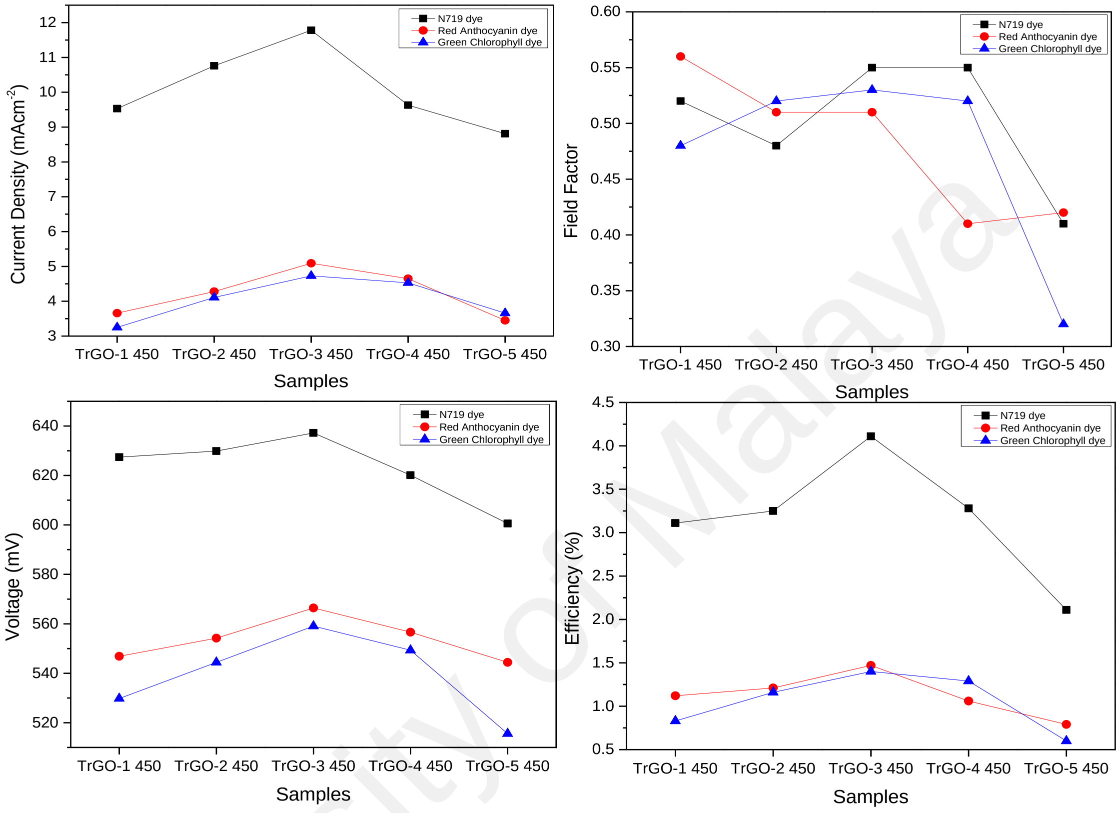

Figure 4.39: DSSCs analysis of all samples; a) current density; b) fill factor; c) voltage short circuit; d) efficiency

By optimizing the loading of TiO_2 dopants attached to the rGO sheets to improve the photovoltaic performance. It has been widely accepted that the photon absorption could be significantly improved with a good combination of weight content and calcination temperature between TiO_2 and rGO. An excessive TiO_2 nanoparticle dopants attached to rGO will cause loss in photons that could have absorbed and eventually lead to electron leakage in the device (Chang et al., 2013). Also, the aim of the present study was to enhance the absorption of the dye via optimizing the ratio of TiO_2 and rGO dopants, crystalline structure and improving the texture of dye to enhance the photovoltaic performance by increasing J_{sc} of DSSCs(Sharma et al., 2013; M. Zhu et al., 2014).

Incorporation of graphene into nanocomposite will attribute to increase in dye loading on the semiconductor oxide, where the chemical defect and high surface area of rGO sheets favours the dye absorption on the semiconductor oxide film. Also, when the surface of photoanode was illuminated with sunlight, the ultrafast electron transport could be enhanced with the support of excellent conductivity of rGO. From the previous study, it was known that the resistance between the grain and path could be minimized by incorporating rGO into TiO_2 as rGO tends to build the bridge between TiO_2 (M. Zhu et al., 2014). This help in enhancing the charge separation, electron collector and transportation of photogenerated electron as well as reducing the probability of charge recombination. This is also beneficial for the photo-generated electron to transfer without suffering from massive resistance (Sharma et al., 2013; Zhao et al., 2013; Zhao et al., 2015; Zhi et al., 2015).

4.4.3 EIS analysis of dye sensitized solar cells

Accordingly, The EIS was then analysed using the stimulated model of internal circuit of DSSCs to identify the resistance of electron charge between each surface materials and internal resistance for DSSC device. EIS test was conducted under the illumination condition of $100mW/cm^2$ over the frequency range of 100kHz to 0.001Hz at the amplitude of 20mV. For electron lifetime of the DSSC will be shown by bode plot where it shifts from low Z' to high Z' value of the Nyquist plot. The device that have the best performance will show a longer electron lifetime span (San Esteban & Enriquez, 2013).

From Fig.4.40 (A, B & C), it shows 3 semicircles where the first semicircle was barely visible due to the large middle frequency semicircle that overlaps the shape of semicircle of the middle frequency, but regardless of that. From Table 4.18, table 4.19 and Table 4.20, the Nyquist plot show almost similar value (± 5value) of R_s and R_{CE} where it describes the materials for counter electrode and electrolyte were same for all DSSCs devices for all type of dye. The variation of value due to adaptation of counter electrode and electrolyte with different dye and morphology of semiconductor oxide photoanode. When the first semicircle decreased, it indicted that the fast electron transfer at counter electrode and electrolyte interface. Furthermore, the second semicircle R_{CT} represents the photoanode/dye/electrolyte resistance. For N719 dye, the value or R_{CT} for TrGO-1 450, TrGO-2 450, TrGO-3 450, TrGO-4 450 and TrGO-5 450 were 131.8Ω, 92.5Ω,74.7Ω, 199.0Ω and 284.3Ω respectively. The green dye recorded 200.2Ω, 172.0Ω, 131.6Ω, 294.0Ω and 334.2Ω for TrGO-1 450, TrGO-2 450, TrGO-3 450, TrGO-4 450 and TrGO-5 450. Meanwhile, red anthocyanin dye R_{CT} value for TrGO-1 450, TrGO-2 450, TrGO-3 450, TrGO-4 450 and TrGO-5 450 were 199.4Ω, 171.8Ω, 129.0Ω, 284.3Ω and 294.2Ω. These values indicate the electrocatalytic activity in the DSSCs where the lowest value of R_{CT} represents the highest electrocatalytic activity then other DSSCs. In this case for red anthocyanin, N719 and natural green chlorophyll dye TrGO-3 450 recorded highest electrocatalytic activity compared to other DSSCs.

Table 4.19: EIS analysis of N719 dye DSSCs.

Sample	R_s(Ω)	R_{CT}(Ω)	R_{CE}(Ω)	Bode Peak (Hz)	Electron Lifetime τ_n(ms)
TrGO-1 450	21.8	131.8	34.1	39.811	4.00
TrGO-2 450	20.9	92.5	35.2	25.119	6.34
TrGO-3 450	19.8	74.7	36.6	15.849	10.00
TrGO-4 450	22.9	199.0	36.7	31.623	5.03
TrGO-5 450	21.7	284.3	37.8	79.433	2.00

Table 4.20: EIS analysis of green chlorophyll dye DSSCs.

Sample	$R_s(\Omega)$	$R_{CT}(\Omega)$	$R_{CE}(\Omega)$	Bode Peak (Hz)	Electron Lifetime τ_n(ms)
TrGO-1 450	22.6	200.2	38.7	50.119	3.18
TrGO-2 450	21.3	172.0	38.1	39.811	4.00
TrGO-3 450	20.3	131.6	37.7	19.953	8.37
TrGO-4 450	22.6	294.0	40.7	50.119	2.00
TrGO-5 450	24.4	334.2	36.7	100.00	1.59

Table 4.21: EIS analysis of red anthocyanin dye DSSCs.

Sample	$R_s(\Omega)$	$R_{CT}(\Omega)$	$R_{CE}(\Omega)$	Bode Peak (Hz)	Electron Lifetime τ_n(ms)
TrGO-1 450	23.9	199.4	33.1	50.119	2.00
TrGO-2 450	22.4	171.8	37.2	19.953	3.18
TrGO-3 450	20.6	129.0	30.9	12.589	8.37
TrGO-4 450	24.7	284.3	34.7	31.623	5.03
TrGO-5 450	24.7	294.2	35.6	100.00	1.59

The resistance of commercial N719 dye DSSC is in denial the lowest among all type of dye, but red anthocyanin dye shows lower resistance compared to green chlorophyll dye for type of natural dye. In the same time, the value of R_{CT} TrGO-3 450 represents the lowest recombination resistance and lowest electron transmission resistance in the photoanode. Incorporation of graphene into nanocomposite will attribute to increase in dye loading on the semiconductor oxide, where the chemical defect and high surface are of rGO sheets favours the dye absorption on the semiconductor oxide film. In addition, when rGO was added into the photoanode, it creates new path in the photoanode structure and the generated electron travels quickly to fill the anode surface (Aung, Hao, Oo, & Boschloo, 2016; Liu et al.; San Esteban & Enriquez, 2013).

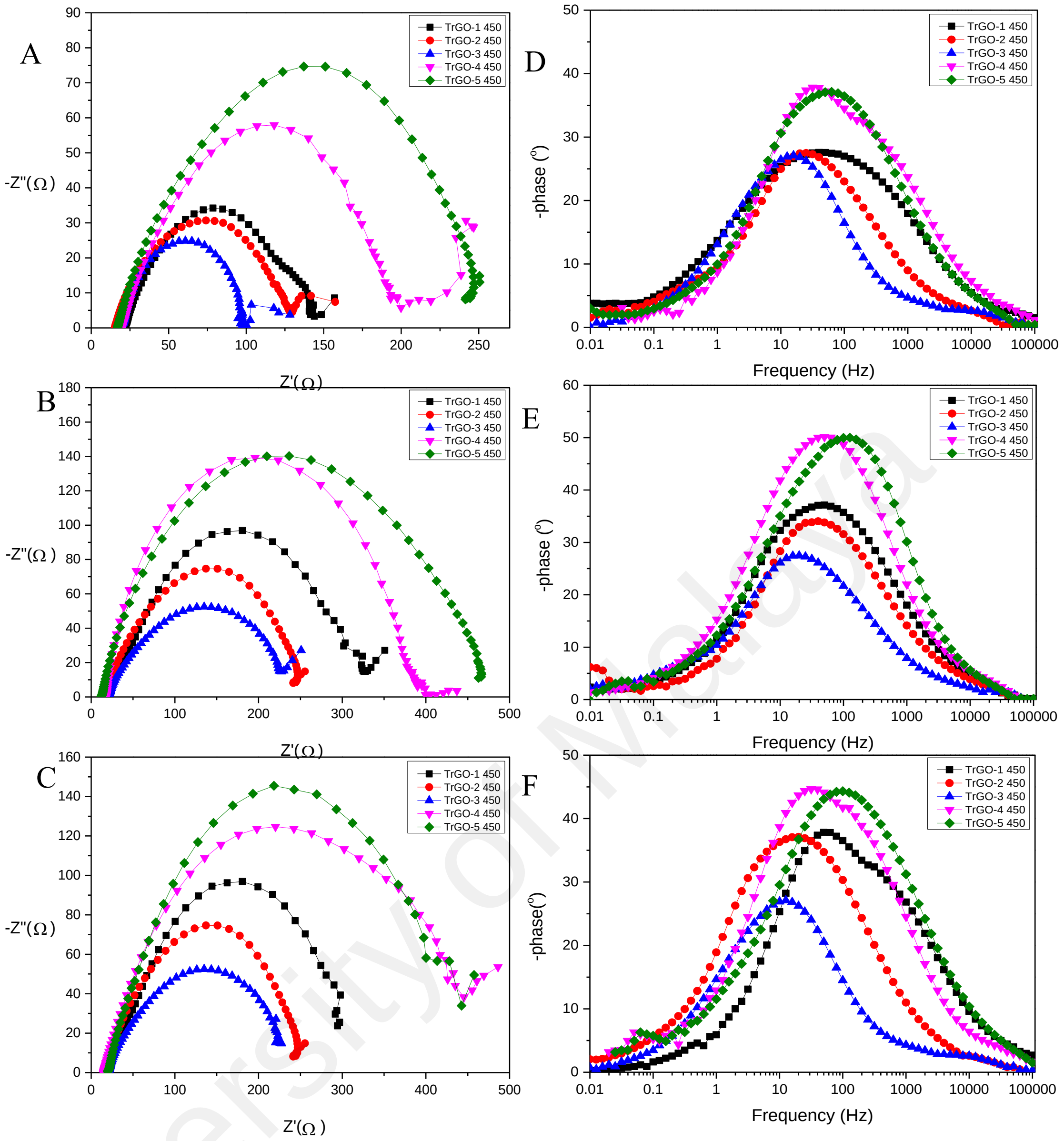

Figure 4.40: EIS analysis (A, B & C) Nyquist plot for commercialize N719 dye, green chlorophyll dye and red anthocyanin dye; (D, E & F) Bode plot for commercialize N719 dye, green chlorophyll dye and red anthocyanin dye

Subsequently, rGO helps in acceleration of the interfacial electron transfer which will reduce the electron-hole recombination. With optimized TiO_2 dopants in rGO film, the minimal defect in the photoanode will create good surface contact for the dye and semiconductor, increased in the performance of DSSCs, supressed the recombination of electron across the semiconductor and enhance the charge transfer between the interfaces of the material (Hu et al., 2017; Liu et al.; San Esteban & Enriquez, 2013). In order to support the EIS analysis, bode plots contribute to the information of electronics transfer and recombination of electron holes lifetime in DSSCs photoanode-electrolyte interface. From the bode plot Figs 4.40 (D, E & F), electron lifetime (τ_n) could be obtained from the peak angular frequency by using the following equation (3.4):

$$\tau_n = \frac{1}{2}\pi f_{max} \tag{3.4}$$

where f_{max} is the peak frequency of bode phase. As shown in Table 4.18, Table 4.19 and Table 4.20 the recorded electron lifetime for N719 dye were 4.00ms, 6.34, 10.00ms, 5.02ms and 2.00ms. For natural dye, red anthocyanin dye recorded 3.18ms, 4.00ms, 8.37ms, 2.00ms and 1.59ms electron lifetime while the electron lifetime for green chlorophyll dye were 3.18ms, 4.00ms, 8.37ms, 2.00ms and 1.59ms. From the bode plot, shifting of the characteristic peak into lower frequency demonstrate with increase in electron transfer. The recombination in the photoanode/dye/electrolyte interface reduced when there is an increase of electron lifetime producing a reduction of recombination (Sharma et al., 2013). From the tables, the increase in electron lifetime was TrGO-3 450 regardless type of dye which suggests the recombination rate of injected electron have improved and leads to faster diffusion rate, thus increasing J_{sc} and PCE values (Sacco et al., 2014; Sharma et al., 2013). Longer electron lifetime shows that rGO contributes to the reduction in electron recombination (San Esteban & Enriquez, 2013) and explained by Zhao et al (Zhao et al., 2013; Zhao et al., 2015) that graphene reacts as a bridge for the electron transfer in TiO_2 photoanode when the electron photogenerated. This contributes less diffusive hindrance and lowers the charge recombination and back transfer reaction when the electron is photogenerated (Zhao et al., 2013; Zhao et al., 2015).

4.4.4 Overall TrGO Photoanode Mechanism

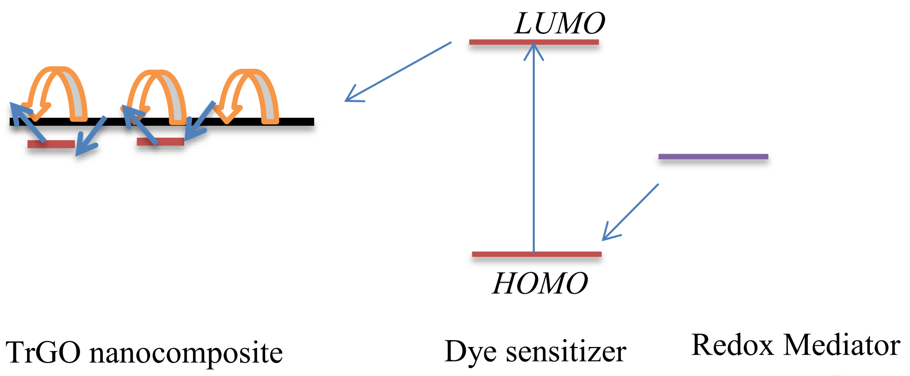

Figure 4.41: Illustration of electron transfer process in DSSC

The electron transfer process is a crucial process in DSSC photoanode due to the electron transfer for on surface interface to another where it will contribute to loss of photogenerated electron. Originally, when an electron transfer process in TiO_2 nanoparticles they may undergo plenty of electron trapping-detraping (Fig. 4.41) events which favour recombination occur. The occurrence of the electron trapping –detraping due to structural defects on Ti grain on TiO_2 and limited surface area (Gong et al., 2017). In this study, rGO was used to increase the surface area and conductivity of the nanocomposite to elevate the photovoltaic efficiency. rGO improves the structure of nanocomposite such as it minimizing the electron trap the surface of the photoanode to ensure ultrafast photogenerated electron to travels in the TrGO surface grain with minimum loss. This could be viewed by EIS spectroscopy and bode plot that TrGO shows reduction in resistance of photoanode/dye/electrolyte interface compared to pure TiO_2. It is supported by the shift of in Nyquist towards low frequency where TrGO shows longer electron lifetime and lower the recombination rate of TrGO nanocomposite.

CHAPTER 5: CONCLUSION AND RECOMENDATION.

5.1 Conclusion

As for conclusion, the three objectives for this thesis have been achieved. For the first objective, to synthesized rGO using Hummer's Method was successfully obtained and used in the second objectives where to incorporating the rGO into TiO_2 to form TrGO nanocomposite. The study was not limited on just synthesizing but optimized the best nanocomposite parameter to achieve optimum TrGO nanocomposite were determined. The conclusion that can be attained from both objective one and two was pure anatase TrGO-3 obtained the most improved and exhibit maximum improvements among all samples in terms of bandgap (2.84eV) and photovoltaic characteristics (refer table 4.2, 4.3 and 4.4). The weight content of rGO for this parameter was 0.03wt/wt% in 11with pH 3. The improvements are shown when we incorporating TrGO-3 semiconductor oxide with different types of dye. In this research, we used 3 types of dye one of it is commercial N719 (synthetic), and two of the dye were crude natural dye with different groups of natural dye (red anthocyanin dye and green chlorophyll dye). By optimizing this content, the natural dye shows an enhancement in terms of photovoltaic characteristics when rGO is incorporated into the photoanode. EIS was used to study the resistance in each layer and the electron lifetime was obtain to prove that it is an effective strategy to enhance photovoltaic characteristics and shortening the electron migration in DSSCs. It is proven that integration of TiO_2 with rGO increase the surface area and improve the electron transport in the photoanode film to decrease the recombination between the photoanode/dye /electrolyte interphase.

The optimization of synthesized pH was done to improve the growth of the crystal and adjusting the crystalline size of TiO_2 that attached on the rGO surface. From

HRTEM and FESEM image, we can conclude that when alteration of pH (pH 1 to pH 5) was done, it gives some effect on the rGO sheet such that the crumpling of rGO less appeared from pH 1 to pH 3 but it crumples more on pH 4 and pH 5. The TiO_2 crystal that grown on rGO shows different patterns of growth and crystalline size. As expected pH 3 TrGO-3 was the best parameter for this optimization as it shows highest photovoltaic characteristics and maximum arc shift to low Z' frequency in bode phase indicate the longer electron lifetime indicates longer electron lifetime where it contributes to lower recombination in DSSCs.

Next, the calcination temperature for TrGO nanocomposite was optimized to obtained the best anatase crystal structure for the photoanode. In the first parameter the samples were calcined 400 °C and in this parameter 450 °C was to improve the crystalline structure of the nanocomposite. From the experiment, the XRD pattern shows improvements in the intensity of the crystalline. The highest peak shows narrow peak where it indicates high crystallinity, but there is a rutile peak on TrGO-3 nanocomposite. In terms of energy band gap, third parameter energy band gap was lower than first parameter may due to small occurrence of rutile peak. In photovoltaic characteristics, TrGO-3 was the highest parameter regardless the type of dye but if both of the parameter (400 °C and 450 °C) were compared on the photovoltaic characteristics, the 400°C shows higher in efficiency and stability on N719 dye while TrGO 450 shows a positive impact on photovoltaic characteristic on natural dye, lower resistance but less stability on the electron lifetime where it is lower than TrGO parameter.

Therefore, we can give a conclusion that the best performance parameter for this study is TrGO-3 with pH3 condition is the best semiconductor oxide for DSSCs study due to it can incorporate well in all types of dye and exhibit comparative DSSC photovoltaic characteristics.

5.2 Recommendation for Future Work

TiO_2 alone is a great material for DSSCs, but there are still limitation that needs to overcome in order to increase the performance of DSSC photovoltaic in terms of photoanode enhancement and dye loading. Graphene is one of materials that being explored due to its astonishing characteristics that improves many material characteristics. In this work, the use of TrGO was found to increase the photovoltaic characteristics, reduced the resistance at the surface interface and lower done the recombination by increasing the electron lifetime. However, the stability of device is still in debate to make it as readily commercial device is still a challenge for all researchers. Several suggestions and recommendations are proposed for further developments:

i. To investigate different TiO_2 structure such as TiO_2 sheet and incorporate with rGO sheet to increase the conductivity of the semiconductor material.
ii. To propose a structure on rGO sheet to increase the dye absorption to the photoanode.
iii. Study the morphology & DSSC characteristics using XPS, time-voltage plot and ICPE for more detail reasoning of the ability of DSSC.
iv. Tailor the natural dye to organic dye to strengthen the stability of anchoring dye into the photoanode surface to reduce the interphase resistance.

REFERENCES

Ahmad, I., McCarthy, J. E., Baranov, A., & Gun'ko, Y. K. (2015). Development of Graphene Nano-Platelet Based Counter Electrodes for Solar Cells. *Materials, 8*(9), 5953-5973.

Al-Alwani, M. A. M., Mohamad, A. B., Ludin, N. A., Kadhum, A. A. H., & Sopian, K. (2016). Dye-sensitised solar cells: Development, structure, operation principles, electron kinetics, characterisation, synthesis materials and natural photosensitisers. *Renewable and Sustainable Energy Reviews, 65*, 183-213.

Amara, H., Latil, S., Meunier, V., Lambin, P., & Charlier, J.-C. (2007). Scanning tunneling microscopy fingerprints of point defects in graphene: A theoretical prediction. *Physical Review B, 76*(11), 115423.

Asim, N., Sopian, K., Ahmadi, S., Saeedfar, K., Alghoul, M. A., Saadatian, O., & Zaidi, S. H. (2012). A review on the role of materials science in solar cells. *Renewable and Sustainable Energy Reviews, 16*(8), 5834-5847.

Aung, S. H., Hao, Y., Oo, T. Z., & Boschloo, G. (2016). Kinetic study of carminic acid and santalin natural dyes in dye-sensitized solar cells. *Journal of Photochemistry and Photobiology A: Chemistry, 325*, 1-8.

Basheer, B., Mathew, D., George, B. K., & Reghunadhan Nair, C. P. (2014). An overview on the spectrum of sensitizers: The heart of Dye Sensitized Solar Cells. *Solar Energy, 108*, 479-507.

Bell, N. On the design and synthesis of titanium dioxide–graphene nanocomposites for enhanced photovoltaic and photocatalytic performance.

Bisquert, J., Fabregat-Santiago, F., Mora-Sero, I., Garcia-Belmonte, G., & Gimén z, S. (2009). Electron lifetime in dye-sensitized solar cells: theory and interpretation of measurements. *The Journal of Physical Chemistry C, 113*(40), 17278-17290.

Blanita, G., & Lazar, M. D. (2013). Review of Graphene-Supported Metal Nanoparticles as New and Efficient Heterogeneous Catalysts. *Micro and Nanosystems, 5*(2), 138-146.

Calogero, G., Citro, I., Crupi, C., & Di Marco, G. (2014). Absorption spectra and photovoltaic characterization of chlorophyllins as sensitizers for dye-sensitized solar cells. *Spectrochimica Acta Part A: Molecular and Biomolecular Spectroscopy, 132*, 477-484.

Chandrasekaran, J., Nithyaprakash, D., Ajjan, K., Maruthamuthu, S., Manoharan, D., & Kumar, S. (2011). Hybrid solar cell based on blending of organic and inorganic materials—an overview. *Renewable and Sustainable Energy Reviews, 15*(2), 1228-1238.

Chang, J. L., Yang, J. L., Ma, P. F., Wu, D. P., Tian, L., Gao, Z. Y., . . . Yang, L. (2013). Hierarchical titania mesoporous sphere/graphene composite, synthesis and application as photoanode in dye sensitized solar cells. *Journal of Colloid and Interface Science, 394*, 231-236.

Chen, J. Z., Yan, Y. C., & Lin, K. J. (2010). Effects of Carbon Nanotubes on Dye-Sensitized Solar Cells. *Journal of the Chinese Chemical Society, 57*(5B), 1180-1184.

Chen, L., Zhou, Y., Tu, W. G., Li, Z. D., Bao, C. X., Dai, H., . . . Zou, Z. G. (2013). Enhanced photovoltaic performance of a dye-sensitized solar cell using graphene-TiO2 photoanode prepared by a novel in situ simultaneous reduction-hydrolysis technique. *Nanoscale, 5*(8), 3481-3485.

Cheng, G., & Stadler, F. J. (2015). Achieving phase transformation and structure control of crystalline anatase TiO2@C hybrids from titanium glycolate precursor and glucose molecules. *Journal of Colloid and Interface Science, 438*, 169-178.

Chergui, Y., Nehaoua, N., & Mekki, D. Comparative Study of Dye-Sensitized Solar Cell Based on ZnO and TiO2 Nanostructures.

de Souza, J. d. S., de Andrade, L. O. M., & Polo, A. S. (2013). Nanomaterials for solar energy conversion: dye-sensitized solar cells based on ruthenium (II) Tris-heteroleptic compounds or natural dyes *Nanoenergy* (pp. 49-80): Springer.

Dey, A., Nangare, V., More, P. V., Khan, M. A. S., Khanna, P. K., Sikder, A. K., & Chattopadhyay, S. (2015). A graphene titanium dioxide nanocomposite (GTNC): one pot green synthesis and its application in a solid rocket propellant. *Rsc Advances, 5*(78), 63777-63785.

Fang, X., Li, M., Guo, K., Zhu, Y., Hu, Z., Liu, X., . . . Zhao, X. (2012). Improved properties of dye-sensitized solar cells by incorporation of graphene into the photoelectrodes. *Electrochimica Acta, 65*, 174-178.

Frank, O., Zukalova, M., Laskova, B., Kurti, J., Koltai, J., & Kavan, L. (2012). Raman spectra of titanium dioxide (anatase, rutile) with identified oxygen isotopes (16, 17, 18). *Physical Chemistry Chemical Physics, 14*(42), 14567-14572.

Gao, Y., Chu, L., Wu, M., Wang, L., Guo, W., & Ma, T. (2012). Improvement of adhesion of Pt-free counter electrodes for low-cost dye-sensitized solar cells. *Journal of Photochemistry and Photobiology A: Chemistry, 245*, 66-71.

Geim, A. K. (2009). Graphene: status and prospects. *science, 324*(5934), 1530-1534.

Gong, J., Liang, J., & Sumathy, K. (2012). Review on dye-sensitized solar cells (DSSCs): Fundamental concepts and novel materials. *Renewable and Sustainable Energy Reviews, 16*(8), 5848-5860.

Gong, J., Sumathy, K., Qiao, Q., & Zhou, Z. (2017). Review on dye-sensitized solar cells (DSSCs): Advanced techniques and research trends. *Renewable and Sustainable Energy Reviews, 68, Part 1*, 234-246.

Grätzel, M. (2003). Dye-sensitized solar cells. *Journal of Photochemistry and Photobiology C: Photochemistry Reviews, 4*(2), 145-153.

Grätzel, M. (2005). Solar energy conversion by dye-sensitized photovoltaic cells. *Inorganic chemistry, 44*(20), 6841-6851.

Gupta, S. K., Desai, R., Jha, P. K., Sahoo, S., & Kirin, D. (2010). Titanium dioxide synthesized using titanium chloride: size effect study using Raman spectroscopy and photoluminescence. *Journal of Raman Spectroscopy, 41*(3), 350-355.

Han, Q., Yu, M., & Liu, J. (2013). Nanocrystalline titanium dioxide prepared by hydrothermal method and its application in dye-sensitised solar cells. *IET Micro & Nano Letters, 8*(5), 238-242.

Hemmatzadeh, R., & Mohammadi, A. (2013). Improving optical absorptivity of natural dyes for fabrication of efficient dye-sensitized solar cells. *Journal of Theoretical and Applied Physics, 7*(1), 1-7.

How, G. T. S., Pandikumar, A., Ming, H. N., & Ngee, L. H. (2014). Highly exposed {001} facets of titanium dioxide modified with reduced graphene oxide for dopamine sensing. *Scientific reports, 4*. doi: 10.1038/srep05044

Hu, W., Zhang, Z., Shen, W., Li, M., & He, R. (2017). Cyclopentadithiophene bridged organic sensitizers with different auxiliary acceptor for high performance dye-sensitized solar cells. *Dyes and Pigments, 137*, 165-173.

Huang, C., Li, C., & Shi, G. (2012). Graphene based catalysts. *Energy & Environmental Science, 5*(10), 8848-8868.

Huang, N. M., Lim, H., Chia, C., Yarmo, M., & Muhamad, M. (2011). Simple room-temperature preparation of high-yield large-area graphene oxide. *International journal of nanomedicine, 6*, 3443.

Isley, S. L., & Penn, R. L. (2008). Titanium Dioxide Nanoparticles: Effect of Sol−Gel pH on Phase Composition, Particle Size, and Particle Growth Mechanism. *The Journal of Physical Chemistry C, 112*(12), 4469-4474.

Ito, S., Murakami, T. N., Comte, P., Liska, P., Grätzel, C., Nazeeruddin, M. K., & Grätzel, M. (2008). Fabrication of thin film dye sensitized solar cells with solar to electric power conversion efficiency over 10%. *Thin Solid Films, 516*(14), 4613-4619.

Ito, S., Saitou, T., Imahori, H., Uehara, H., & Hasegawa, N. (2010). Fabrication of dye-sensitized solar cells using natural dye for food pigment: Monascus yellow. *Energy & Environmental Science, 3*(7), 905-909.

J.Gong, K. S., J.Gong. (2012). *Review on dye-sensitized solar cell (DSSCs): Fundamental concepts and novel material*. Paper presented at the Renewable and Sustainable Energy Reviews 16.

Jin, C., Liu, B., Lei, Z., & Sun, J. (2015). Structure and photoluminescence of the TiO2 films grown by atomic layer deposition using tetrakis-dimethylamino titanium and ozone. *Nanoscale Research Letters, 10*(1), 1-9. Jo, W.-K., & Kang, H.-J. (2013).

Titanium dioxide–graphene oxide composites with different ratios supported by Pyrex tube for photocatalysis of toxic aromatic vapors. *Powder Technology, 250*, 115-121.

Jumeri, F. A., Lim, H. N., Zainal, Z., Huang, N. M., Pandikumar, A., & Lim, S. P. (2015). Dual functional reduced graphene oxide as photoanode and counter electrode in dye-sensitized solar cells and its exceptional efficiency enhancement. *Journal of Power Sources, 293*, 712-720.

Karimi, L., Yazdanshenas, M., Khajavi, R., Rashidi, A., & Mirjalili, M. (2014). Using graphene/TiO2 nanocomposite as a new route for preparation of electroconductive, self-cleaning, antibacterial and antifungal cotton fabric without toxicity. *Cellulose, 21*(5), 3813-3827.

Kay, A., & Grätzel, M. (1996). Low cost photovoltaic modules based on dye sensitized nanocrystalline titanium dioxide and carbon powder. *Solar energy materials and solar cells, 44*(1), 99-117.

Kim, A., Kim, J.-E., Kim, M.-Y., Ha, S.-W., Tien, N. T. T., & Kang, M.-S. (2012). Photovoltaic efficiencies on dye-sensitized solar cells assembled with graphene-linked TiO 2 anode films. *Bulletin of the Korean Chemical Society, 33*(10), 3355-3360.

Lai, C. W., Low, F. W., Chong, S. W., Wong, C. P. P., Siddick, S., Juan, J. C., & Hamid, S. B. A. (2015). An Overview: Recent Development of Titanium Dioxide Loaded Graphene Nanocomposite Film for Solar Application. *Current Organic Chemistry, 19*(19), 1882-1895.

Li, S., Luo, Y., Lv, W., Yu, W., Wu, S., Hou, P., . . . Cheng, H. M. (2011). Vertically Aligned Carbon Nanotubes Grown on Graphene Paper as Electrodes in Lithium-Ion Batteries and Dye-Sensitized Solar Cells. *Advanced Energy Materials, 1*(4), 486-490.

Liang, Y., Wang, H., Casalongue, H. S., Chen, Z., & Dai, H. (2010). TiO2 nanocrystals grown on graphene as advanced photocatalytic hybrid materials. *Nano Research, 3*(10), 701-705.

Ling, Y., Cooper, J. K., Yang, Y., Wang, G., Munoz, L., Wang, H., . . . Li, Y. (2013). Chemically modified titanium oxide nanostructures for dye-sensitized solar cells. *Nano Energy, 2*(6), 1373-1382.

Liu, L., Zeng, B., Meng, Q., Zhang, Z., Li, J., Zhang, X., . . . Wang, H. Titanium dioxide/graphene anode for enhanced charge-transfer in dye-sensitized solar cell. *Synthetic Metals*.

Ludin, N. A., Mahmoud, A., Mohamad, A. B., Kadhum, A. A. H., Sopian, K., & Karim, N. S. A. (2014). Review on the development of natural dye photosensitizer for dye-sensitized solar cells. *Renewable & Sustainable Energy Reviews, 31*, 386-396.

Maurya, I. C., Srivastava, P., & Bahadur, L. (2016). Dye-sensitized solar cell using extract from petals of male flowers Luffa cylindrica L. as a natural sensitizer. *Optical Materials, 52*, 150-156.

Mehmood, U., Ahmed, S., Hussein, I. A., & Harrabi, K. (2015). Improving the efficiency of dye sensitized solar cells by TiO2-graphene nanocomposite photoanode. *Photonics and Nanostructures-Fundamentals and Applications, 16*, 34-42.

Meng, X. B., Geng, D. S., Liu, J. A., Li, R. Y., & Sun, X. L. (2011). Controllable synthesis of graphene-based titanium dioxide nanocomposites by atomic layer deposition. *Nanotechnology, 22*(16).

Min, Y., Zhang, K., Zhao, W., Zheng, F., Chen, Y., & Zhang, Y. (2012). Enhanced chemical interaction between TiO 2 and graphene oxide for photocatalytic decolorization of methylene blue. *Chemical Engineering Journal, 193*, 203-210.

Narayan, M. R. (2012). Review: dye sensitized solar cells based on natural photosensitizers. *Renewable and Sustainable Energy Reviews, 16*(1), 208-215.

Nazeeruddin, M. K., Baranoff, E., & Grätzel, M. (2011). Dye-sensitized solar cells: a brief overview. *Solar Energy, 85* (6), 1172-1178.

Nithya, A., Rokesh, K., & Jothivenkatachalam, K. Biosynthesis, Characterization and Application of Titanium Dioxide Nanoparticles.

O'regan, B., & Grfitzeli, M. (1991). A low-cost, high-efficiency solar cell based on dye-sensitized. *nature, 353*, 737-740.

Pablo, C. V., Enrique, R. R., Jose, R. G., Enrique, M. P., Juan, L. H., & Eddie, A. M. (2016). Construction of dye-sensitized solar cells (DSSC) with natural pigments. *Materials Today-Proceedings, 3*(2), 194-200.

Pagliaro, M., Palmisano, G., Ciriminna, R., & Loddo, V. (2009). Nanochemistry aspects of titania in dye-sensitized solar cells. *Energy & Environmental Science, 2*(8), 838-844.

Qu, J., & Lai, C. (2013). One-dimensional TiO 2 nanostructures as photoanodes for dye-sensitized solar cells. *Journal of Nanomaterials, 2013*, 2.

Raghavan, N., Thangavel, S., & Venugopal, G. (2015). Enhanced photocatalytic degradation of methylene blue by reduced graphene-oxide/titanium dioxide/zinc oxide ternary nanocomposites. *Materials Science in Semiconductor Processing, 30*, 321-329.

Raj, C. C., & Prasanth, R. (2016). A critical review of recent developments in nanomaterials for photoelectrodes in dye sensitized solar cells. *Journal of Power Sources, 317*, 120-132.

Roy-Mayhew, J. D., & Aksay, I. A. (2014). Graphene Materials and Their Use in Dye-Sensitized Solar Cells. *Chemical Reviews, 114*(12), 6323-6348.

Roy-Mayhew, J. D., Bozym, D. J., Punckt, C., & Aksay, I. A. (2010). Functionalized graphene as a catalytic counter electrode in dye-sensitized solar cells. *ACS nano, 4*(10), 6203-6211.

S.Anandan. (2007). Recent improvments and arising challenges in dye-sensitized solar cell. *Solar Energy Material & Solar Cell*, 843-846.

Sacco, A., Porro, S., Lamberti, A., Gerosa, M., Castellino, M., Chiodoni, A., & Bianco, S. (2014). Investigation of Transport and Recombination Properties in Graphene/Titanium Dioxide Nanocomposite for Dye-Sensitized Solar Cell Photoanodes. *Electrochimica Acta, 131*, 154-159.

Samsudin, E. M., Hamid, S. B. A., Juan, J. C., Basirun, W. J., & Kandjani, A. E. (2015). Surface modification of mixed-phase hydrogenated TiO2 and corresponding photocatalytic response. *Applied Surface Science, 359*, 883-896.

San Esteban, A. C. M., & Enriquez, E. P. (2013). Graphene–anthocyanin mixture as photosensitizer for dye-sensitized solar cell. *Solar Energy, 98, Part C*, 392-399.

Sengupta, D., Das, P., Mondal, B., & Mukherjee, K. (2016). Effects of doping, morphology and film-thickness of photo-anode materials for dye sensitized solar cell application – A review. *Renewable and Sustainable Energy Reviews, 60*, 356-376.

Senthil, T. S., Muthukumarasamy, N., Agilan, S., Balasundaraprabhu, R., & Kumaran, C. K. S. (2013). Effect of surface morphology on the performance of natural dye sensitized TiO2 thin film solar cells. In S. Velumani & N. Muthukumarasamy (Eds.), *Advances in Nanoscience and Nanotechnology* (Vol. 678, pp. 326-330).

Shalini, S., Prabhu, R. B., Prasanna, S., Mallick, T. K., & Senthilarasu, S. (2015). Review on natural dye sensitized solar cells: Operation, materials and methods. *Renewable & Sustainable Energy Reviews, 51*, 1306-1325.

Sharma, G. D., Daphnomili, D., Gupta, K. S. V., Gayathri, T., Singh, S. P., Angaridis, P. A., . . . Coutsolelos, A. G. (2013). Enhancement of power conversion efficiency of dye-sensitized solar cells by co-sensitization of zinc-porphyrin and thiocyanate-free ruthenium(II)-terpyridine dyes and graphene modified TiO2 photoanode. *Rsc Advances, 3*(44), 22412-22420.

Shearer, C. J., Cherevan, A., & Eder, D. (2014). Chapter 16 - Application of Functional Hybrids Incorporating Carbon Nanotubes or Graphene A2 - Tanaka, K. In S. Iijima (Ed.), *Carbon Nanotubes and Graphene (Second Edition)* (pp. 387-433). Oxford: Elsevier.

Shi, M., Shen, J., Ma, H., Li, Z., Lu, X., Li, N., & Ye, M. (2012). Preparation of graphene–TiO $_2$ composite by hydrothermal method from peroxotitanium acid and its photocatalytic properties. *Colloids and Surfaces A: Physicochemical and Engineering Aspects, 405*, 30-37.

Singh, E., & Nalwa, H. S. (2015). Graphene-Based Dye-Sensitized Solar Cells: A Review. *Science of Advanced Materials, 7*(10), 1863-1912. doi: 10.1166/sam.2015.2438

Singh, V., Joung, D., Zhai, L., Das, S., Khondaker, S. I., & Seal, S. (2011). Graphene based materials: Past, present and future. *Progress in Materials Science, 56*(8), 1178-1271.

Su’ait, M. S., Rahman, M. Y. A., & Ahmad, A. (2015). Review on polymer electrolyte in dye-sensitized solar cells (DSSCs). *Solar Energy, 115*, 452-470.

Sugathan, V., John, E., & Sudhakar, K. (2015). Recent improvements in dye sensitized solar cells: A review. *Renewable and Sustainable Energy Reviews, 52*, 54-64.

Tang, Y.-B., Lee, C.-S., Xu, J., Liu, Z.-T., Chen, Z.-H., He, Z., . . . Chen, L. (2010). Incorporation of graphenes in nanostructured TiO2 films via molecular grafting for dye-sensitized solar cell application. *ACS nano, 4*(6), 3482-3488.

Tripathi, B., Yadav, P., Pandey, K., Kanade, P., Kumar, M., & Kumar, M. (2014). Investigating the role of graphene in the photovoltaic performance improvement of dye-sensitized solar cell. *Materials Science and Engineering: B, 190*, 111-118.

Tsega, M., & Dejene, F. B. (2017). Influence of acidic pH on the formulation of TiO2 nanocrystalline powders with enhanced photoluminescence property. *Heliyon, 3*(2), e00246.

Wan, H. (2004). Dye sensitized solar cells. *University of Alabama, published research paper*.

Wang, H., Leonard, S. L., & Hu, Y. H. (2012). Promoting Effect of Graphene on Dye-Sensitized Solar Cells. *Industrial & Engineering Chemistry Research, 51*(32), 10613-10620. doi: 10.1021/ie300563h

Wang, P., He, F., Wang, J., Yu, H., & Zhao, L. (2015). Graphene oxide nanosheets as an effective template for the synthesis of porous TiO2 film in dye-sensitized solar cells. *Applied Surface Science, 358, Part A*, 175-180.

Wu, J., Wang, J., Lin, J., Xiao, Y., Yue, G., Huang, M., . . . Yin, S. (2013). Dual functions of YF3: Eu3+ for improving photovoltaic performance of dye-sensitized solar cells. *Scientific reports, 3*.

Wu, T.-T., & Ting, J.-M. (2013). Preparation and characteristics of graphene oxide and its thin films. *Surface and Coatings Technology, 231*, 487-491.

Xiang, Q., Yu, J., & Jaroniec, M. (2012). Graphene-based semiconductor photocatalysts. *Chemical Society Reviews, 41*(2), 782-796.

Yang, S., Feng, X., Ivanovici, S., & Müllen, K. (2010). Fabrication of graphene-encapsulated oxide nanoparticles: towards high-performance anode materials for lithium storage. *Angewandte Chemie International Edition, 49*(45), 8408-8411.

Yu, J. C., Zhang, L., Zheng, Z., & Zhao, J. (2003). Synthesis and characterization of phosphated mesoporous titanium dioxide with high photocatalytic activity. *Chemistry of Materials, 15*(11), 2280-2286.

Zhang, L., Yuan, S.-m., & Lu, X.-j. (2014). Amperometric nonenzymatic glucose sensor based on a glassy carbon electrode modified with a nanocomposite made from nickel(II) hydroxide nanoplates and carbon nanofibers. *Microchimica Acta, 181*(3-4), 365-372.

Zhao, J. C., Wu, J. H., Yu, F. D., Zhang, X. P., Lan, Z., & Lin, J. M. (2013). Improving the photovoltaic performance of cadmium sulfide quantum dots-sensitized solar cell by graphene/titania photoanode. *Electrochimica Acta, 96*, 110-116.

Zhao, J. C., Wu, J. H., Zheng, M., Huo, J. H., & Tu, Y. G. (2015). Improving the photovoltaic performance of dye-sensitized solar cell by graphene/titania photoanode. *Electrochimica Acta, 156*, 261-266.

Zhi, J., Cui, H. L., Chen, A., Xie, Y., & Huang, F. Q. (2015). Efficient highly flexible dye sensitized solar cells of three dimensional graphene decorated titanium dioxide nanoparticles on plastic substrate. *Journal of Power Sources, 281*, 404-410.

Zhu, M., Li, X., Liu, W., & Cui, Y. (2014). An investigation on the photoelectrochemical properties of dye-sensitized solar cells based on graphene–TiO2 composite photoanodes. *Journal of Power Sources, 262*, 349-355.

Zhu, Y., Murali, S., Cai, W., Li, X., Suk, J. W., Potts, J. R., & Ruoff, R. S. (2010). Graphene and graphene oxide: synthesis, properties, and applications. *Advanced materials, 22*(35), 3906-3924.

LIST OF PUBLICATIONS AND PAPERS PRESENTED

i. Siti Zubaidah, S., Chin Wei, L., Joon Ching, J., & Sharifah Bee, H. (2017). Reduced Graphene Oxide–Titania Nanocomposite Film for Improving Dye-Sensitized Solar Cell (DSSCs) Performance. *Current Nanoscience, 13*(5), 494-500.

ii. Siti Zubaidah, S., Chin Wei, L., Joon Ching, J.,(2018). An Investigation of the Dye-sensitized Solar Cell Performance using Graphene-Titania (TrGO) Photoanode with Conventional Dye and Natural Green Chlorophyll Dye. *Materials Science in Semiconductor Processing,* Vol.74, 267-276, ISSN 1369-8001.